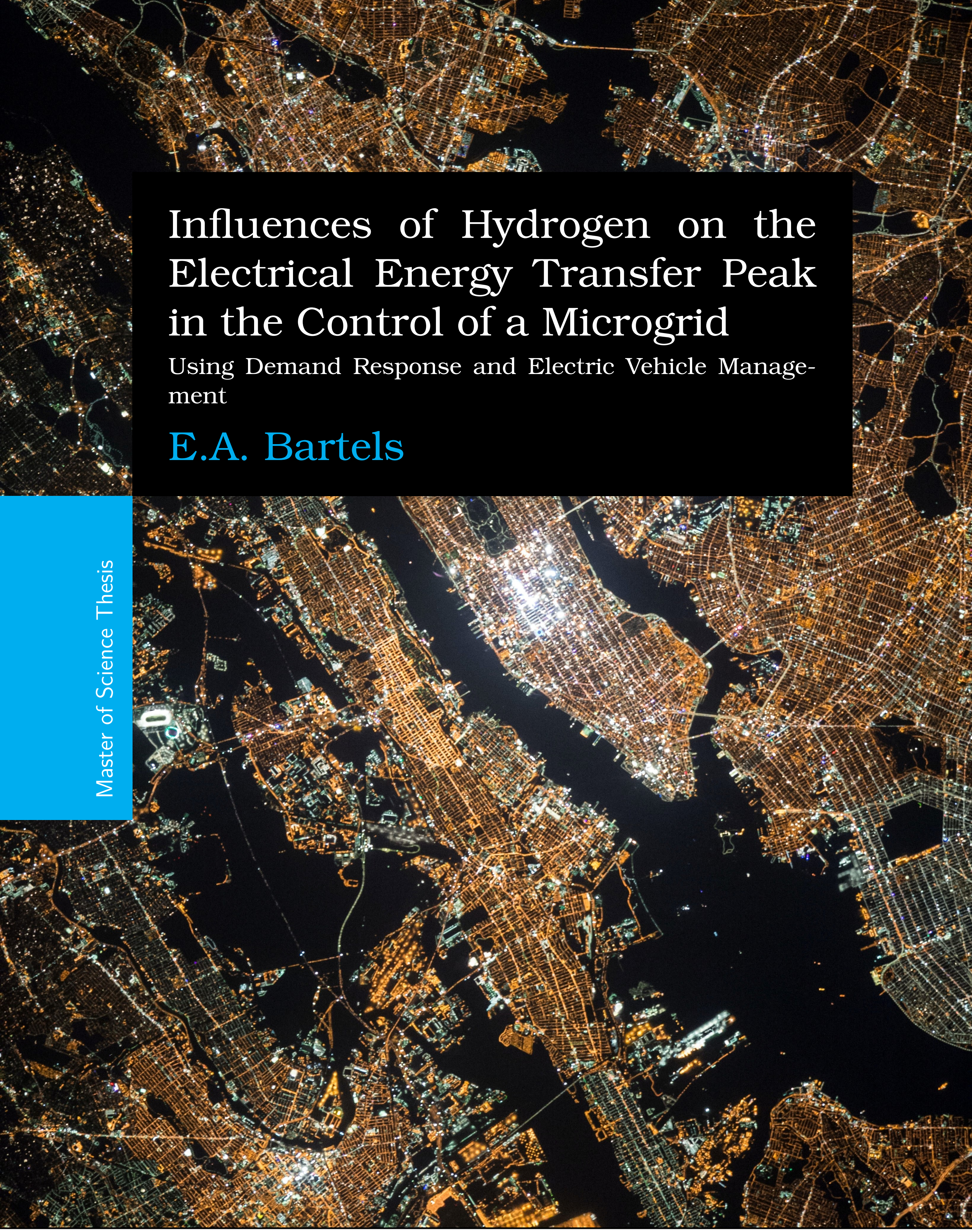

Influences of Hydrogen on the Electrical Energy Transfer Peak in the Control of a Microgrid

Using Demand Response and Electric Vehicle Management

E.A. Bartels

Master of Science Thesis

Delft University of Technology

Delft Center for Systems and Control

Influences of Hydrogen on the Electrical Energy Transfer Peak in the Control of a Microgrid

Using Demand Response and Electric Vehicle Management

Master of Science Thesis

For the degree of Master of Science in Systems and Control at Delft University of Technology

E.A. Bartels

November 10, 2020

Faculty of Mechanical, Maritime and Materials Engineering (3mE) · Delft University of Technology

Abstract

A future rise in electrical energy demand is expected due to the electrification of the thermal energy supply and the rise in popularity of the Electric Vehicle (EV). This rise in the electrical energy demand results in needed investments in the electrical energy infrastructure to prevent congestion at the transformer due to the higher peak of energy transfer between the microgrid and utility grid. Smart control strategies as EV management and Demand Response (DR) programs are used to lower the peak of electrical energy transfer. In this thesis, the focus is on how the introduction of hydrogen will influence the peak of electrical energy transfer between the microgrid and utility grid to reduce future electrical grid investments. The stochastic processes in the microgrid are forecasted with the best-obtained forecasting models. Using a mixed logic dynamical formulation of the hybrid model of the microgrid, different Model Predictive Control (MPC) control strategies are implemented to solve the multi-objective mixed-integer linear programming problem. Microgrids with different levels of hydrogen penetration are compared. It is concluded that the introduction of hydrogen to a future microgrid will reduce the peak of electrical energy transfer, i.e., reduce future investments in the electrical grid. However, it does result in higher overall economic costs due to the high increase in energy import costs. Furthermore, an increase in the degradation of the EVs due to their more intensive use is concluded when introducing hydrogen to the microgrid. Two stochastic MPC methods, scenario- and tree-based MPC are compared to the nominal controller to see if better performance can be obtained for a hydrogen-based microgrid. Better overall performance of the stochastic MPC strategies is obtained in the winter but could not be realized in the summer. Only tree-based MPC shows a reduction in the peak of electrical energy transfer.

Table of Contents

Chapter 1

Introduction

The reduction of greenhouse gases to mitigate the global average temperature rise has been a worldwide topic of great concern over the past decade. During the United Nations Climate Change Conference in 2015, 195 governments signed an agreement for a long-term goal of keeping the increase of the global average temperature this century below two degrees and aiming for an increase of a maximum of one and a half degrees. This agreement is commonly known as the Paris agreement [126]. To prevent exceeding this maximum of two degrees rising of the global average temperature, scientists have determined that human society needs to reduce the electricity produced by burning fossil fuels from 70% in 2010 to 20% in 2050 [63]. Therefore, more energy needs to be produced by renewable energy sources. However, due to the intermittent nature of these renewable energy resources, there is a need for more flexibility in the energy grid [46] and a rise of complexity for the energy management [79].

The implementation of microgrids seems to be a possible key solution to the integration of these renewable energy resources in the energy grid [139]. Microgrids consist of interconnected loads, distributed energy resources, and energy storage systems. These microgrids can be seen as a miniature version of the larger utility grid. A connection to the utility grid is sometimes available, but in other cases, the microgrid needs to be self-supplied and operate in an islanded mode [77]. Due to the distribution of the energy resources by implementing a microgrid, improved reliability, power quality, and reduced distribution loss are realized [99, 101].

Furthermore, changes are happening in the transport sector as well to reduce the emission of greenhouse gases by replacing the internal combustion engine vehicle with an Electric Vehicle (EV) [20]. The increased use of EVs has a strong effect on the energy demand in the microgrid due to their relatively high consumption of energy [99]. This increase in energy demand in the microgrid results in needed economic investments in the infrastructure of the energy grid to prevent congestion at the transformer during high consumption times [138]. Therefore, in future microgrids, the focus should be on the peak of electrical energy transfer between the microgrid and utility grid.

In these future microgrids, smart strategies can be used to create a framework where renewable energy sources can be implemented and reduce the peak of electrical energy transfer to prevent unnecessary investments in the energy grid. The impact of the increasing energy demand by the addition of EVs in the microgrid can be reduced by using smart EV management. In this EV management, the EVs are charged at convenient moments, i.e., when there is an abundance, or less shortage, of energy in the microgrid. Moreover, EVs can contribute to mitigate the problem for energy distribution in the microgrid while being used as a power plant or energy storage system to provide energy at times of high energy demand in the microgrid [9, 52, 99]. Another strategy is the use of Demand Response (DR) programs where the consumption pattern of the consumers in the microgrid is altered. The use of DR programs has proven to generate more flexibility in the grid and reduce the electrical energy transfer peak [101, 119].

A new source of energy is emerging in both the energy and transport sector, hydrogen [20, 94]. The popularity of hydrogen is expected to increase in the next years due to its storing capabilities, cheap transport of energy, and capability to be produced without the emission of greenhouse gases [80]. Hydrogen offers a great solution to the distribution of generated renewable energy, e.g., when generated on offshore wind farms. Fuel cell EVs are emerging due to some beneficial specifications compared to the battery EVs, e.g., greater range and faster refueling [94, 125]. This introduction of hydrogen to the microgrid alters its behaviour. Therefore, different performance regarding the peak of electrical energy transfer between the microgrid and utility grid can be obtained.

1-1 Research Objective

In the presented context, the problem is formulated that the rising electrical energy demand in the microgrid will cause needed investments in the electrical energy grid. Some strategies can be applied to reduce these investments as smart EVs management and the implementation of DR programs. However, the influence of hydrogen in a microgrid on these electrical energy grid investments is unknown. Therefore, the research question of this thesis is formulated as

> *How does the introduction of hydrogen to the microgrid influence the peak of electrical energy transfer between the microgrid and utility grid?*

To answer this question, a comparison should be made between microgrids with different levels of penetration of hydrogen. The performances of these different microgrids can be compared to conclude on the influence of hydrogen on the performance. Hence, the first sub-question to the research question is formulated as

1. *What is the difference in the peak of electrical energy transfer for different microgrids with a different level of penetration of hydrogen?*

These microgrids will be controlled with a nominal Model Predictive Control (MPC) framework that has proven to provide good performance on the energy management of a microgrid [9, 17, 107, 131]. For the control of the microgrid, different stochastic processes in the microgrid are forecasted, i.e., the energy demand of the buildings and power generation by renewable energy sources. The errors in these forecasts can be considered in the optimization by using stochastic MPC strategies, potentially improving the performance of the microgrid [108]. A comparison should be made between the different stochastic MPC strategies and the nominal MPC, to see if the peak of electrical energy transfer could be reduced. Hence, the second sub-question to answer the research question is formulated as

2. *Can stochastic MPC strategies improve the performance of the microgrid and will it reduce the peak of electrical energy transfer?*

1-2 Thesis Contribution

This research aims to provide a primary indication of the difference in the performance and reduction of the peak of electrical energy transfer of the microgrid when hydrogen is introduced. A future microgrid is constructed based on predicted developments in the Netherlands. Moreover, the data used in the optimization of the microgrid are real data sets from the Netherlands. Hence, this study focuses on the specific context of the Netherlands. For the different stochastic processes, multiple forecasting models are developed based on historical data of the stochastic process and exogenous inputs. The best performing forecasting model for each stochastic process is concluded that can be used in other case studies in the Netherlands. Moreover, different stochastic MPC strategies are implemented and compared for a hydrogen-based microgrid. Their performance is compared and conclusions are made if the proposed stochastic MPC strategies can improve the performance of the microgrid.

1-3 Thesis Outline

This thesis report comprises six more chapters. In Chapter 2, a description of the future electric and thermal microgrid is presented. Furthermore, different distributed energy resources are discussed and smart strategies are introduced that can be applied in the microgrid, i.e., smart EV management and DR programs. Chapter 3 describes the modelling of the proposed microgrid. In Chapter 4, the different stochastic processes in the microgrid are forecasted using multiple models. The best performing point forecasting models are concluded and scenarios for the stochastic processes are generated. In Chapter 5, the different MPC control strategies that are used in the microgrid are explained. Moreover, the objective function for the optimization is constructed. To answer the research question, different case studies are presented in Chapter 6. The results from the case studies are obtained and discussed. Lastly, in Chapter 7, the conclusions of this thesis and different proposals for future work are given. A draft of a paper based on the findings in this thesis is attached in Appendix I.

Chapter 2

Electric and Thermal Microgrid

Due to the increase of renewable energy sources and their intermittent behaviour, power fluctuations in the energy grid have become more common. Decentralization of electrical and thermal energy is the natural consequence of the integration of these renewable energy sources. Moreover, the current energy infrastructure is not built to cope with the predicted rise of energy demand that is caused by the electrification of the thermal energy supply and the presence of the Electric Vehicle (EV) in the energy grid. A microgrid can provide a solution to these problems. In a microgrid, distributed energy resources are used to compensate for the energy supply discrepancies in the microgrid. In this chapter, firstly, the electric and thermal microgrid is described. The general structure and control of microgrids are presented, and a hypothetical future microgrid with hydrogen technology integration is sketched. Furthermore, commonly used control objectives in a microgrid are discussed. Secondly, the distributed energy resources in the microgrid that will be used in this study are explained. Thirdly, EVs are discussed and focus is on the management of EVs in microgrids. Lastly, Demand Response (DR) in the microgrid and the response of different consumers are explained.

2-1 Microgrids

This section presents the structure and control of electric and thermal microgrids. Furthermore, a future microgrid in the year 2050 in the Netherlands is sketched. Lastly, different objectives for microgrids, commonly used in the literature, are explained and evaluated.

2-1-1 General Structure

Microgrids can be explained as smaller versions of the utility grid. They can be self-sustainable and operate in islanded mode, or be connected to the utility grid to exchange power to compensate for internal discrepancies in the power [77]. The energy in microgrids comes from local distributed energy resources or is bought from the utility grid. These distributed energy resources can be divided into two categories, i.e., resources where energy is generated or stored.

The energy demand in the microgrid comprises the electrical and thermal energy demand of buildings. These buildings are divided into three different consumer groups [6]: industrial, commercial, and residential consumers, i.e., large factories, local retail stores (small) up to theaters (big), and houses, respectively. In this thesis, only small commercial and residential buildings are considered since the focus is on habitable districts. Their consumption pattern and stochastic behaviour are further discussed in Section 4-3 and 4-4. The introduction of EVs in the microgrid are originally considered as extra energy demand in the microgrid. However, using smart EV management, they also operate as a distributed energy resource by storing and generating energy.

2-1-2 Control Structure

A hierarchical control structure of three levels is used for power management in microgrids: primary, secondary, and tertiary control [92,106]. Primary control stabilizes the frequency and voltage in the electrical network using droop controllers within a sampling time of milliseconds. Secondary control compensates for the steady-state deviations in voltage and frequency caused by the primary control within sampling times varying from seconds to minutes. Tertiary control is the highest control of power management that controls the power flow within the microgrid and between the microgrid and utility grid with a sampling time varying from minutes to days. In this thesis, the focus is on the tertiary control between a microgrid and the utility grid.

Three main approaches are used for the tertiary control of the microgrid: centralized, decentralized, and distributed approach [104, 106]. In this thesis, a centralized approach is used where a central controller collects the information of all units in the microgrid and determines a control action for these units at a single point [104]. This method provides easy implementation and obtains the best achievable performance for a solvable optimization of the microgrid [106]. However, extensive communication is needed between the central controller and the controlled units, resulting in high computational complexity [104].

2-1-3 Microgrids in 2050

In this thesis, a hydrogen-based microgrid is considered. Since hydrogen in the energy grid has not yet emerged, a future microgrid is sketched where hydrogen-based distributed energy resources and fuel cell EVs are present. The construction of the future microgrid is based on a national study in the Netherlands that describes the energy infrastructure of the Netherlands in the year 2050 with no emission of greenhouse gases [20], removing natural gas from the energy infrastructure and replacing it with ‘green’ gas or hydrogen. This study proposes four scenarios: regional, national, European, and international management. Each scenario can be used on its own or be combined with others. A combination of these scenarios is used to construct the hydrogen-based microgrid in this thesis. It is assumed that the following four developments will occur before the year 2050 based on [20]:

1. **Active involvement of citizens:** The intrinsic motivation due to the great attention given to the climate problem as well as the pressure from society will contribute to the active involvement of citizens in the energy transition.

2. **Regional management:** More responsibility is laid on local governmental organizations. They are responsible for leading the local energy transition, decreasing their energy consumption, and increasing their local 'green' energy generation.

3. **National management:** Large projects are established to obtain more energy from renewable energy sources, e.g., large wind parks in the North Sea or Photovoltaic (PV) parks in the polder. A large national hydrogen infrastructure will be built to transport the energy from these sources.

4. **European management:** Greenhouse gas taxes will be introduced to increase the use of 'green' energy at European level. This tax concerns all sectors and increases progressively up till 2050.

The impact of these developments on the future microgrid in the year 2050 in the Netherlands, assuming no strong international management actions are taken, are [20]:

- **Residential consumers:** Growth in energy consumption of 1% per year till 2050 on electric devices and the electrification of the thermal energy supply will lead to a rise in the net electricity use of residential buildings, despite the predicted 10% increase in efficient use of electricity. New residential buildings will install heat pumps in combination with local batteries to supply the thermal energy demand. However, in existing districts with poor isolation, chemical energy carriers as hydrogen should be burned to generate thermal energy as well. Therefore, a hybrid heat pump, that combines a heat pump and gas condensing boiler, will be a good alternative to the general heat pump. Due to the extrinsic and intrinsic motivation to be actively involved in the energy transition, people will be more willing to participate in local programs to reduce their emission of greenhouse gases or to save energy. Therefore, the willingness to participate in DR programs is high.

- **Hydrogen:** Large national projects for getting energy from renewable energy sources will lead to a problem of transportation of this energy. The large wind parks in the North Sea are an example of them. This energy will be efficiently stored as hydrogen to be used on the mainland. Countries in the European Union will create large projects to obtain energy from renewable energy sources as well due to greenhouse gas taxes. Therefore, in times of local shortage or abundance in hydrogen, hydrogen can be exported and imported between the European countries. These above developments will result in a large hydrogen infrastructure in Europe that will replace the current natural gas infrastructure to transport the hydrogen.

- **Mobility:** Municipalities will set environmental zones for 'green vehicles' only, especially in the cities. Moreover, more investment will be made for the proper charging infrastructure for EVs. This is in line with the ambition of the people that want to reduce their local emission of greenhouse gases. However, since many will still want to go for the cheapest way of living, the European Union introduces the taxes on greenhouse gases that will motivate them to switch to the 'greener' EVs. The generation of hydrogen and the investments in proper hydrogen infrastructure will result in high penetration of fuel cell EVs in the private transport sector. Nevertheless, more battery EVs will still be present than fuel cell EVs due to their economic advantages.

- **Photovoltaic panels:** PV panels will become cheaper over time, and due to the greenhouse gas taxes, people will only profit more from this investment. Moreover, since people are motivated to shift to EVs, this extra energy demand will make PV panels on their roof even more appealing. These PV panels will reduce their energy costs, and they can take their measurements for reducing the local energy impact.

2-1-4 Objectives in Microgrids

Different control objectives are considered for tertiary control in microgrids depending on a difference in incentives. The main objectives found in the literature are:

- **Discomfort**: Minimizing the daily discomfort of the consumer. Discomfort can be created since devices are operating at different times than the usual consumption pattern or the temperature in the buildings is lowered.
- **Durability**: Minimizing the degradation of different energy resources in the microgrid. By smooth operation as control actions, the degradation can be minimized.
- **Economic**: Minimizing the financial costs of the microgrid. Generally, these costs are based on the import and export of energy with the utility grid. However, maintenance and operational costs are sometimes included as well.
- **Environmental**: Minimizing the emission of greenhouse gases. This can be achieved by maximizing the use of renewable energy sources and, therefore, decreasing the use of plants that emit greenhouse gases.
- **Grid demand**: Minimizing the power flow with the utility grid. The overload of the grid, especially at the peak demand, needs to be reduced. This objective causes a microgrid to be more self-supplied, i.e., more towards islanded mode.

In Table 2-1, an overview is given of the objectives found in the literature. It can be concluded that the economic objective is generally included. Discomfort, durability, environmental, and grid demand objectives are often combined with the economic objective to prevent constructing a distorted picture of the possibilities, e.g., if the grid demand can be improved by 5%, but the costs of the microgrid will double, this will most likely not result in realistic suitable solutions. In this thesis, the focus is on the grid demand of the microgrid by considering the other objectives as well. However, since it is expected that there is no emission of greenhouse gases by microgrids in 2050 [20], the environmental objective is left out.

2-2 Distributed Energy Resources in Microgrids

In this section, the different distributed energy resources that will be integrated into our microgrid are presented. Techno-economic aspects of the different resources are evaluated, and their likelihood of implementation in the future Dutch energy infrastructure is discussed. If not stated otherwise, the investment costs are based on the year 2050, while the lifetime and maintenance costs are based on current values since no accurate predictions are available.

Table 2-1: Overview of the objectives in microgrids found in the literature.

Papers	Discomfort	Durability	Economic	Environmental	Grid demand
[11,17,18,31,37,42] & [65,96,102,107,133]			✓		
[3,87,97,110]	✓		✓		
[36]		✓	✓		
[5,6,68,85,118,135]			✓	✓	
[9,49,144]			✓		✓
[21,129,131]					✓
[78]	✓	✓	✓		
[100]	✓		✓		✓

2-2-1 Energy Storage Systems

An energy storage system captures the energy in the microgrid and converts it to an efficient form of storage, so it can be used at a later time. Large benefits can be obtained by using these energy storage systems in the microgrid, e.g., short-term power supply, providing a framework for integrating renewable energy resources, arbitrage, and grid stability [123]. In the proposed microgrid, no extra thermal storage is considered apart from the integrated thermal storage in the Combined Heat and Power (CHP) plant. In this section, two other energy storage systems that are included in the proposed microgrid are explained, i.e., electrical energy and hydrogen storage.

Electrical Energy Storage

The most common electrical energy storage system is the battery. Other electrical energy storage systems that are often used in microgrids are supercapacitors and superconducting magnetic energy storage. However, these two electrical energy storage systems are mostly used for fast charge and discharge capabilities for voltage and frequency regulations, i.e., primary and secondary control issues in the microgrid [123]. From the different types of batteries [41,91,123], the lithium-ion battery is chosen due to the high energy density of the battery and recommendation made in [41]. The disadvantage of this lithium-ion battery is the high investment costs, as seen in Table 2-2. These investment costs are based on the maximum capacity of the stored energy of the battery. The maintenance costs are given for every kWh of energy exchanged during the operational time while implemented in the microgrid without associated inverter costs [107]. Despite the maintenance costs are relatively low, they can still have a large impact on the economic costs of the microgrid when the battery is intensively used. Since the lifetime of a battery is strongly based on the number of cycles, intenser use of the battery will shorten the lifetime.

Hydrogen Storage

Hydrogen storage is a chemical energy storage system. The main advantage of hydrogen storage is that hydrogen can be stored in fuel tanks with high energy density resulting in compact storage that surpasses the energy density of most batteries [94]. However, hydrogen

Table 2-2: Economic parameters of the battery, electrolyzer, and Photovoltaic (PV) panels [9, 20, 48, 93, 107, 122].

Specifications	Battery	Electrolyzer	PV panels
Lifetime [years]	10	20	40
Investment	300 [€ /kWh]	450 [€ /kW]	330 [€ /kW]
Maintenance [c€ /kWh]	7.84	15	≈ 0

cannot be easily stored due to its low density and needs to be compressed, cooled, or a combination of both. In this thesis, the hydrogen is stored by compression in a reservoir connected to the electrolysis system as proposed in [9]. Therefore, the economic parameters of the hydrogen storage are included in the values for the electrolyzer.

2-2-2 Electrolyzer

Electrolyzers provide a solution to creating hydrogen without the emission of greenhouse gases, in contrast to the current industrial manner where hydrogen is extracted using petroleum fuels [80]. Distributed electrolyzers can be implemented in districts to compromise for the abundance in electrical energy from PV panels and generate hydrogen for the thermal demand of buildings or fuel cell EVs [20]. It is not specified which fuel cells in the electrolyzer will most likely be used in the future microgrid, but an approximation is made of the expected best performing technique. As written in Section 2-2-1, a hydrogen storage tank is integrated into the electrolyzer. In Table 2-2, an overview is given of the economic costs of an electrolyzer with a hydrogen storage tank. In this overview, the investment and maintenance costs are based on the maximum consumed electrical energy to produce hydrogen. Despite the investment of an electrolyzer is relatively high, the electrolyzer can still be profitable due to its long lifespan. The maintenance costs are relatively high, e.g., compared to the maintenance of the battery, but these costs can be compensated by the extra feature the electrolyzer brings to the microgrid to convert electrical energy to hydrogen. This feature is especially beneficial in low consumption hours when there is a lot of electrical energy generation, e.g., by the PV panels. Moreover, it is expected that the maintenance costs will decrease in the future [94]. It is important to mention that the lifetime and maintenance costs are based on the fact that no fast on and off switching of the electrolyzer will occur.

2-2-3 Photovoltaic Panels

The most common renewable energy source that is applied in a microgrid is solar energy using PV panels. Micro wind turbines are sometimes used as well [122], but their presence in the Dutch energy infrastructure is negligible [20]. In many papers, the focus is on introducing PV panels in a microgrid and therefore lowering the environmental and economic costs [67, 122]. Similar reasoning indicates that PV panels will be highly used in distributed energy networks in a microgrid in the Netherlands [20] in 2050. A simple physical model can be used to calculate the generated power from these PV panels [48]:

$$
\begin{aligned}
P_{\mathrm{PV}}(k) &= P_{\mathrm{STC}} \frac{G_{\mathrm{c}}(k)}{G_{\mathrm{STC}}} \left[1 + \alpha \left(T_{\mathrm{c}}(k) - T_{\mathrm{STC}}\right)\right], \quad \text{with} \\
T_{\mathrm{c}}(k) &= T_{\mathrm{amb}}(k) + (\mathrm{NOCT} - 20) \frac{G_{\mathrm{c}}(k)}{800}.
\end{aligned} \tag{2-1}
$$

The nominal power P_{STC}, the global irradiance G_{STC}, and the cell temperature T_{STC} are under standard test conditions (1000 W/m^2 and 25 °C). The air mass coefficient that is commonly used to characterize the performance of solar cells under standardized conditions is assumed to be AM1.5. This is almost universal when characterizing terrestrial PV panels [112]. Furthermore, α is the negative power temperature coefficient, and NOCT the nominal operating cell temperature. These values are commonly given by the manufactures of the PV panels. The global irradiance G_{c} and ambient temperature T_{amb} at time step k are estimated to calculate the cell temperature T_{c} and generated PV power P_{PV}. The above equation describes the ratio between the produced PV power and the different variables, where the total effective area of the PV panel is included in the value of the nominal power to be used.

The maximum possible solar irradiance is strongly related to the latitudinal location, the day of the year, and time of day due to the rotation and revolution of the earth around the sun [89]. Furthermore, the actual obtained solar irradiance is highly stochastic due to external influences that will be further discussed in Section 4-2-1, e.g., cloud covering. The temperature of the solar cells influences the possible electricity production since higher temperatures decrease the effectiveness of the PV panels.

In Table 2-2, an overview is given of the economic costs of PV panels, where the investment costs are based on the installed maximum power that can be generated. The future yearly investment costs of solar panels are low due to the long lifetime of the panels and a strong expected decrease in the investment costs in the coming years [20]. This aligns with the trend that has been noticed that every time the cumulative production of PV panels doubled, the price went down by 25% [50]. The investment costs are based on the installed maximum power that can be generated. Furthermore, the maintenance costs are assumed to be negligible. These economic benefits make the implementation of PV panels in the microgrid almost certain.

2-2-4 Thermal Devices

Two distributed energy sources are used to generate thermal energy within the microgrid, i.e., hybrid heat pumps and micro-CHP plants.

Hybrid Heat Pumps

As discussed in Section 2-1-3, heat pumps will be implemented in new buildings. A heat pump transfers heat energy from a thermal reservoir using electrical energy. The thermal reservoir can be deep in the ground, transferring heat from the warm soil to the colder building. Great energy savings can be achieved by using these heat pumps [35]. However, in the existing buildings, a combination of the boiler and the heat pump will be used due to lack of thermal infrastructure and isolation [20], the hybrid heat pump. Due to the two different sources of energy that can be used to produce heat, hybrid heat pumps have great potential for increasing the energy savings of the microgrid as well as minimizing the grid demand [35, 74].

In Table 2-3, an overview is given of the economic costs of hybrid heat pumps. A distinction is made for the investment and maintenance costs for hybrid heat pumps that run on 'green' gas or hydrogen. The electric maintenance costs are applicable when electrical energy is used to generate thermal energy instead of gas. It is important to notice that the expected investment costs in 2050 will be around 30% higher when hydrogen is used due to the more expensive system that is needed. The current maintenance costs of the fuel cell make a hydrogen-based hybrid heat pump highly unlikely to be integrated into the microgrid. However, considering these maintenance costs will decrease in the coming years [94], these fuel cell-based hybrid heat pumps are implemented. Fast on and off switching of the hybrid heat pump or switching from generating energy from thermal or electrical energy will influence the maintenance costs since start-up and shut-down costs are now integrated into the maintenance costs. Therefore, fast switching between modes needs to be prevented.

Table 2-3: Economic parameters of a hybrid heat pump and micro-Combined Heat and Power (μ-CHP) plant [14, 20, 26, 103, 107, 124, 142].

Specification	**Hybrid heat pump**	**μ-CHP plant**
Lifetime [years]	15	10
Investment gas based [€ /kW]	620	2,500
Investment hydrogen based [€ /kW]	760	2,500
Electric maintenance [c€ /kW]	2	-
Gas boiler maintenance [c€ /kW]	5	-
Internal combustion engine maintenance [c€ /kW]	-	1.5
Fuel cell maintenance [c€ /h]	64	64

Micro-Combined Heat and Power Plant

In conventional electrical power generation, the byproduct heat is usually wasted. In CHP plants, using cogeneration technology as seen in Figure 2-1, the heat is captured and can be used on-site or stored. In a microgrid, smaller variants of the CHP plants are considered, i.e., micro-CHP or μ-CHP plants. These μ-CHP plants are often a collective name of a prime mover technology and a thermal storage system to use the excess thermal energy at a later time. Different prime mover technologies for μ-CHP plants are currently on the market having different total efficiencies and power-to-heat ratios [90]. In this thesis, μ-CHP plants with an internal combustion engine are considered when running on 'green' gas since it is the most well-established technology [65]. Moreover, μ-CHP plants with fuel cells are considered when hydrogen is the energy source. In the current vision of the energy landscape in the Netherlands, μ-CHP plants will not take a significant role [20] due to the lack of thermal infrastructure. However, if the focus will shift to more local self-sustaining microgrids, μ-CHP plants can be implemented to provide better performance. Therefore, μ-CHP plants are considered in this thesis, but only on a relatively small scale compared to the overall energy consumption of the microgrid.

In Table 2-3, an overview is given of the economic costs of the μ-CHP plants. By the absence of data, the investment costs are based on current internal combustion engine investments and representative of both technologies in the future due to the decrease in economic costs for

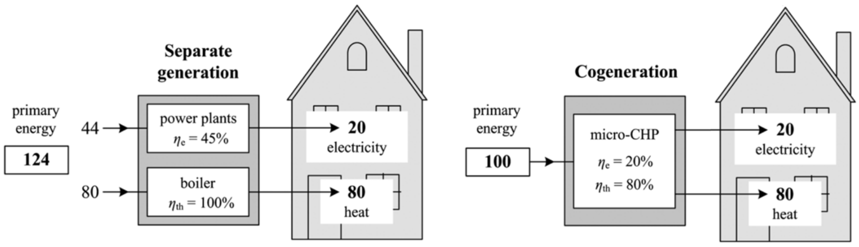

Figure 2-1: Comparison between separate generation and cogeneration [65].

fuel cells [90, 94, 103]. Both prime movers will have acceptable lifetimes of 10 years [26, 103]. The investment costs of the μ-CHP plant are much higher than of the hybrid heat pumps. However, due to the use of cogeneration as well as the integrated thermal storage, economic benefits can be obtained resulting in the repayment of these extra investments. The large difference in maintenance costs for the different technologies in the μ-CHP plant is almost similar to that of the hybrid heat pump. According to similar reasoning as for the hybrid heat pump, both technologies for the prime mover are considered in the microgrid. Fast switching on and off of the μ-CHP plant should be avoided since it causes an increase in maintenance costs and a decrease in the lifetime of the μ-CHP plant [59].

2-3 Electric Vehicles

Combustion engine vehicles will be replaced by EVs in the coming years [20]. In this section, the two different types of EVs are briefly explained that are considered in this thesis, i.e., battery and fuel cell EV. Then, smart EV management strategies are explained and the response of the EVs on these strategies.

2-3-1 Types of Electric Vehicles

The battery EVs are assumed to have lithium-ion batteries due to their higher energy density, longer durability, and higher power density compared to other suitable types of batteries [8]. The fuel cell EV that is powered by hydrogen is assumed to use a proton exchange membrane fuel cell due to their high power density, efficiency, and low operating temperature facilitating the swift start-up of the vehicle compared to other fuel cells [80]. Although battery EVs currently dominate the EV market, fuel cell EVs are expected to obtain a large share in the market [20] because their price will be competitive to that of the battery EVs by the year 2030 [94]. Moreover, fuel cell EVs can be more attractive than battery EVs due to their faster charging time and higher range [94].

2-3-2 Electric Vehicle Management

Smart EV management can be implemented in a microgrid where smart charging or refueling of the EV is done and the EV can be used as an energy storage system or power plant when parked. Due to these strategies, a microgrid can be more flexible and self-sustainable, i.e., less power exchange with the utility grid will be needed [9, 36, 86, 100, 129]. Moreover, the EV can provide energy in times of great energy demand, reducing the peak of electrical energy demand [86]. The three EV management strategies in a microgrid are [86]:

1. **Vehicle-to-home:** In vehicle-to-home, the EV can give power to the home grid in case of high energy prices or when there is a shortage in energy supply. This structure mostly contains a single EV and smart home [86]. This strategy is the most simple strategy but the least flexible since it mostly considers the energy flow of a single household.
2. **Vehicle-to-vehicle:** In this strategy, a group of EVs share their power among each other. Vehicle-to-vehicle is mainly executed in large parking lots. This framework is considered less simple but more flexible in comparison with vehicle-to-home [86].
3. **Vehicle-to-grid:** In vehicle-to-grid, EVs are connected and exchange power to the energy grid [86]. This strategy focuses on large groups of EVs and utilizes smart homes, parking lots, and fast-charging stations for their power exchange. This strategy has a flexible framework and can provide better results than the other strategies [86], but the current low use of EVs and missing infrastructure result in the hard implementation of it [52].

In this study, vehicle-to-grid is chosen since a microgrid is considered with a large amount of EVs and the assumption is made that in a future scenario, the implementation of it will be possible. Moreover, this strategy can provide the most beneficial results on the performance of the microgrid [36, 130].

2-3-3 Response to Electric Vehicle Management

The response to EV management is different for battery and fuel cell EVs. To the best of our knowledge, the difference between those EVs has not been researched yet. Existing literature on the EV management strategies can be found, however, it is applied exclusively to battery EVs [3, 18, 36, 78, 85, 100, 129] or fuel cell EVs [9]. For both types of EVs, promising results were obtained using these strategies, i.e., increase of the performance of the microgrid for economic, environmental, and grid demand objectives.

A consequence of these strategies is the increase in degradation of the battery or fuel cell in the EVs [43,129,141]. Therefore, generating much electrical energy to the microgrid from the EVs as well as the frequent switching on and off of the EV should be prevented. Furthermore, when the EVs are in stationary mode, i.e., when they can be used for generating electricity, they only operate at partial load. For the battery EV, the most important reason for that is to prevent the accelerated degradation of the battery due to intensive usage [129]. For fuel cell EVs, to operate at partial load is specifically necessary to guarantee that the on-board utilities of the vehicle will still be able to regulate the fuel cell's temperature [9].

Lastly, the use of these management strategies results in fear of the users that the EV will not be sufficiently charged upon departure, i.e., range anxiety [52]. On the other hand, assuring that the EVs will be fully charged upon departure will increase the conservatism in the microgrid, resulting in less performance for certain objectives, e.g., for the economic and grid demand objective. Therefore, constraints are set assuring enough electrical energy or hydrogen will be present in the EV upon departure.

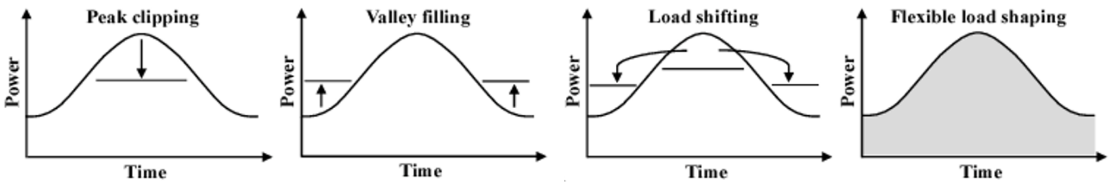

Figure 2-2: Different changes in the consumption pattern due to demand response programs [81].

2-4 Demand Response

Since the introduction of renewable energy sources in the microgrid, the power supply in microgrids has lost some of its flexibility due to the stochastic nature of these sources. For balancing the generation and consumption of energy, the focus shifted more to controlling the loads in the microgrid, rather than controlling the energy generation [105]. DR programs can be used to control these loads, i.e., the energy demand of the buildings, and change the consumption pattern of the consumers. This change in the consumption pattern is realized in different ways, as shown in Figure 2-2. Due to the participation in a DR program, the peak of energy demand can be lowered, more consumption can be insinuated during low consumption times, loads can be shifted, and flexible load shaping can be realized [16, 69, 72]. The energy demand of buildings is divided into three different categories to distinguish the possibilities of control for these loads. These categories, whereof the latter two can be controlled using a DR program, are [98, 115, 135]:

1. **Critical loads:** Loads that have to be met at all times, e.g., refrigerator.
2. **Curtailable loads:** Loads that can temporarily be lowered or switched off, e.g., heating of the building.
3. **Rescheduable loads:** Loads that can be shifted in time with two different subcategories:
   (a) **Uninterruptible loads:** Loads that have to complete their task when started, e.g., dishwasher.
   (b) **Interruptible loads:** Loads that can be interrupted when started, e.g., charging of an EV.

How the consumption pattern needs to change depends on the different objectives for the microgrid. For DR programs in microgrids, three general objectives are most common [16]: discomfort, economic, and grid demand. Besides, combinations of these objectives are used as a single objective to realize desired results [16]. As concluded in Section 2-1-4, these objectives will all be considered in the microgrid.

2-4-1 Demand Response Programs

Different DR programs can be implemented to control the loads in the microgrid and can be classified into two categories: price-based programs and incentive-based programs. In the first category, the price of energy consumption for the consumers alters over time that influences the consumption pattern. Therefore, utilities create an enticement to reduce electrical energy consumption at a particular time frame. In the second category, consumers have to change their consumption patterns to be awarded with certain incentives. Thus, the utilities pay the consumers for their participation in certain programs [1,2,69,119]. The incentive-based direct load control is chosen as a DR program since it can provide good performance on lowering the peak of electrical energy transfer and is suitable for the low consumption consumers considered in the microgrid [2]. In this program, the utility has a degree of control over the energy demand of the consumer. It must be noted that the implementation of DR programs is at the expense of comfort and certain investment costs [4, 69, 127], of which the investment costs are not included in this study.

2-4-2 Consumer Response

Commercial and residential consumers react differently to DR programs and their incentives. Residential consumers are more responsive to DR programs because a great part of their load is curtailable or rescheduable [69, 96]. However, it is important to consider the preferences of residential consumers, e.g., not turning on the washing machine in the middle of the night due to noise pollution. The desire of commercial consumers to respond to DR programs highly depends on the share of their electricity bill in their total costs and their discomfort costs for participation in DR programs [69]. The commercial consumers respond less to DR programs than residential consumers, despite their higher energy consumption [96]. Due to the industrial nature of commercial consumers, they are not able to reschedule many loads [145], i.e., due to the fixed hours where many commercial consumers operate, there is low flexibility, and the available incentives to reschedule their loads are not strong [69]. Due to the relatively little response and strong economic incentives needed for commercial consumers, it is chosen that only residential consumers will participate in the DR program.

2-5 Conclusions

In this chapter, the electric and thermal microgrid is presented and discussed. A future hydrogen-based microgrid is constructed for the year 2050. The different distributed energy resources in this microgrid are discussed. Furthermore, the role of EVs in the microgrid is analyzed and it is concluded to use vehicle-to-grid as a smart EV management strategy in the microgrid. It is chosen to implement direct load control as a DR program for the residential consumers in the microgrid. How these distributed energy resources and smart strategies will function in the microgrid is further explained in Chapter 3.

Chapter 3

Microgrid Modelling

A hybrid model is used to describe the dynamics of the microgrid. In this hybrid model, there is an interaction between continuous and discrete dynamics of the system, e.g., the different charging and discharging modes having their own dynamics for a battery. The model is rewritten to a mixed logical dynamical model to tackle the nonlinearities in the hybrid model, as in [9, 65, 107]. In a mixed logical dynamical model, the system is described by linear dynamic equations subject to linear mixed-integer inequalities, i.e., inequalities involving both continuous and binary variables [19]. Due to the fact that no nonlinear mixed-integer inequalities are present in the system anymore, the computational complexity of the problem is generally decreased.

In this chapter, the different components in the microgrid and the connection to the utility grid are firstly described. Secondly, the stochastic processes present in the microgrid are given and it is described how they will affect the modelled microgrid. Thirdly, the modelling of the Demand Response (DR) program is presented. Lastly, different constraints are explained that are modelled in the microgrid. Note that in this chapter, the modelling of the microgrid is written in piecewise affine form for the sake of readability. However, in the actual implementation, a mixed logic dynamical model has been used.

3-1 Components in the Microgrid

In this section, the models of the different components in the microgrid are given. The dynamics of the components are given and it is explained how certain values of the dynamics are determined, e.g., travel schedule for the Electric Vehicle (EV). Moreover, the connection to the utility grid is modelled. In Appendix A, a descriptive overview is given of rewriting the presented piecewise affine models to mixed logic dynamical models.

3-1-1 Energy Storage Systems

Two energy storage systems in the microgrid are modelled besides the integrated thermal storage in the μ-Combined Heat and Power (CHP) plant, i.e., the battery and hydrogen storage system. The distinction between these two systems is that for the hydrogen storage system, the charging and discharging efficiency are assumed to be 100% since the efficiencies are already incorporated in the electrolyzer. Therefore, the modelling is slightly different as will be explained in this subsection.

Battery

The dynamics to determine the stored energy in a battery x_{bat} at the next time step $k+1$, depend on the different mode the battery is in, i.e., the battery is charging or discharging. If the binary variable $\delta_{\text{bat}}(k) = 1$, the battery is charging and if $\delta_{\text{bat}}(k) = 0$, the battery is discharging. Therefore, the battery can be described by the following equation:

$$x_{\text{bat}}(k+1) = \begin{cases} x_{\text{bat}}(k) + \eta_{\text{bat}}^{\text{c}} u_{\text{bat}}(k), & \text{if } \delta_{\text{bat}}(k) = 1 \\ x_{\text{bat}}(k) + \frac{1}{\eta_{\text{bat}}^{\text{d}}} u_{\text{bat}}(k), & \text{if } \delta_{\text{bat}}(k) = 0 \end{cases},$$

where u_{bat} is the exchanged electrical energy, $\eta_{\text{bat}}^{\text{c}}$ the charging efficiency, and $\eta_{\text{bat}}^{\text{d}}$ the discharging efficiency. The state of the battery and the electrical energy exchanged to or from the battery cannot exceed their minimal and maximal bounds, i.e., $\underline{x}_{\text{bat}} \leq x_{\text{bat}}(k) \leq \overline{x}_{\text{bat}}$ and $\underline{u}_{\text{bat}} \leq u_{\text{bat}}(k) \leq \overline{u}_{\text{bat}}$. Moreover, an extra constraint on the energy transfer is set to distinguish if energy is coming in or leaving the battery, i.e., if the battery is in charging or discharging mode. Therefore, the constraint $\delta_{\text{bat}}(k) = 1 \iff u_{\text{bat}}(k) \geq 0$ is added.

Hydrogen Storage Tank

Since no charging and discharging efficiencies are considered in the hydrogen storage tank, the model is much simpler compared to that of the battery. No logic binary variables need to be used to describe the dynamics for the amount of hydrogen stored in the tank x_{hst}:

$$x_{\text{hst}}(k+1) = x_{\text{hst}}(k) + u_{\text{hst}}(k),$$

where u_{hst} is the exchanged hydrogen. Similar to the battery, bounds are set on the amount of stored and exchanged hydrogen, i.e., $\underline{x}_{\text{hst}} \leq x_{\text{hst}} \leq \overline{x}_{\text{hst}}$ and $\underline{u}_{\text{hst}} \leq u_{\text{hst}} \leq \overline{u}_{\text{hst}}$.

3-1-2 Electrolyzer

The electrolyzer converts consumed electrical energy u_{elc} into hydrogen H_{elc} when the system is on. When the system is off, the electrolyzer will not produce any hydrogen. Therefore, using the logic variable δ_{elc}, the system at time step k can be described as on or off, i.e., $\delta_{\text{elc}}(k) = 1$ or $\delta_{\text{elc}}(k) = 0$, respectively. The electrolyzer can be written as

$$H_{\text{elc}}(k) = \begin{cases} \alpha_{\text{elc}} u_{\text{elc}}(k), & \text{if } \delta_{\text{elc}}(k) = 1 \\ 0, & \text{if } \delta_{\text{elc}}(k) = 0 \end{cases},$$

where α_{elc} is the model parameter related to the specifications of the system as proposed in [9]. The amount of electrical energy that is consumed is constrained by $0 \leq u_{\text{elc}}(k) \leq \overline{u}_{\text{elc}}$. If the electrolyzer is turned off, the consumed electrical energy needs to be zero, i.e., $\delta_{\text{elc}}(k) = 0 \implies u_{\text{elc}}(k) = 0$.

3-1-3 Hybrid Heat Pump

The hybrid heat pump produces thermal energy Q_{HP} by consuming electrical energy $u_{\mathrm{HP}}^{\mathrm{el}}$, gas $u_{\mathrm{HP}}^{\mathrm{gas}}$, or hydrogen $u_{\mathrm{HP}}^{\mathrm{hyd}}$, as explained in Section 2-2-4. Since the model is similar for gas and hydrogen, it is presented as a hybrid heat pump that consumes electrical energy and gas. Two logic binary variables are introduced to represent if at time step k the hybrid heat pump is running on electrical energy $\left(\delta_{\mathrm{HP}}^{\mathrm{el}}(k)=1\right)$, on thermal energy $(\delta_{\mathrm{HP}}^{\mathrm{gas}}(k)=1)$, or if the system is off $\left(\delta_{\mathrm{HP}}^{\mathrm{el}}(k)=\delta_{\mathrm{HP}}^{\mathrm{gas}}(k)=0\right)$. Therefore, the hybrid heat pump can be modelled as

$$Q_{\mathrm{HP}}(k)=\begin{cases}\eta_{\mathrm{HP}}^{\mathrm{el}}u_{\mathrm{HP}}^{\mathrm{el}}(k), & \text{if } \delta_{\mathrm{HP}}^{\mathrm{el}}(k)=1 \ \wedge \ \delta_{\mathrm{HP}}^{\mathrm{gas}}(k)=0\\ \eta_{\mathrm{HP}}^{\mathrm{gas}}u_{\mathrm{HP}}^{\mathrm{gas}}(k), & \text{if } \delta_{\mathrm{HP}}^{\mathrm{el}}(k)=0 \ \wedge \ \delta_{\mathrm{HP}}^{\mathrm{gas}}(k)=1\\ 0, & \text{if } \delta_{\mathrm{HP}}^{\mathrm{el}}(k)=\delta_{\mathrm{HP}}^{\mathrm{gas}}(k)=0\end{cases},$$

where $\eta_{\mathrm{HP}}^{\mathrm{el}}$ is the electrical efficiency and $\eta_{\mathrm{HP}}^{\mathrm{gas}}$ the efficiency of burning gases such as hydrogen. The maximal consumed energy is constrained by the equations $0 \leq u_{\mathrm{HP}}^{\mathrm{el}}(k) \leq \overline{u}_{\mathrm{HP}}^{\mathrm{el}}$ and $0 \leq u_{\mathrm{HP}}^{\mathrm{gas}}(k) \leq \overline{u}_{\mathrm{HP}}^{\mathrm{gas}}$. The consumption of energy, electrical or gas, will be zero if that mode is off, i.e., $\delta_{\mathrm{HP}}^{\mathrm{el}}(k)=0 \Longrightarrow u_{\mathrm{HP}}^{\mathrm{el}}(k)=0$ and $\delta_{\mathrm{HP}}^{\mathrm{gas}}(k)=0 \Longrightarrow u_{\mathrm{HP}}^{\mathrm{gas}}(k)=0$. Since the hybrid heat pump will not consume electrical energy and uses the boiler at simultaneous time, a constraint is added that the logical binary variables cannot both be equal to one at time step k, i.e., $\delta_{\mathrm{HP}}^{\mathrm{el}}(k)+\delta_{\mathrm{HP}}^{\mathrm{gas}}(k) \leq 1$.

3-1-4 Micro-Combined Heat and Power Plant

The μ-CHP plant produces electrical P_{CHP} and thermal energy Q_{CHP} simultaneously. Moreover, a thermal storage unit is integrated with an amount of energy stored x_{CHP}. The production of energy depends on the amount of consumed gas or hydrogen u_{CHP}. Similarly to the hybrid heat pump, two logic binary variables are introduced to indicate whether the $\mu-$CHP system is turned on or off, i.e., $\delta_{\mathrm{CHP}}(k)=1$ or $\delta_{\mathrm{CHP}}(k)=0$ at time step k, respectively. The system of a μ-CHP plant can therefore be described by

$$\begin{aligned}P_{\mathrm{CHP}}(k)&=\begin{cases}\eta_{\mathrm{CHP}}^{\mathrm{el}}u_{\mathrm{CHP}}(k), & \text{if } \delta_{\mathrm{CHP}}(k)=1\\ 0, & \text{if } \delta_{\mathrm{CHP}}(k)=0\end{cases}\\ x_{\mathrm{CHP}}(k+1)&=\begin{cases}x_{\mathrm{CHP}}(k)+\eta_{\mathrm{CHP}}^{\mathrm{th}}u_{\mathrm{CHP}}(k)-Q_{\mathrm{CHP}}(k), & \text{if } \delta_{\mathrm{CHP}}(k)=1\\ x_{\mathrm{CHP}}(k)-Q_{\mathrm{CHP}}(k), & \text{if } \delta_{\mathrm{CHP}}(k)=0\end{cases}\end{aligned},$$

where $\eta_{\mathrm{CHP}}^{\mathrm{el}}$ and $\eta_{\mathrm{CHP}}^{\mathrm{th}}$ are the electrical and thermal efficiency of the plant. The consumed energy and stored energy are bounded by $0 \leq u_{\mathrm{CHP}}(k) \leq \overline{u}_{\mathrm{CHP}}$ and $\underline{x}_{\mathrm{CHP}} \leq x_{\mathrm{CHP}}(k) \leq \overline{x}_{\mathrm{CHP}}$. The minimum stored thermal energy needs to be higher than a determined threshold $\underline{x}_{\mathrm{CHP}} > 0$. Furthermore, the consumed energy is zero if the system is turned off at time step k, i.e., $u_{\mathrm{CHP}}(k)=0 \Longleftrightarrow \delta_{\mathrm{CHP}}(k)=0$.

3-1-5 Electric Vehicles

The dynamics of the two different EVs are modelled based on the model of a fuel cell EV described in [9]. Their main underlying difference in dynamics is the conversion of hydrogen to electrical energy in the fuel cell EV. Moreover, the transportation schedules and the energy costs per trip of the EVs in the microgrid are presented.

Battery Electric Vehicle

The battery EV dynamics are based on the dynamics of the battery but include more modes since the EV can be in transportation. The EV can be refilled with electrical energy, generate electrical energy to the microgrid, be in transportation, and arrive after its trip. The amount of electrical energy stored in the battery EV x_{BEV} is based on the electrical energy u_{BEV} transferred and the energy costs of a trip h_{BEV}. The model of the battery EV is written as

$$x_{\mathrm{BEV}}(k+1) = \begin{cases} x_{\mathrm{BEV}}(k) + \eta^{\mathrm{c}}_{\mathrm{BEV}} u_{\mathrm{BEV}}(k), & \text{if refilling} \\ x_{\mathrm{BEV}}(k), & \text{if no generation} \\ x_{\mathrm{BEV}}(k) + \frac{1}{\eta^{\mathrm{d}}_{\mathrm{BEV}}} u_{\mathrm{BEV}}(k), & \text{if generation} \\ x_{\mathrm{BEV}}(k), & \text{if transportation} \\ x_{\mathrm{BEV}}(k) - h_{\mathrm{BEV}}(k), & \text{if arrival} \end{cases}, \tag{3-1}$$

where $\eta^{\mathrm{c}}_{\mathrm{BEV}}$ and $\eta^{\mathrm{d}}_{\mathrm{BEV}}$ are the charging and discharging efficiencies, respectively. Constraints are set on the total energy storage of the battery $\underline{x}_{\mathrm{BEV}} \leq x_{\mathrm{BEV}}(k) \leq \overline{x}_{\mathrm{BEV}}$ as well as on the transferred energy $\underline{u}_{\mathrm{BEV}} \leq u_{\mathrm{BEV}}(k) \leq \overline{u}_{\mathrm{BEV}}$. The value of the transferred energy is managed in a similar way as in the battery: $u_{\mathrm{BEV}}(k) \geq 0 \iff$ refilling mode, and $u_{\mathrm{BEV}}(k) < 0 \iff$ generation mode. Note that, as explained in Section 2-3-3, the charging and discharging of the EV will be done at partial load. Furthermore, constraints are introduced to prevent the battery EV from being in different modes simultaneously.

Fuel Cell Electric Vehicle

The fuel cell EV is modelled in similar way as the battery EV to estimate the amount of hydrogen x_{FEV} in the tank. However, a difference is that the refilled energy $u^{\mathrm{hyd}}_{\mathrm{FEV}}$ and energy costs of a trip h_{FEV} are expressed in hydrogen, while in generation mode electrical energy $u^{\mathrm{el}}_{\mathrm{FEV}}$ is produced. Furthermore, the dynamics of the battery in the battery EV are replaced by the dynamics of a fuel cell to get the model for a fuel cell EV [9]:

$$x_{\mathrm{FEV}}(k+1) = \begin{cases} x_{\mathrm{FEV}}(k) + u^{\mathrm{hyd}}_{\mathrm{FEV}}(k), & \text{if refilling} \\ x_{\mathrm{FEV}}(k), & \text{if no generation} \\ x_{\mathrm{FEV}}(k) - \left(\alpha_{\mathrm{FEV}} u^{\mathrm{el}}_{\mathrm{FEV}}(k) + \beta_{\mathrm{FEV}}\right), & \text{if generation} \\ x_{\mathrm{FEV}}(k), & \text{if transportation} \\ x_{\mathrm{FEV}}(k) - h_{\mathrm{FEV}}(k), & \text{if arrival} \end{cases},$$

where α_{FEV} and β_{FEV} are the model parameters of the fuel cell in the EV. These model parameters are based on the specifications of the fuel stack in the EV [10, 113]. Constraints are set on the hydrogen storage, transferred hydrogen, and the electrical energy transferred, i.e., $\underline{x}_{\mathrm{FEV}} \leq x_{\mathrm{FEV}}(k) \leq \overline{x}_{\mathrm{FEV}}$, $0 \leq u^{\mathrm{hyd}}_{\mathrm{FEV}}(k) \leq \overline{u}^{\mathrm{hyd}}_{\mathrm{FEV}}$, and $0 \leq u^{\mathrm{el}}_{\mathrm{FEV}}(k) \leq \overline{u}^{\mathrm{el}}_{\mathrm{FEV}}$, respectively. The maximum generated electrical energy is based on the fact the fuel cell will operate at partial load when in generation mode. Furthermore, constraints are introduced to prevent the fuel cell EV from being in different modes simultaneously.

Trip Characteristics

A stochastic part for the EV modelling is the trip pattern as well as the fuel costs of these trips. Assumptions need to be made to model these stochastic processes. For real data on the arrival and departure time of EVs, a data set of charging patterns of EVs in the Netherlands form ElaadNL has been obtained. These charging sessions can be clustered into three groups by the method described in [111]: charge-near-home, park-to-charge, and charge-near work. In this method, the charging sessions are clustered based on the duration of charging and the time of the day. Furthermore, it is concluded in [111] that the arrivals are earlier in the summer and spring than in the autumn and winter. Moreover, people stay out of home longer during weekends resulting in later arrival times compared to the weekdays. The obtained data set is clustered and the charge-near-home data are used to describe different arrival and departure time patterns for the EVs in the microgrid.

The energy costs per trip are calculated based on the average kilometres driven per year. The yearly average driven distance per vehicle in the Netherlands was 12,984 kilometres in 2018 [33]. In the obtained data set, the charging frequency of vehicles was around one session a day. Therefore, it is calculated that per trip an average of 35.57 kilometres is driven. In this reasoning, it is assumed that the driving behaviour will not change when switching from internal combustion engine vehicles to EVs. From [111], it is estimated that 54.4% of the charging sessions are charge-near-home sessions. Therefore, not all the energy for the EV will be refilled in the microgrid, but also at work or in public charging poles elsewhere. It is assumed that 19.35 kilometres worth of fuel is the average energy cost per trip for the EVs in the microgrid. Since different vehicles will have different driving patterns, a multivariate random Gaussian sampling is used to obtain different trip costs for different EVs.

Important assumptions are made to describe the above trip characteristics. It is assumed that the arrival and departure times are known and that every single EV has its unique constant driven kilometres per trip. The stochastic properties of the trip characteristics are therefore neglected and the model is simplified. This will result in less realistic performance of the microgrid. However, since the large trips on average are home to work distances that are on daily basis and similar for most weekdays, the reality is closely approached. Moreover, the smaller trips, e.g., to the local grocery store, will not take long and do not use much fuel. Therefore, their influence on the performance of the microgrid will be relatively small. In conclusion, this assumption simplifies the model but it is expected that it will not lead to a radical different performance of the microgrid. A recommendation in future work is to do include the stochastic behaviour of the EVs if sufficient data are available, as is proposed in Section 7-3.

3-1-6 Utility Grid

The microgrid remains connected to the utility grid at all times. Therefore, it is able to import or export electrical energy, hydrogen, or 'green' gas at a certain price. To model the utility grid, a binary logic variable δ_{UG} is introduced to determine if energy u_{UG} is bought ($\delta_{\mathrm{UG}}(k) = 1$) or sold ($\delta_{\mathrm{UG}}(k) = 0$) to the utility grid at time step k with $u_{\mathrm{UG}}(k) \geq 0 \iff \delta_{\mathrm{UG}}(k) = 1$. The economic costs C_{UG} for the microgrid, from the imported and exported energy with the utility grid, are modelled as

$$C_{\mathrm{UG}}(k) = \begin{cases} c^{\mathrm{P}}(k)u_{\mathrm{UG}}(k), & \text{if } \delta_{\mathrm{UG}}(k) = 1 \\ c^{\mathrm{S}}(k)u_{\mathrm{UG}}(k), & \text{if } \delta_{\mathrm{UG}}(k) = 0 \end{cases},$$

where $c^{\mathrm{P}}(k)$ and $c^{\mathrm{S}}(k)$ are the purchase and sale price of energy at time step k, respectively. The transferred energy is constrained by the maximum allowed energy transfer between the microgrid and the utility grid, i.e., $\underline{u}_{\mathrm{UG}}(k) \leq u_{\mathrm{UG}}(k) \leq \overline{u}_{\mathrm{UG}}(k)$.

Energy Price

For the purchase and sale price of electricity, a time-of-use price is computed. The electrical energy price varies greatly throughout the day and shows strong weekly patterns. Therefore, a weekly import price is computed for every time step during the week based on the national data of the Netherlands from Entsoe of previous years [45]. A 20% increase in this price is added due to rising electrical energy price [20]. The purchasing price of hydrogen and 'green' gas is fixed throughout the day based on the data of [20]. The sale price of energy is assumed to be equal to the net import price, i.e., excluding taxes and transportation costs. The ratio of this net import price to the import price is based on the data of [66].

3-2 Stochastic Processes

Different stochastic processes are present in the microgrid and affecting the system dynamics as external disturbances. Their behaviour has to be modelled and identified to account for these external disturbances. In the microgrid the following stochastic processes are present:

1. Electrical energy demand of the residential buildings (P_{res}).
2. Thermal energy demand of the residential buildings (Q_{res}).
3. Electrical energy demand of the small commercial buildings (P_{com}).
4. Thermal energy demand of the small commercial buildings (Q_{com}).
5. Electrical power generation of the Photovoltaic (PV) panels (P_{PV}).

Forecasting models are needed to identify the behaviour of these stochastic processes. However, these forecasting models contain errors that have to be considered in the model. Therefore, at every time step a difference is present between the forecasted and real values of the stochastic processes. Different control strategies that will be covered in Chapter 5 will consider these errors and their uncertainty. A low level controller needs to be implemented to compensate for this difference in forecasted and real values of the stochastic processes. In the model of the microgrid, the actual value of the stochastic process is formulated as a summation of the point forecast $(\hat{\cdot})$ and its error $(\tilde{\cdot})$ as

$$\begin{aligned} P_{\text{res}} &= \hat{P}_{\text{res}} + \tilde{P}_{\text{res}}, \\ Q_{\text{res}} &= \hat{Q}_{\text{res}} + \tilde{Q}_{\text{res}}, \\ P_{\text{com}} &= \hat{P}_{\text{com}} + \tilde{P}_{\text{com}}, \\ Q_{\text{com}} &= \hat{Q}_{\text{com}} + \tilde{Q}_{\text{com}}, \\ \text{and } P_{\text{PV}} &= \hat{P}_{\text{PV}} + \tilde{P}_{\text{PV}}. \end{aligned}$$

The detailed behaviour of these stochastic processes and how they are forecasted are discussed in Chapter 4.

3-3 Demand Response

The electrical and thermal demand of the residential buildings will participate in the DR program direct load control. Therefore, the utility has a degree of control over a part of the residential load. This section presents how the curtailed and rescheduled load is modelled.

3-3-1 Curtailable Load

Curtailable loads D_{c} can temporarily be lowered or switched off. The variable $\beta_{\text{c}}(k)$ with $0 \leq \beta_{\text{c}}(k) \leq 1$ shows the percentage of preferred power level to be curtailed at time step k. Thus, if no curtailment is allowed, $\beta_{\text{c}}(k) = 0$ at time step k [107]. In the model it is assumed that a part of the thermal energy can only be lowered against discomfort costs, i.e., that the temperature in the building becomes lower than preferred, or higher in hot climates. The curtailed load Q_{c} is expressed by

$$Q_{\text{c}}(k) = \beta_{\text{c}}(k) D_{\text{c}}(k).$$

3-3-2 Rescheduable Load

Rescheduable loads D_{r} can be shifted in time, but in contrast to the curtailable loads, they have to be fulfilled after a certain time. These loads are divided, as explained in Section 2-4, into two subcategories: uninterruptible and interruptible loads. In this thesis, only uninterruptible loads are considered. However, the smart charging of EVs due to the implementation of the EV management strategies can be considered as an interruptible load in the microgrid.

Fractions of the electrical and thermal energy are considered to be rescheduable. The only electric devices that are considered to be rescheduable are dishwashers. These devices are chosen due to their regular consumption pattern and their time of use. Dishwashers are used in the evening where, in general, large peaks of electrical energy demand are visible. Similar as to the curtailable load, a variable $\beta_{\text{r}}(k)$ with $0 \leq \beta_{\text{r}}(k) \leq 1$ is introduced to indicate the percentage of preferred level to be rescheduled at time step k. This results in the equation of rescheduled load for electrical and thermal energy demand as

$$P_{\text{r}}(k) = \beta_{\text{r}}^{\text{el}}(k) D_{\text{r}}^{\text{el}}(k) \text{ and } Q_{\text{r}}(k) = \beta_{\text{r}}^{\text{th}}(k) D_{\text{r}}^{\text{th}}(k),$$

where P_r and Q_r are the rescheduled electrical and thermal load, respectively. These rescheduled loads have to be consumed at other time steps. Since these loads are uninterruptible ones, they have to be satisfied in consecutive time steps. The amount of load that is consumed at each time step is a constant denoted as $D_\mathrm{rc}^\mathrm{el}$ or $D_\mathrm{rc}^\mathrm{th}$ for the electrical and thermal energy, respectively. A binary variable δ_rc is introduced to determine if the rescheduled load is consumed ($\delta_\mathrm{rc}(k) = 1$) or not ($\delta_\mathrm{rc}(k) = 0$) at time step k. This leads to a constraint of the consumed rescheduled load per time step as

$$P_\mathrm{rc}(k) = D_\mathrm{rc}^\mathrm{el}\delta_\mathrm{rc}^\mathrm{el}(k) \text{ and } Q_\mathrm{rc}(k) = D_\mathrm{rc}^\mathrm{th}\delta_\mathrm{rc}^\mathrm{th}(k),$$

where $P_\mathrm{rc}(k)$ and $Q_\mathrm{rc}(k)$ are the consumed electrical and thermal energy at time step k. It is assured that the energy is uninterruptedly consumed by the constraints:

$$\begin{aligned}
\delta_\mathrm{rc}^\mathrm{el}(k) - \delta_\mathrm{rc}^\mathrm{el}(k-1) &\leq \delta_\mathrm{rc}^\mathrm{el}(\tau), \quad \text{with } \tau = k+1, \ldots, k + T_\mathrm{rc}^\mathrm{el} - 1, \\
\delta_\mathrm{rc}^\mathrm{th}(k) - \delta_\mathrm{rc}^\mathrm{th}(k-1) &\leq \delta_\mathrm{rc}^\mathrm{th}(\tau), \quad \text{with } \tau = k+1, \ldots, k + T_\mathrm{rc}^\mathrm{th} - 1,
\end{aligned}$$

where $T_\mathrm{rc}^\mathrm{el}$ and $T_\mathrm{rc}^\mathrm{th}$ are the time needed for the unsatisfied rescheduled electrical l_r^el and thermal load l_r^th to be fully consumed, respectively. The unsatisfied rescheduled loads are updated at each time step to estimate how much electrical and thermal load needs to be consumed as

$$\begin{aligned}
l_\mathrm{r}^\mathrm{el}(k) &= \sum_{i=1}^{k-1} P_\mathrm{r}(i) - \sum_{i=1}^{k} P_\mathrm{rc}(i), \\
l_\mathrm{r}^\mathrm{th}(k) &= \sum_{i=1}^{k-1} Q_\mathrm{r}(i) - \sum_{i=1}^{k} Q_\mathrm{rc}(i).
\end{aligned}$$

The rescheduled load has to be consumed before reaching a defined time step F. For example, a dishwasher can be rescheduled in the evening to a later time step, but one wants that the program is done by the coming morning. Therefore, no unsatisfied load should be present at that time step, i.e., $l_\mathrm{r}^\mathrm{el}(F^\mathrm{el}) = 0$ and $l_\mathrm{r}^\mathrm{th}(F^\mathrm{th}) = 0$.

3-4 Constraints

In the microgrid, several main constraints are introduced besides the more practical ones explained in previous sections. To prevent the fast degradation of multiple devices in the microgrid a constraint is introduced. Furthermore, to tackle the problem of range anxiety introduced by smart EV management, constraints are set on the storage of fuel in the EV. Lastly, the power balance in the system is presented that guarantees the energy saturation in the microgrid.

3-4-1 Degradation

To tackle the problem of fast degradation for multiple components in the microgrid, a constraint is added as introduced in [107]. A constraint is set on the minimum time the system is turned on T_{ON} or off T_{OFF}. In this constraint, binary logic variables are introduced to define if the system is on ($\delta = 1$) or off ($\delta = 0$). Note that in the previous section, these modes were respectively the charging and discharging mode of the battery and battery EV. The constraint is expressed without resorting to any additional variable as

$$\begin{aligned} &\delta(k) - \delta(k-1) \leq \delta(\tau), && \text{with } \tau = k+1, \ldots, k + T_{\mathrm{ON}} - 1, \\ &\delta(k-1) - \delta(k) \leq 1 - \delta(\tau), && \text{with } \tau = k+1, \ldots, k + T_{\mathrm{OFF}} - 1. \end{aligned} \tag{3-2}$$

The first line in this equation ensures the system satisfies the minimal 'on time' and the second line the minimal 'off time'. This constraint is used to prevent fast switching between modes in the battery, electrolyzer, $\mu-$CHP plant, hybrid heat pump, and both types of EVs. For the hybrid heat pumps, both for thermal energy generated by electrical energy consumption and by gas, the constraint is added. Moreover, for the EVs, this constraint is introduced for both the modes refilling and generation.

3-4-2 Range Anxiety

The use of EV management results in fear of the users that the EV will not be sufficiently charged upon departure, i.e., range anxiety [52]. In the model, it is chosen that it is not necessary that the EV should be fully charged upon departure since this will lead to conservative results and the exact departure time is generally not known in real life. However, the following constraint is introduced to ensure a certain state of charge $\underline{x}^{\mathrm{t}}_{\mathrm{EV}}$ is reached when the vehicle turns into transportation mode $\left(\delta^{\mathrm{t}}_{\mathrm{EV}} = 1\right)$:

$$x_{\mathrm{EV}}(k) \geq \underline{x}^{\mathrm{t}}_{\mathrm{EV}} \delta^{\mathrm{t}}_{\mathrm{EV}}(k),$$

where $x_{\mathrm{EV}}(k)$ is the fuel storage of the EV at time step k. Since not all trips are known beforehand, one wants to ensure as well that enough fuel is in the EV before the EV will be generating electricity to the microgrid. Therefore, another constraint is added that assures a minimal state of charge $\underline{x}^{\mathrm{g}}_{\mathrm{EV}}$ in the EV is set before the EV can be in generation mode ($\delta^{\mathrm{g}}_{\mathrm{EV}} = 1$):

$$x_{\mathrm{EV}}(k) \geq \underline{x}^{\mathrm{g}}_{\mathrm{EV}} \delta^{\mathrm{g}}_{\mathrm{EV}}(k),$$

where $\underline{x}^{\mathrm{g}}_{\mathrm{EV}} < \underline{x}^{\mathrm{t}}_{\mathrm{EV}}$.

3-4-3 Power Balance

The different types of energies in the microgrid have to be balanced at every time step. A constant ratio between energy and power at each time interval is assumed due to the constant sampling time. In the microgrid, different types of energies are considered: electrical energy, thermal energy, hydrogen, and 'green' gas. The power balances are given using the variables introduced in the previous sections as

$$
\begin{aligned}
&u_{\mathrm{UG}}^{\mathrm{el}}(k)+P_{\mathrm{PV}}(k)+P_{\mathrm{CHP}}(k)+u_{\mathrm{FEV}}^{\mathrm{el}}(k)=P_{\mathrm{res}}(k)+P_{\mathrm{com}}(k)+P_{\mathrm{rc}}(k)-P_{\mathrm{r}}(k)\\
&+u_{\mathrm{bat}}(k)+u_{\mathrm{BEV}}(k)+u_{\mathrm{elc}}(k)+u_{\mathrm{HP}}^{\mathrm{el}}(k),\\
&Q_{\mathrm{CHP}}(k)+Q_{\mathrm{HP}}(k)=Q_{\mathrm{res}}(k)+Q_{\mathrm{com}}(k)+Q_{\mathrm{rc}}(k)-Q_{\mathrm{r}}(k)-Q_{\mathrm{c}}(k),\\
&u_{\mathrm{UG}}^{\mathrm{gas}}(k)=u_{\mathrm{CHP}}^{\mathrm{gas}}(k)+u_{\mathrm{HP}}^{\mathrm{gas}}(k),\\
&u_{\mathrm{UG}}^{\mathrm{hyd}}(k)+H_{\mathrm{elc}}(k)=u_{\mathrm{CHP}}^{\mathrm{hyd}}(k)+u_{\mathrm{HP}}^{\mathrm{hyd}}(k)+u_{\mathrm{FEV}}^{\mathrm{hyd}}(k).
\end{aligned}
\tag{3-3}
$$

In above equations, $(\cdot)^{\mathrm{el}}$, $(\cdot)^{\mathrm{gas}}$, and $(\cdot)^{\mathrm{hyd}}$ represent the energy that is generated or consumed as electricity, gas, and hydrogen, respectively. For almost all the power balances a connection to the utility grid that can act as an infinite buffer is present. The net imbalance of the microgrid can be compensated by importing or exporting more energy from the utility grid. The thermal power balance does not have this connection. However, since the generation of thermal energy is more of a conversion of other types of energy to thermal energy, the connections to the utility grid in the other power balances act indirectly as an infinity buffer for the thermal power balance.

3-5 Conclusions

In this chapter, it is explained how the electric and thermal microgrid is modelled. Firstly, the different components in the microgrid are modelled using binary logic variables representing their different modes. In the modelling of the EVs it is assumed that the trip characteristics are known beforehand. This assumption simplifies the model but it is concluded that these assumptions will not result in a radical difference in the performance of the microgrid. Secondly, the stochastic processes are listed and their influence on the model is discussed. Forecasting models are needed to determine the predicted values and corresponding errors of these processes. Thirdly, DR for residential buildings is modelled where a distinction is made between curtailable and rescheduable load. Only thermal energy is chosen to be curtailed, but both electrical (dishwashers) and thermal energy are able to be rescheduled. Lastly, general constraints are added to the model. To tackle the degradation of different components in the microgrid, a constraint is set on the minimal time this component has to stay in the same mode. Furthermore, constraints tackling range anxiety are included to prevent the state of charge of the EVs to be too low in the point of view of the consumers when set for departure. The last added constraint is the power balance wherein the energy balance of the microgrid is assured.

Chapter 4

Forecasting of Stochastic Processes

In this chapter, different forecasting models are presented to forecast the stochastic processes in the microgrid. These processes are the Photovoltaic (PV) power, electrical and thermal energy demand of residential buildings, and electrical and thermal energy demand of commercial buildings. Firstly, the different models are presented and explained. Secondly, these models are analyzed for each stochastic process and the best model is chosen. Lastly, scenarios are generated for the stochastic processes based on the distribution of the forecasting error, including the underlying interdependence structure of the prediction errors.

4-1 Point Forecasting

In point forecasting, unique values are forecasted for a stochastic process. The different approaches for point forecasting can be divided into physical-based, statistical-based, and hybrid models. In general, physical approaches use numerical weather prediction and the forecast is calculated from a physical model. In statistical approaches, historic data measurements are used to train a model. Using online available data, a forecast is generated by the trained model. The hybrid approach uses a combination of a physical and statistical approach. A naive approach called the persistence approach is often compared to the more advanced models and serves as a benchmark model. An overview of these models in the literature is given in Figure 4-1.

In this thesis, it is chosen to use the persistence approach and different statistical approaches. Three different statistical models are used: two conventional approaches, i.e., linear regression and a seasonal autoregressive integrated moving average with exogenous inputs, and an Artificial Neural Network (ANN). In this section, the motivation behind and explanation of these models are presented. All the models are evaluated by the root mean square error and weighted average prediction error. These metrics are chosen since the root mean square error penalizes large outliers that will influence the performance of the microgrid considerably, and the weighted average prediction error gives a more general overview of the prediction error.

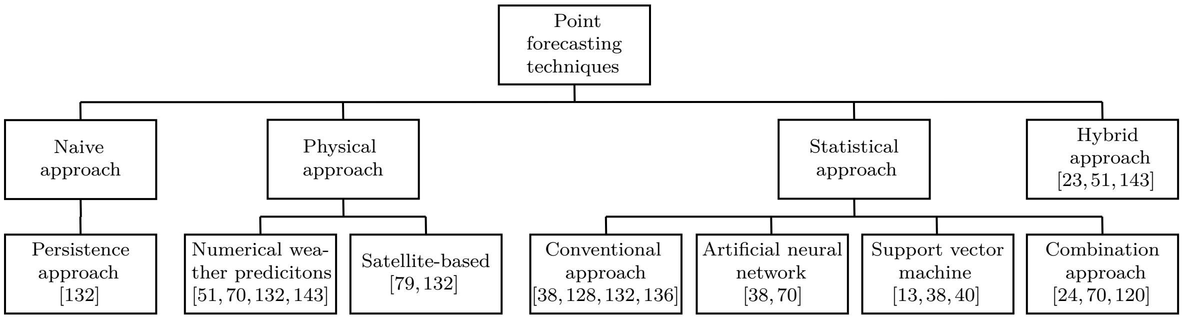

Figure 4-1: Overview of different point forecasting techniques found in the literature.

4-1-1 Persistence Approach

The persistence approach is a naive approach that assumes that the forecast values are the same as past observed values, e.g., for PV power generation, the solar irradiance during the day is similar to that of the previous day for each time step. For the energy demand of buildings, an assumption can be made that the value for next time steps are similar to the previous time step. However, increasing the forecasting horizon will significantly reduce the accuracy of the model [132]. For day-ahead forecasting, a day-to-day persistence method can be used [116]. Due to its naive approach and simplicity, the model is generally used as a benchmark model.

4-1-2 Linear Regression

Linear regressions are widely used to forecast simple models that have an underlying linear correlation structure in the time series. This model is often used due to its simplicity. When nonlinear relationships describe the correlations in the time series better, a more complex estimation method should be used [62]. The forecasted values are based on the measured values of previous time steps and can include seasonality. Exogenous influences can be added as a linear time series to the model. Drawbacks of this method are the poorer performance compared to smarter forecasting models for complex processes and the fact that data should be stationary to use the model. The model is trained by using historic data to calculate the coefficients for the constructed linear regression model.

4-1-3 Autoregressive Moving Average

A conventional statistical approach model used for forecasting is the autoregressive moving average model based on the Box-Jenkins method [25]. This model shows reliable predictions when there exists an underlying linear correlation structure in the time series. Furthermore, a favorable aspect of the model is its flexibility, since it can represent multiple types of time series by using different orders [132]. A main difference with the linear regression model is that it includes the moving average. Therefore, unobserved errors of previous forecasts are included for predicting the value of the next time steps. With the autoregressive moving average model, one assumes that the data show no characteristics of non-stationarity [38]. When non-stationarity data are considered, a generalization of the model can be used by creating an autoregressive integrated moving average model. Inherent seasonal effects of the data can be added to the model by adding seasonality to the model. Lastly, exogenous inputs with a high correlation to the forecasting data can be added to improve the performance of the model. Considering all extensions, a seasonal autoregressive integrated moving average model can be constructed as

$$\phi_{\mathrm{p}}(L)\Phi_{\mathrm{P}}(L^{\mathrm{s}})\nabla^{\mathrm{d}}\nabla_{\mathrm{s}}^{\mathrm{D}}X_t = \theta_{\mathrm{q}}(L)\Theta_{\mathrm{Q}}\left(L^{\mathrm{s}}\right)\varepsilon_{\mathrm{t}} + \beta_{\mathrm{k}}x'_{\mathrm{k,t}}.$$

In the above equation, the P, D, and Q are the seasonal autoregressive order, seasonal difference order, and seasonal moving average order, respectively. The quantity $\phi_{\mathrm{p}}(L)$ is the regular autoregressive polynomial of order p and $\theta_{\mathrm{q}}(L)$ the regular moving average polynomial of order q, while $\Phi_{\mathrm{P}}(L^{\mathrm{s}})$ is the seasonal autoregressive polynomial of order P and $\Theta_{\mathrm{Q}}(L^{\mathrm{s}})$ the seasonal moving average polynomial of order Q. Furthermore, L is the lag operator, L^{s} is the seasonal lag operator, X_{t} represents the forecast variable, ∇^{d} the differentiating operator, $\nabla_{\mathrm{s}}^{\mathrm{D}}$ the seasonal differentiating operator, and ε_{t} white noise. The exogenous part in the equation is $\beta_{\mathrm{k}}x'_{\mathrm{k,t}}$, where $x'_{\mathrm{k,t}}$ is the exogenous input and β_{k} the coefficient value of the exogenous input of the k^{th} exogenous input variable.

4-1-4 Artificial Neural Network

An ANN is a series of algorithms inspired by the neural network in a biological brain. It is trained by using a historical data set where it computes nonlinear relationships between the in- and outputs of the model. In general, an ANN consists of an input layer, output layer, and multiple hidden layers that make the connection between the input and output layer. Each layer is composed of one or more neurons where an activation function in the neurons determines the nonlinear mapping characteristics across the ANN [54]. This approach is widely used since it does not require mathematical expressions, it is self-learning, easy to implement, and short online computation time is needed. This approach is especially used for detecting complex nonlinear relations between the input and output [70]. However, drawbacks of the model are that it needs a significant amount of historical data to be properly trained and overfitting may occur [38].

The ANN has many different structures and applications. For forecasting time series, supervised learning algorithms are used to train the ANN. In this thesis, a long short-term memory recurrent ANN, as first introduced in [64], is used to forecast the stochastic processes. Recurrent networks are fundamentally different from the traditional feedforward neural network since they can establish a temporal correlation between previous information and current circumstances [76]. Therefore, decisions made at a previous time step influences the decision for coming time steps in the ANN. These recurrent ANNs are trained by the popular back-propagation through time. Due to the gradient vanishing or exploring in the training of the ANN, long-range dependencies are difficult to learn. This problem can be overcome by using long short-term recurrent ANNs that uses a memory cell to capture these long-range dependencies [64, 76]. The long short-term recurrent ANNs used in this thesis are modelled with multiple layers using a mini-batch gradient descent. This is done to increase the training speed of the ANN compared to the batch gradient descent, but preventing the regularizing effect of using a stochastic gradient descent where a batch size of one is used. A detailed mathematical expression of the long short-term memory recurrent ANN and different gradient descent methods are found in the Appendix B.

4-2 Photovoltaic Power

For the forecasting of solar energy, a physical model is used since no real data of the energy generation of PV panels are available. Therefore, variables need to be forecasted as input to the physical model of Eq. (2-1). Two stochastic processes have to be forecasted: solar irradiance and ambient temperature. In this section, these two stochastic processes are forecasted per hour using weather data from the Koninklijk Nederlands Meteorologisch Instituut for weather station 240 located near Schiphol [75].

4-2-1 Solar Irradiance

The solar irradiance has seasonal patterns [88] due to the orbit of the Earth around the sun and the obliquity of the Earth [13]. Furthermore, the stochastic behaviour of the solar irradiance comes from atmospheric conditions, e.g., cloud cover, and also from irradiance reflected from the surroundings. Many studies use a clear sky model where the global horizontal solar irradiance is computed as if it is a clear sky day $G_{\mathrm{c}}^{\mathrm{cs}}$, i.e., without any clouds [15,44]. Therefore, the stochastic component is excluded and a clear sky global horizontal solar irradiance can be obtained for every hour in the year. With these values, the clear sky index τ can be computed as the normalization of the measured solar irradiance $G_{\mathrm{c}}(k)$:

$$\tau(k) = \frac{G_{\mathrm{c}}(k)}{G_{\mathrm{c}}^{\mathrm{cs}}(k)}.$$

Multiple models are available to calculate the clear sky global horizontal solar irradiance, e.g., Bird's clear sky model [22]. A poor match between the used data set and the clear sky days of the Bird's model was obtained due to unknown measurement errors and the extra measured reflected irradiation. Therefore, the clear sky model is obtained from the data, and absent data are computed using a statistical smoothing technique based on weighted quantile regressions, as presented in Appendix C [15]. In general, a limiting factor of developing clear sky data is the absence or quality of the data [13], i.e., in the winter there are not many clear sky observations to train the model and this increases the error of the quantile regression. Therefore, data of the past 20 years are used, increasing the number of clear sky observations.

In Figure 4-2, an overview is given of the solar irradiance per day and the clear sky indices. The clear sky indices are assumed to be stationary and can be used for the linear regression models. In the early and late hours, it is seen that there is a more deviating distribution resulting in an expected poorer performance on the linear regression forecasting models. However, the solar irradiance at those time steps is relatively low and will therefore not have a large impact on the performance of the forecasting models. A yearly trend for the clear sky indices is visible from the boxplot in Figure 4-3. The distribution of the clear sky indices differs between seasons and two categories can be defined for which different models can be constructed: the sunnier spring and summer seasons, and the cloudier winter and autumn seasons. Note that the outliers visible in the figure are due to mismatches with the clear

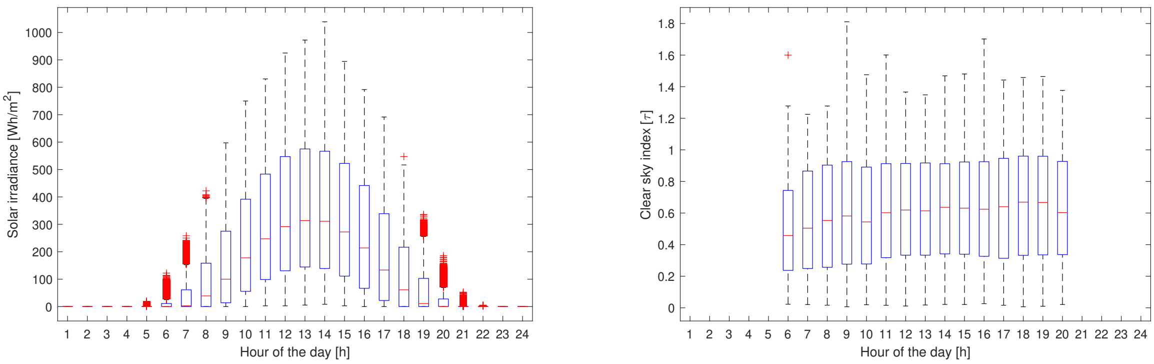

Figure 4-2: In the left graph the distribution of the solar irradiance throughout the day is presented. In the right graph, the distribution of the clear sky index throughout the day is presented.

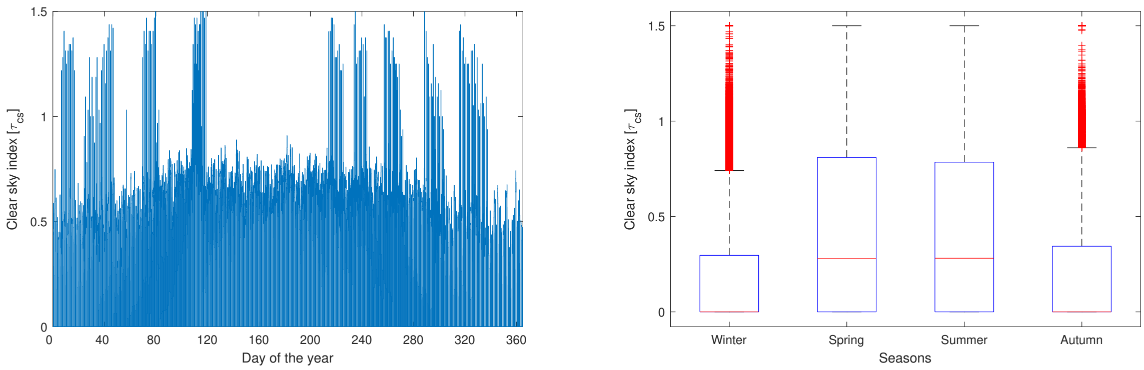

Figure 4-3: In the left graph, the mean clear sky indices of the last sixteen years are presented per hour. In the right graph, a boxplot of the clear sky index is presented with respect to the meteorological seasons of the year.

sky days in early hours and will therefore have a negligible influence on the forecast of solar irradiance. From the autocorrelation of the clear sky index, as presented in Appendix D, it is concluded that the indices of one hour and 24 hours earlier influence are most related to the current clear sky index. The literature has shown that multiple exogenous inputs can be considered in the forecasting models based on the geographical location: temperature, humidity, rainfall, snowfall, and wind speed [7, 13, 38, 40, 132]. Another promising exogenous input is snow that blocks the measured solar irradiance, similar to that it blocks the solar irradiance coming on the PV panels. In the data set, a logic binary variable indicates if there is a presence of snow on the ground. The correlation coefficients, given in Appendix D, between the clear sky indices and exogenous inputs are analyzed, and it is concluded that the highest correlation coefficients are for the temperature, presence of snow, and humidity.

Linear Regression For the linear regression model, the clear sky index of the current hour and 23 hours before is used to forecast the clear sky index for the next hour. Thus, the daily seasonality of the clear sky index is considered in the linear regression. It is analyzed to use exogenous inputs for the forecasting model, and only including the snow as exogenous input results in a smaller forecasting error. This results in the following linear equation for the clear sky index τ at time step k, where $S(k)$ is binary and indicates the presence of snow:

$$\hat{\tau}(k+1) = \alpha_1 \tau(k) + \alpha_2 \tau(k-23) + \alpha_3 S(k),$$

with $\boldsymbol{\alpha} = [\alpha_1, \alpha_2, \alpha_3]$ being a vector of the optimized parameters. Two different models are computed for the two different categories of the seasons. In the sunnier category, where no snow is expected to fall, α_3 is not optimized and set to zero.

Another linear regression model that has the same characteristics as the above model is computed, but for the first hour of light during the day, persistence forecasting is used. This is done to obtain less error when the prediction horizon grows due to large errors obtained in the forecasting for the first light hour of the day.

Seasonal Autoregressive Moving Average A seasonal autoregressive moving average is used to forecast the clear sky index depending on the previous hour and 24 hours before. Seasonal differencing is used to compensate for the change in variance throughout different days in the year, as concluded from Figure 4-3. No differencing is needed between sequential time steps since τ is assumed to be a stationary variable, as seen in Figure 4-2. Adding exogenous inputs did not lead to smaller errors for the forecasting model. The model to calculate is described as

$$(1-\phi_1 L)\left(1-\Phi_{24}L^{24}\right)\left(1-L^{24}\right)y_t = c + (1+\theta_1 L)\left(1+\Theta_{24}L^{24}\right)\varepsilon_t, \tag{4-1}$$

where L is the lag operator, ϕ the autoregressive parameter, θ the moving average parameter, ϵ_t the error, and c a constant value.

Artificial Neural Network A long short-term memory recurrent ANN is used to forecast the solar irradiance and trained with a mini-batch size of 32 while using the data of the past 48 hours. This model does not use the clear sky indices, but the measured solar irradiance. Therefore, the day of the year and hour of the day are included as exogenous inputs to include the measured seasonalities. Furthermore, the temperature and presence of snow are used as exogenous inputs in the model. Including the humidity in the model resulted in larger prediction errors on the test data.

Results All the models are tested and the root mean squared error and the weighted average prediction error are calculated up to a prediction horizon of 18 hours for the year 2013. As a benchmark model, a persistence model is calculated that assumes the solar irradiance to be similar to 24 hours before. An overview of the calculated errors is given in Figure 4-4. For the root mean square error, it is clearly visible that the ANN performs as the best model for larger prediction horizons. However, the weighted average error is significantly higher. Since outliers will expect to result in a lower performance of the microgrid due to the large influence it has on the PV power generation, it is chosen to use the ANN model.

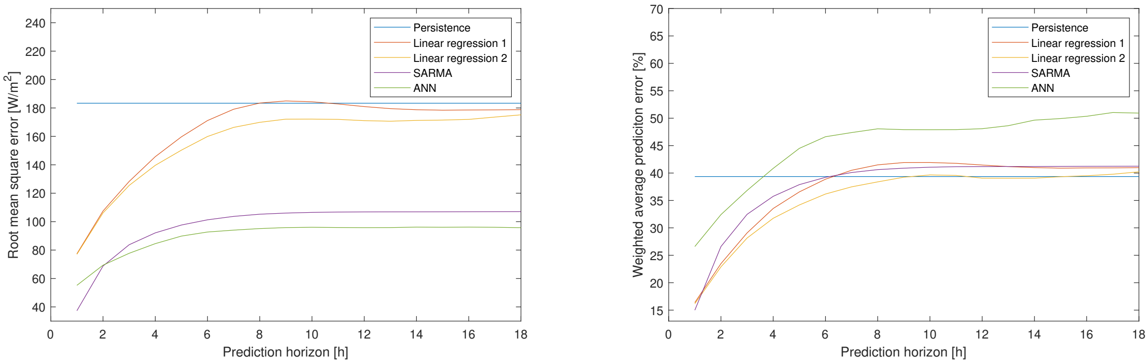

Figure 4-4: Overview of the calculated errors of the different forecasting models for solar irradiance, where linear regression 2 is the model including the persistence forecast, SARMA is the seasonal autoregressive moving average model, and ANN the artificial neural network.

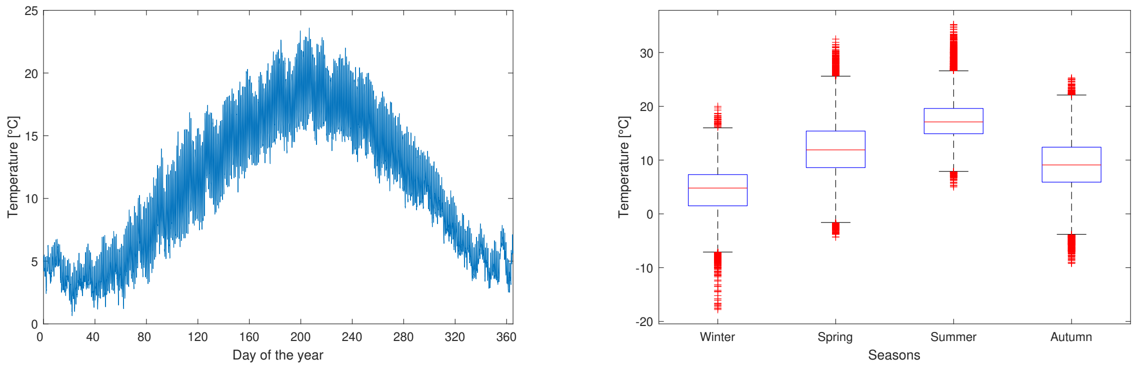

Figure 4-5: In the left graph the mean ambient temperature of the last sixteen years is presented. In the right graph, a boxplot of the ambient temperature is presented with respect to the seasons of the year.

4-2-2 Ambient Temperature

The ambient temperature shows a clear yearly trend between the seasons, as presented in Figure 4-5. Therefore, one can consider different models during the year or use seasonal differencing to overcome this trend. The ambient temperature shows a daily trend as well. However, to use the linear regression methods, the data are normalized over the mean to create stationary data respectively to the hour of the day as presented in Appendix D. The autocorrelation, as presented in Appendix D, is analyzed and it is chosen to use the data from one to five and 24 hours before for the forecasting. Furthermore, the correlation coefficients between the ambient temperature and some meteorological exogenous inputs are calculated in Appendix D. It is concluded that solar irradiance and humidity have the strongest correlation, but these values are still low. Therefore, it is not expected that adding these exogenous inputs will lead to smaller errors in the forecasting models.

Linear Regression The linear regression uses the stationary data of the previous five hours and that of 24 hours ago. For the linear regression, no external variables are considered since they did not increase the performance of the forecast. The parameters of the linear regression model are estimated for the four different seasons throughout the year due to the different characteristics in each season, as concluded from Figure 4-5. The linear regression is written as

$$\begin{aligned} T_{\mathrm{amb}}(k+1) = {} & \alpha_1^{\mathrm{i}} T_{\mathrm{amb}}(k) + \alpha_2^{\mathrm{i}} T_{\mathrm{amb}}(k-1) + \alpha_3^{\mathrm{i}} T_{\mathrm{amb}}(k-2) \\ & + \alpha_4^{\mathrm{i}} T_{\mathrm{amb}}(k-3) + \alpha_5^{\mathrm{i}} T_{\mathrm{amb}}(k-4) + \alpha_6^{\mathrm{i}} T_{\mathrm{amb}}(k-23), \end{aligned}$$

where T_{amb} is the temperature on time step k and $\boldsymbol{\alpha}^{\mathrm{i}} = [\alpha_1^{\mathrm{i}}, \ldots, \alpha_6^{\mathrm{i}}]$ the predicted vector parameter for each season $i = \{\text{winter, spring, summer, autumn}\}$.

Seasonal Autoregressive Integrated Moving Average The nonstationary data set is used in this model since it obtains a smaller error compared to the normalized data set. Using the integrated extension on a autoregressive moving average model, the model assumes the data become stationary after differencing. Seasonality is added in the model to include the daily seasonality and, therefore, indirectly the strong yearly seasonality. Adding exogenous inputs to the model did not result in a smaller error in the model and were therefore excluded. The seasonal autoregressive integrated moving average model uses the same sequence of time steps as the linear regression and is written down as

$$\begin{aligned} & \left(1 - \phi_1 L - \cdots - \phi_5 L^5\right)\left(1 - \Phi_{24} L^{24}\right)(1 - L)\left(1 - L^{24}\right) y_t = \\ & c + \left(1 + \theta_1 L + \cdots + \theta_5 L^5\right)\left(1 + \Theta_{24} L^{24}\right) \varepsilon_t, \end{aligned}$$

where the variables have similar definitions as in Eq. (4-1).

Artificial Neural Network A long short-term memory recurrent ANN is implemented that uses the temperature data of 48 hours and is trained with mini-batches of size 32. Multiple exogenous inputs are included in the model: day of the year, the hour of the day, and the ambient air pressure at sea level. Other exogenous inputs with relatively high correlation, e.g., solar irradiance, did not improve the model.

Results All the models are tested and the root mean squared error and the weighted average prediction error are calculated up to a prediction horizon of 18 hours for the year 2013. As a benchmark model, a persistence model is calculated that assumes the temperature to be similar to 24 hours before. An overview of the calculated errors is given in Figure 4-6. From both metrics, it is clearly visible that the seasonal autoregressive integrated moving average model obtains the smallest error. One should expect the ANN to obtain at least similar performance, but this could not be obtained.

4-3 Residential Energy Demand

The forecasting of the residential energy demand is done with the Liander data set that is complete for 67 households for the year 2013 [84]. Data of the 67 households are added together to create the most general training set and different forecasting models are constructed

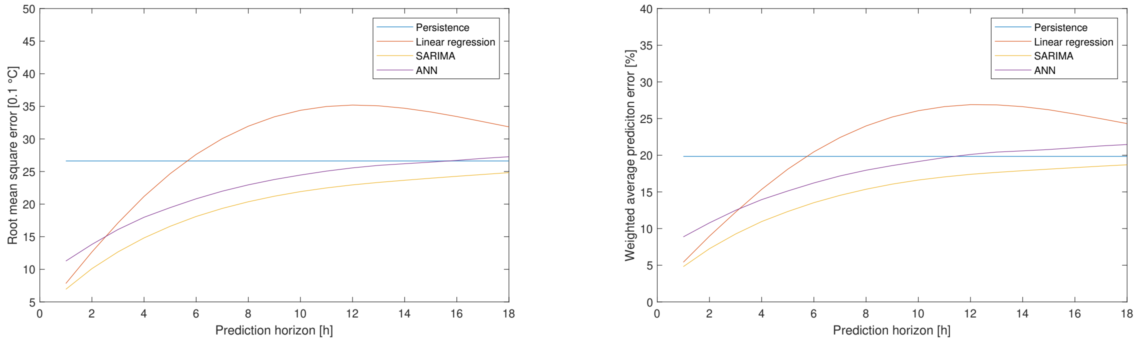

Figure 4-6: Overview of the calculated errors of the different forecasting models for temperature, where SARIMA is the seasonal autoregressive integrated moving average model and ANN the artificial neural network.

for the electrical and thermal energy demand. The data for the electrical energy demand are given per quarter of an hour and the data for the thermal energy demand are given per hour.

4-3-1 Forecasting Models

The yearly trend is analyzed from the data set, assuming 2013 was a general year of energy consumption for these households. From Figure 4-7, a clear trend is visible in both the electrical and thermal energy demand. The electrical energy demand is clearly less in the days when there is more daylight. For the thermal energy demand , even a stronger correlation is visible with the days in the year. In the colder months, more thermal energy is used and the distribution is larger in absolute terms. In conclusion, it can be interesting to use different forecasting models dependent on the season, especially for forecasting the thermal demand, due to the different data characteristics during the year.

In Figure 4-8, a small variation is visible during weekdays and the weekends for both the electrical and thermal energy demand. For both demands, more energy is consumed during the middle of the day at the weekends than the weekdays. People will get up later during the weekends and will be more at home, consuming more energy. The distinctive residential energy consumption curve during the day is clearly visible from Figure 4-8. The electrical energy has a high peak after 18:00 hours when people start to come home from work during the week. The thermal demand has a more constant distribution during the day, and it is visible that in the nightly hours, the thermal energy consumption drops significantly.

To use linear regression models, the data are made stationary by normalizing the data through division by the mean per time step during the day, as visualized in Appendix D. From the autocorrelation, as presented in Appendix D, it is chosen that for the electrical energy demand the data of the previous 45 minutes and of 23:45-24:15 hours before are used. For the thermal demand, the data of the last two hours are used as well as the data of the 23 - 25 hours before. Correlation coefficients of meteorological exogenous inputs, as presented in Appendix D, are analyzed, and it is concluded that only a high correlation is obtained between the temperature and thermal demand.

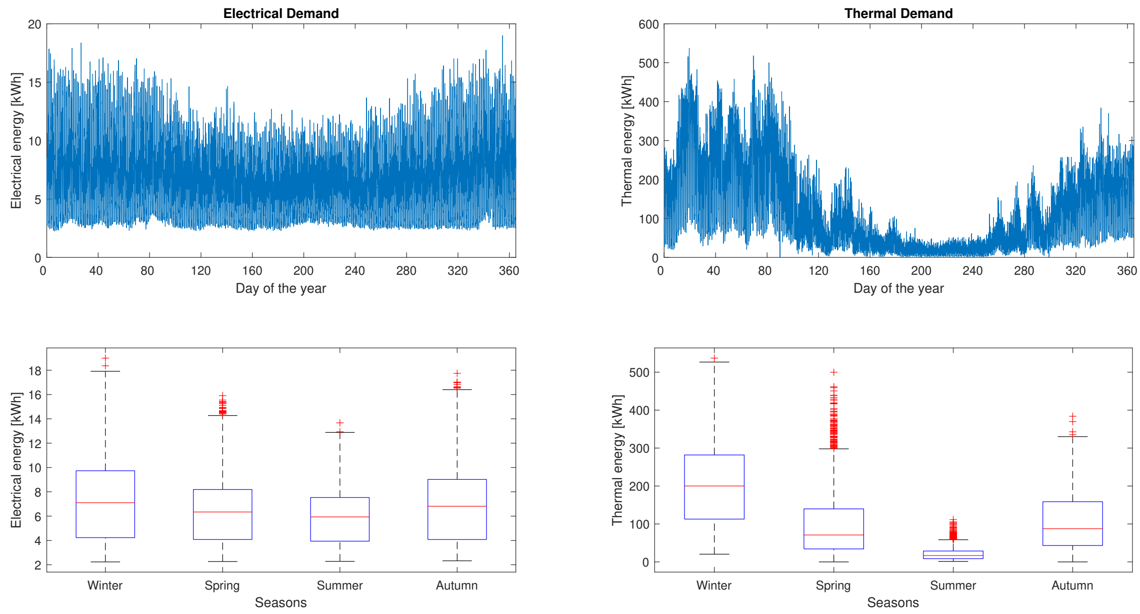

Figure 4-7: Average yearly trend of the energy demand of residential buildings.

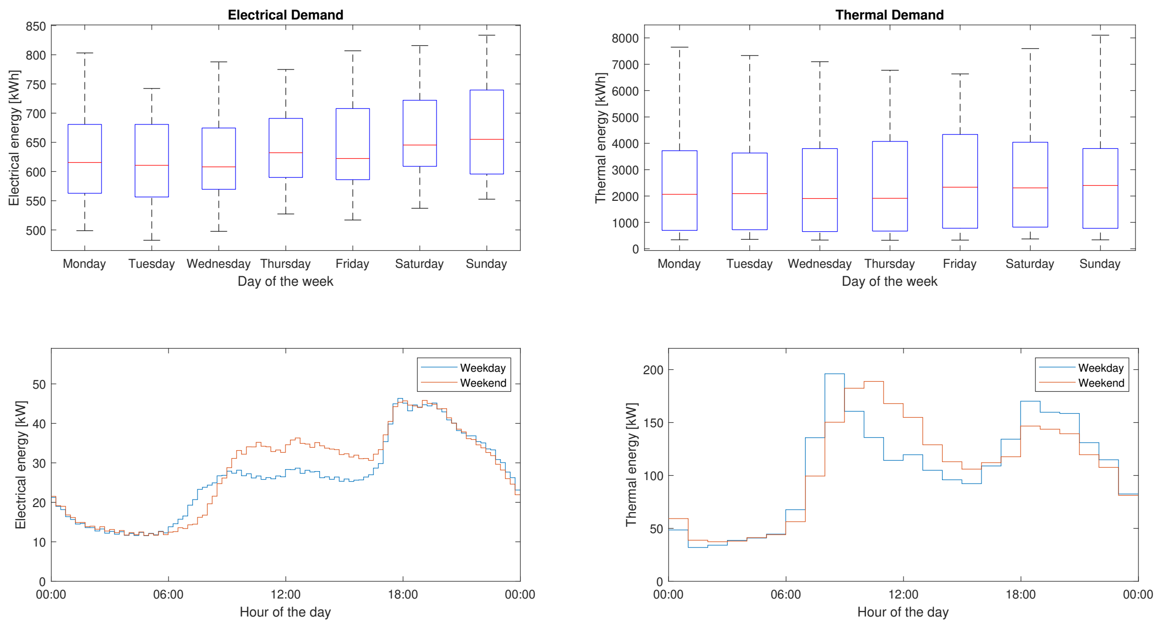

Figure 4-8: Average weekly trend of the energy demand of residential buildings.

Linear Regression The stationary data are used for linear regression. Despite the high correlation coefficient between the temperature and thermal demand, including this exogenous input did not result in better performance. For the thermal demand, there is a significant difference in the distribution of the data in the different seasons of the year, as seen in Figure 4-10. Therefore, a different model will be used for every season to predict the parameters of the thermal demand. The equations of the linear regressions for the residential electrical and thermal energy demand are

$$\begin{aligned} P_{\text{res}}(k+1) &= \alpha_1^{\text{el}} P_{\text{res}}(k) + \alpha_2^{\text{el}} P_{\text{res}}(k-1) + \alpha_3^{\text{el}} P_{\text{res}}(k-2) + \alpha_4^{\text{el}} P_{\text{res}}(k-94) \\ &\quad + \alpha_5^{\text{el}} P_{\text{res}}(k-95) + \alpha_6^{\text{el}} P_{\text{res}}(k-96) \\ Q_{\text{res}}(k+1) &= \alpha_1^{\text{th,i}} Q_{\text{res}}(k) + \alpha_2^{\text{th,i}} Q_{\text{res}}(k-1) + \alpha_3^{\text{th,i}} Q_{\text{res}}(k-22) + \alpha_4^{\text{th,i}} Q_{\text{res}}(k-23) \\ &\quad + \alpha_5^{\text{th,i}} Q_{\text{res}}(k-24), \end{aligned} \tag{4-2}$$

where P_{res} and Q_{res} are the electrical and thermal residential energy demand, respectively. Furthermore, $\boldsymbol{\alpha}^{\text{el}} = [\alpha_1^{\text{el}}, \ldots, \alpha_6^{\text{el}}]$ is a vector of the optimized parameters for the electrical energy demand and $\boldsymbol{\alpha}^{\text{th,i}} = [\alpha_1^{\text{th,i}}, \ldots, \alpha_5^{\text{th,i}}]$ a vector of the optimized parameters for the thermal demand for different seasons during the year $i = \{\text{winter, spring, summer, autumn}\}$.

Seasonal Autoregressive Integrated Moving Average In this model, the nonstationary data set is used since a lower prediction error is obtained compared to the stationary data set. Moreover, the integrated part is used and it is assumed that the data become stationary after differencing. Daily seasonal differencing is used to include the yearly seasonality. No exogenous inputs are considered since they did not improve the performance of the model. The models used for the electrical and thermal energy demand are, respectively,

$$\begin{aligned} &\left(1 - \phi_1 L - \cdots - \phi_3 L^3\right)\left(1 - \Phi_{96} L^{96}\right)(1 - L)\left(1 - L^{96}\right) y_t = \\ &c + \left(1 + \theta_1 L + \cdots + \theta_3 L^3\right)\left(1 + \Theta_{96} L^{96}\right) \varepsilon_t \text{ and} \\ &\left(1 - \phi_1 L - \phi_2 L^2\right)\left(1 - \Phi_{23} L^{23} - \cdots - \Phi_{25} L^{25}\right)(1 - L)\left(1 - L^{24}\right) y_t = \\ &c + \left(1 + \theta_1 L + \theta_2 L^2\right)\left(1 + \Theta_{23} L^{23} + \cdots + \Theta_{25} L^{25}\right) \varepsilon_t. \end{aligned}$$

The variables in the above equation have similar definitions as in Eq. (4-1).

Artificial Neural Network A long short-term memory recurrent ANN is implemented using data of the past 48 hours and the model is trained with mini-batches of size 32. In both models, the following exogenous inputs are included: the hour of the day and day of the week. The day of the year is not included since only data are available of one single year. For the thermal demand forecasting, the temperature data of the past 12 hours are also included.

4-3-2 Results

All the models are tested and the root mean squared error and the weighted average prediction error are calculated up to a prediction horizon of 18 hours for the year 2013. As a benchmark

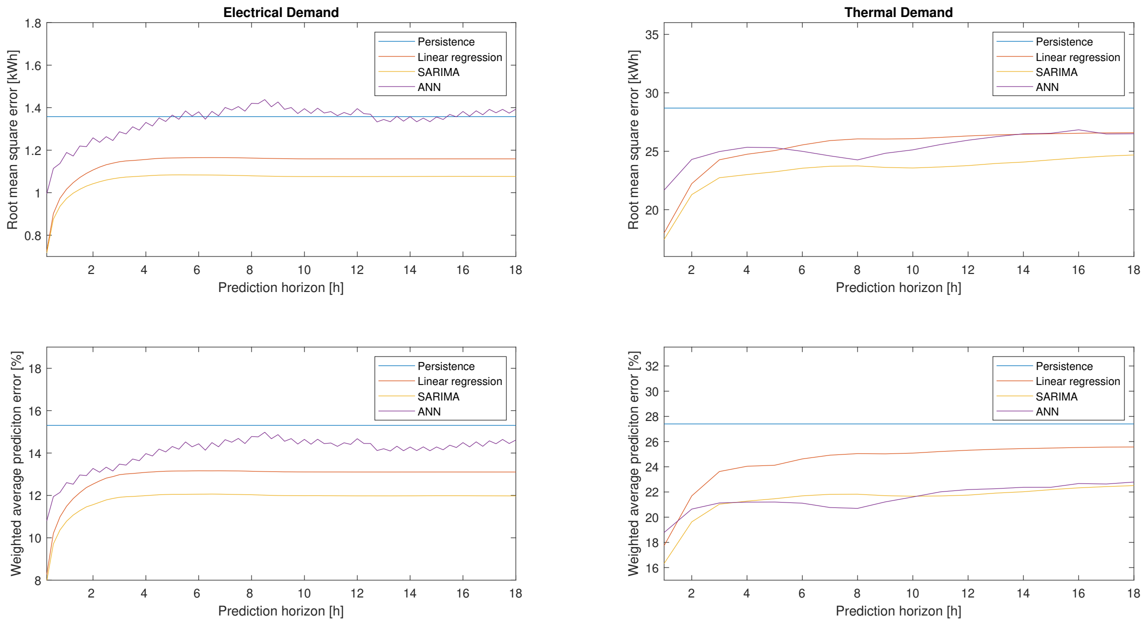

Figure 4-9: Overview of the calculated errors of the different forecasting models for the residential energy demands, where SARIMA is the seasonal autoregressive integrated moving average model and ANN the artificial neural network.

model, a persistence model is calculated that assumes the energy demand to be similar to 24 hours before. An overview of the calculated errors is given in Figure 4-9. From both metrics, it is concluded that the seasonal autoregressive integrated moving average model obtains the smallest errors for both energy demands. One should expect the ANN to obtain at least similar performance, but this could not be achieved due to the lack of training data.

4-4 Commercial Energy Demand

The forecasting of the commercial energy demand is done with the data from De Energiemanager commissioned by NEDU [39]. These data give the average energy demand of stores in the Netherlands in a yearly percentage. The data are for the electrical and thermal energy demand per quarter of an hour and hour, respectively. Assuming that a general store uses around 10,000 kWh electricity and 5000 m^3 gas per year [140], the demand of a small store in the Netherlands is calculated during the year. Forecasting models are constructed for the electrical energy demand per quarter of an hour and for the thermal energy demand per hour.

4-4-1 Forecasting Models

A yearly trend is visible in the electrical and thermal energy demand, as seen in Figure 4-10. Especially for the thermal demand, a considerable difference in the distribution of the data per season is visible. Therefore, it might be interesting to use different forecasting models

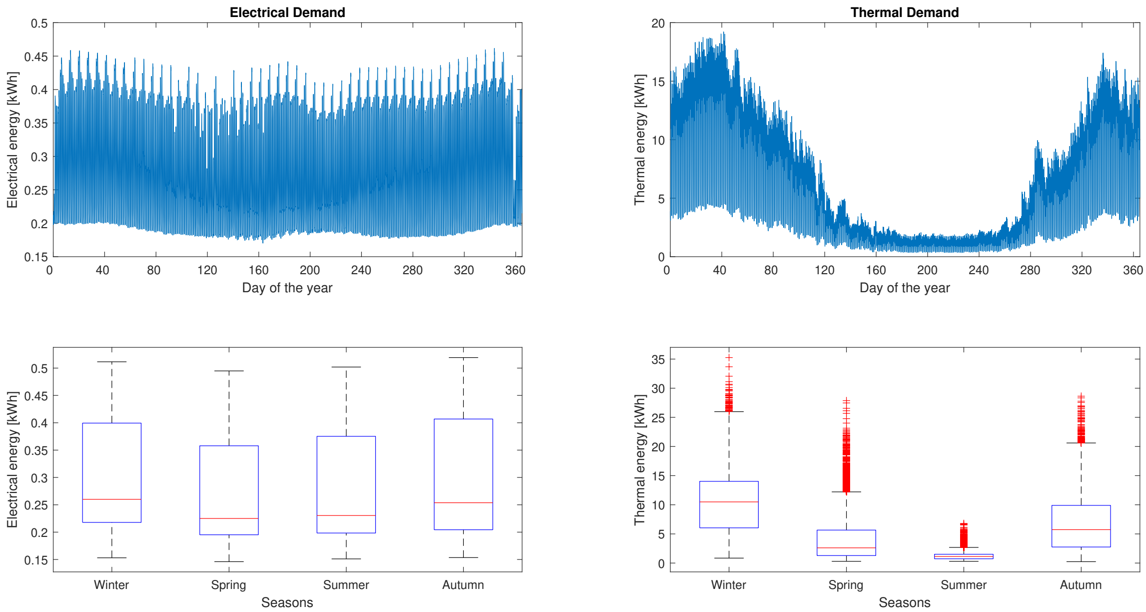

Figure 4-10: Average yearly trend of the energy demand of commercial buildings.

dependent on the season. The electrical energy demand for commercial buildings is strongly influenced by the opening hours of the buildings which differ for weekends compared to the weekdays, as seen in Figure 4-11. Most of the energy is consumed during the opening hours, and the electrical energy peak is during the middle of the day. The thermal demand is not influenced much by the type of day and has a more similar pattern to that of the residential thermal demand.

To use linear regression models, the data are made stationary by normalizing the data through division by the mean per time step during the day, as visualized in Appendix D. From the autocorrelation, as presented in Appendix D, it is chosen that for the electrical energy demand, data of the previous 30 minutes back in time as well as of 168 hours before (week) are used. For the thermal energy demand, the data of the previous hour are used as well as of 23-25 hours before. Correlation coefficients of meteorological exogenous inputs, as presented in Appendix D, are analyzed, and it is concluded that only a high correlation is obtained between the temperature and thermal demand.

Linear Regression The stationary data are used for linear regression. No exogenous inputs were used since they did not result in smaller forecasting error. For the thermal demand, there is a significant difference in the distribution of the data in the different seasons of the year, as seen in Figure 4-10. Therefore, a different model will be used for every season to predict the parameters of the thermal demand. Making two different models for weekdays and weekends did not improve the model for both the electrical and thermal energy demand. The equations of the linear regressions for electrical and thermal energy demand of commercial buildings are

$$
\begin{aligned}
P_{\text{com}}(k+1) &= \alpha_1^{\text{el}} P_{\text{com}}(k) + \alpha_2^{\text{el}} P_{\text{com}}(k-1) + \alpha_3^{\text{el}} P_{\text{com}}(k-671) \\
Q_{\text{com}}(k+1) &= \alpha_1^{\text{th,i}} Q_{\text{com}}(k) + \alpha_2^{\text{th,i}} Q_{\text{com}}(k-22) + \alpha_3^{\text{th,i}} Q_{\text{com}}(k-23) + \alpha_4^{\text{th,i}} Q_{\text{com}}(k-24),
\end{aligned}
$$

where P_{com} and Q_{com} are the electrical and thermal commercial energy demand, respectively. The other variables having similar definitions as in Eq. (4-2).

Seasonal Autoregressive Integrated Moving Average In this model, the nonstationary data set is used since it obtained smaller errors compared to the normalized data set. Moreover, the integrated extension is used and it is assumed that the data become stationary after differencing. Daily seasonal differencing is used to include the yearly seasonality. No exogenous inputs are used since they did not result in lower errors. Different models are constructed for the electrical energy demand demand for the weekdays and weekends. The model used for the electrical and thermal energy demand are, respectively,

$$
\begin{aligned}
&\left(1 - \phi_1^{\text{i}} L - \phi_2 L^2\right)\left(1 - \Phi_{672}^{\text{i}} L^{672}\right)(1 - L)\left(1 - L^{672}\right) y_t = \\
&c^{\text{i}} + \left(1 + \theta_1^{\text{i}} L + \theta_2^{\text{i}} L^2\right)\left(1 + \Theta_{672}^{\text{i}} L^{672}\right)\varepsilon_t \\
&(1 - \phi_1 L)\left(1 - \Phi_{23} L^{23} - \cdots - \Phi_{25} L^{25}\right)(1 - L)\left(1 - L^{24}\right) y_t = \\
&c + (1 + \theta_1 L)\left(1 + \Theta_{23} L^{23} + \cdots + \Theta_{25} L^{25}\right)\varepsilon_t.
\end{aligned}
$$

The variables in the above equation have similar definitions as in Eq. (4-1), with $i = \{\text{weekdays, weekends}\}$.

Artificial Neural Network A long short-term memory recurrent ANN is implemented using data of the previous 24 hours and the same day a week before with mini-batches of size 32 for the electrical energy demand. For the thermal energy demand, data of the previous 48 hours are used and the model is trained with mini-bathes of size 24. For both stochastic processes the hour of the day, day of the week, and day of the year are used as exogenous inputs to the model. Furthermore, the temperature is added as exogenous input for the thermal energy demand.

4-4-2 Results

All the models are tested and the root mean squared error and the weighted average prediction error are calculated up to a prediction horizon of 18 hours for the year 2013. As a benchmark model, a persistence model is calculated that assumes the energy demand to be similar to 24 hours before. An overview of the calculated errors is given in Figure 4-12. From the figure, it can be concluded that the ANN performs better for prediction horizons larger than six hours for the electrical energy demand, i.e., the cumulative error of the linear regression model exceeds the ANN. Since the prediction horizon will be larger than six hours in the case studies of this thesis, the ANN is chosen to be the most suitable model. The seasonal autoregressive integrated moving average model gives an unexpected high error for the electrical energy demand. The model was able to forecast the weekends accurately, but high errors were obtained during the weekdays. For the thermal energy demand, it is concluded that the ANN obtains the smallest errors.

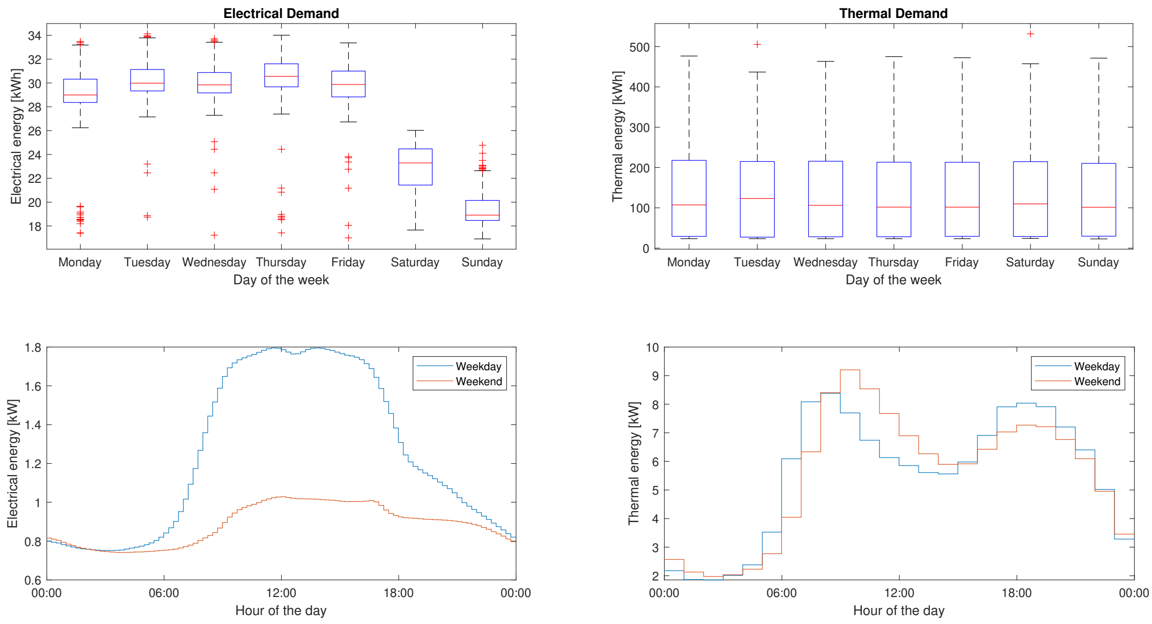

Figure 4-11: Average weekly trend of the energy demand of commercial buildings.

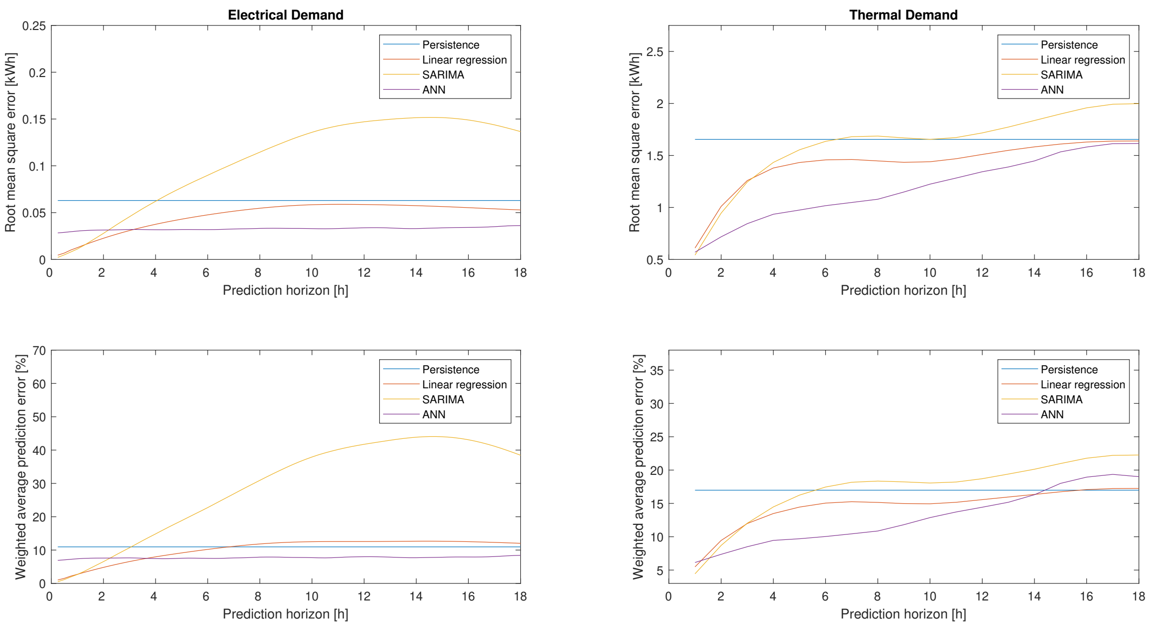

Figure 4-12: Overview of the calculated errors of the different forecasting models for the commercial energy demands, where SARIMA is the seasonal autoregressive integrated moving average model and ANN the artificial neural network.

4-5 Scenario Generation

By including the expected error of the point forecasting, scenarios can be generated for the stochastic processes to obtain a more accurate forecast. Before these scenarios can be generated, distributions of the forecasting errors should be computed by a probabilistic forecasting model.

Three different types of probabilistic forecasting approaches are mostly used in the literature: parametric, non-parametric, and ensemble approach. The parametric approach assumes that the distribution can be approximated by pre-defined distribution structures. For the stochastic processes used in this thesis, this approach is mainly not used or does not show good performance [53]. Since the different point forecasting methods differ substantially in performance, the ensemble approach as described in [70] is not preferable. Hence, a non-parametric approach is used to describe the distribution. A linear quantile regression, as described in Appendix C, is computed as a non-parametric model to calculate the quantiles of the error distribution of each stochastic process. The quantiles are calculated for each distinctive time step during the day in the prediction horizon. By fitting a smooth curve through the set of quantiles of each time step during the day in each step in the prediction horizon, a continuous cumulative quantile distribution is obtained. This distribution is inversed to obtain the cumulative distribution of the error in each hour of the day for the prediction horizon. It must be noted that possibly more accurate distributions can be obtained with more sophisticated machine learning methods as quantile regression forest, ANNs, or gradient boosting techniques [83]. However, these methods exceed the goal of this thesis.

From these cumulative distributions, scenarios can be generated for the different stochastic processes using a sampling-based method. To include the interdependence structure of prediction errors, a method inspired by [109] is used. This method relies on the fundamental property of reliable probabilistic predictions that the prediction errors can by transformation be made Gaussian. A unique covariance matrix is made to capture the interdependence structure for each distribution per hour per time step in the prediction horizon. Using a multivariate Gaussian random number generator with zero mean and the computed covariance matrix, scenarios are generated. Note that probably more accurate and complex interdependence structures can be obtained using the copula theory [109]. A detailed description of this method is found in Appendix E.

4-6 Conclusions

Different point forecasting models are implemented for the stochastic processes in this thesis: persistence approach, linear regression, autoregressive moving average, and ANN. The solar irradiance and ambient temperature are forecasted to calculate the expected PV power. It is concluded that for the solar irradiance and commercial buildings the ANN obtains the smallest errors. Seasonal autoregressive integrated moving average models obtained the smallest errors for the ambient temperature and the residential buildings. For the forecasting of the residential energy demand, this can be explained due to the lack of a large training data set. Lastly, scenarios are generated using linear quantile regression to compute the error distributions and a multivariate Gaussian random number generator, including the interdependence structure of the different stochastic processes.

Chapter 5

Control Strategies

Different control strategies are used in the literature for the tertiary control problem within a microgrid. An important aspect in these control strategies is how to deal with the errors in the stochastic processes of Chapter 4. In some studies, optimal scheduling models are used to solve the scheduling problems for the tertiary control of a microgrid in, e.g., a day-ahead scenario. These algorithms use a predefined control structure to decide when it is the best time for certain appliances in the microgrid to be operated to obtain the best performances [137]. The advantages of such methods are their low complexity and easy implementation. However, improvements in the performance can be obtained by using closed-loop scheduling models as Model Predictive Control (MPC) [17, 107, 131]. In this chapter, firstly, nominal MPC and a low-level controller to adjust for the errors in the forecasts are introduced. Secondly, stochastic MPC strategies are introduced that might improve the performance of the microgrid by including the uncertainties of the point forecasts. Lastly, the control objective of the optimization is given.

5-1 Model Predictive Control

MPC is a widely used control strategy since its adoption in the process industry [95]. This adoption was mainly due to the conceptual simplicity of MPC and the ability to easily handle complex systems with hard constraints on the system as well as on the inputs. In this section, the principles of nominal MPC are explained and a low-level controller is introduced to compensate for the errors in the forecasts.

5-1-1 Nominal

There has been a vast amount of literature on nominal MPC for discrete-time systems where the known states $\boldsymbol{x}$ and inputs $\boldsymbol{u}$ are constrained, described as

$$\begin{aligned} &\boldsymbol{x}^{+} = f(\boldsymbol{x},\ \boldsymbol{u}), \quad \boldsymbol{y} = h(\boldsymbol{x}), \\ &\boldsymbol{x} \in \mathbb{X},\ \boldsymbol{u} \in \mathbb{U},\ f \in \mathbb{R}^{n} \times \mathbb{R}^{m} \to \mathbb{R}^{n},\ \boldsymbol{y} \in \mathbb{R}^{b},\ \text{and } h \in \mathbb{R}^{n}, \end{aligned} \tag{5-1}$$

with $\boldsymbol{x}^{+}$ representing the successor states and $\boldsymbol{y}$ the outputs of the system. In this system, the state is assumed to be observable. At each event of the state or time, the optimal control problem is solved while simulating future states in a receding horizon fashion. The length of the finite-horizon, wherein these future states lie, is called the prediction horizon. For this prediction horizon, a control sequence is computed with the length of the control horizon. The first control of the computed sequence is implemented in the system and the process is repeated for the next control step. Due to this method, future output in the chosen prediction horizon can be considered while choosing the control input. Increasing the control horizon can improve the performance of the optimal control problem, but increases the computation time.

The use of MPC on hybrid systems is not as extensively researched as standard linear processes with linear constraints [27]. The main drawback of hybrid systems is the computational burden due to the introduction of the integer variables in the optimization. The complexity is NP-hard and to test if a new feasible solution improves the best one so far is an NP problem [27]. Another drawback is the loss of convexity and it is therefore not known if a feasible solution is the global optimum.

5-1-2 Low-Level Controller

No constraints satisfaction nor recursive feasibility can be guaranteed by using the nominal MPC due to the errors in the point forecasts, i.e., violations of the constraints can occur [95]. For example, the rescheduled Q_{r} and curtailed thermal energy Q_{c} can exceed the maximum defined fraction of the real consumed thermal energy. Moreover, due to the errors in the forecast, a difference occurs in the electrical and thermal power balance of Eq. (3-3) due to differences in the stochastic processes $P_{\mathrm{PV}},\ P_{\mathrm{res}},\ P_{\mathrm{com}},\ Q_{\mathrm{res}}$, and Q_{com}. An online low-level controller is assumed to be available to adjust for these discrepancies.

This low-level controller adjusts the maximum possible thermal energy that can be rescheduled and curtailed. Then, it checks if an abundance or shortage of thermal energy is present. A shortage of thermal energy is compensated by burning extra imported 'green' gas or hydrogen using the hybrid heat pumps. If this is not possible, extra electrical energy is consumed by the heat pumps to generate the thermal energy. During an abundance of thermal energy, similar steps are taken but the abundance in gas or hydrogen is subtracted from the imported quantity. The electrical energy difference is computed out of the error of the electrical stochastic processes and the extra electrical energy needed for the hybrid heat pumps. The utility grid compensates for this electrical energy difference by purchasing or selling electrical energy. Feasibility is assumed to be ensured since there are no constraints on the imported energy and the hybrid heat pumps can provide more thermal energy than the maximum thermal demand measured in the historic data. A more detailed description of the low-level controller is given in Appendix F.

5-2 Stochastic Model Predictive Control

Due to the errors in the point forecasts, the system in Eq. (5-1) is not necessarily stable, i.e., infeasibility can occur [56, 95]. To prevent this, the system can be described as a perturbed model containing additive disturbances $\boldsymbol{w}$:

$$\begin{aligned} &\boldsymbol{x}^{+} = f(\boldsymbol{x},\ \boldsymbol{u},\ \boldsymbol{w}), \quad y = h(\boldsymbol{x}), \\ &\boldsymbol{x} \in \mathbb{X},\ \boldsymbol{u} \in \mathbb{U},\ \boldsymbol{w} \in \mathbb{W},\ f \in \mathbb{R}^n \times \mathbb{R}^m \rightarrow \mathbb{R}^n,\ \boldsymbol{y} \in \mathbb{R}^b,\ \text{and } h \in \mathbb{R}^n. \end{aligned} \tag{5-2}$$

The disturbance can be bounded or described by a mathematical formulation, e.g., probability distributions. Different extensions on the nominal MPC are possible to deal with the uncertainties of the point forecasts for the stochastic processes. In this section, a brief comparison is made between robust and stochastic MPC. Furthermore, two stochastic MPC methods that can deal with the nonlinearities of the mixed-integer linear programming problem are explained and adapted to the control of the microgrid in this thesis [47]: scenario-based and tree-based MPC. Note that in these stochastic MPC methods, the low-level controller from Section 5-1-2 will still be applied.

5-2-1 Robust versus Stochastic

The two different methods considering the uncertainty, as described in Eq. (5-2), are robust and stochastic MPC. In robust MPC, the uncertainty is assumed to be bounded and for all required realizations of the disturbances $\boldsymbol{w} = \{w(0),\ w(1), \ldots, w(N-1)\} \in \mathbb{W}^N$ the control constraints need to be satisfied [95]. This guarantees feasibility for the bounded disturbances but results in a conservative solution. To decrease the conservatism of the results, stochastic MPC will be used in this thesis where the constraints are assumed to be stochastic. In this method, the constraints are softened, i.e., the constraints do not need to be satisfied for all possible realizations of the disturbances [95]. In the optimization of stochastic MPC, a trade-off is made between the control performance and the probability of state constraint violation [60].

5-2-2 Scenario-Based Model Predictive Control

In the scenario-based approach, the state distribution is approximated by generating scenarios. A single finite-horizon input trajectory is computed that is feasible for all the sampled scenarios, i.e., the state constraints should hold for all the sampled scenarios [117]. The finite-horizon input trajectory is calculated by the cost function that computes the state and input costs over the prediction horizon as an average over the scenarios as

$$\min_{\boldsymbol{u}} \sum_{\mathrm{i}=1}^{\mathrm{N_s}} J\left(\boldsymbol{x}_{\mathrm{i}},\ \boldsymbol{u}\right), \tag{5-3}$$

where $\boldsymbol{u}$ describes the control inputs, N_{s} the number of scenarios, J the cost function, and $\boldsymbol{x}$ the states. A high number of scenarios is needed to obtain good performance, but one has to keep in mind that the computational complexity increases greatly with the number of scenarios. Furthermore, an infinite number of scenarios would converge to the performance of the nominal MPC with the point forecasting prediction. Erratic behaviour of sampled scenarios with unlikely outliers will influence the results much since it has to be feasible for all scenarios. One can choose to decrease the number of generated scenarios to exclude these outliers [117]. Another more efficient method is to use posterior scenario removal methods that can be used to obtain less conservative results [28]. Since highly unlikely outliers have a small chance of occurring due to Gaussian random number generator that is based on the cumulative distribution of the point forecast, and a more robust controller is preferred, it is chosen not to implement scenario removal.

Differences between the scenarios for the power balances from Eq. (3-3) will occur. To assure feasibility, some control inputs influencing the electrical and thermal power balance should be different for each scenario or a feasible bound for the constraints should be defined. For the electrical power balance, the utility grid will act as a buffer. Each scenario has its 'own' electric utility grid regulating the transfer of electrical energy. For the thermal power balance, the thermal energy generated for each scenario will be different. The hybrid heat pumps will be in the same mode for each scenario, but their electrical energy or gas consumed will be different for each scenario. It was also considered to determine a bound where a single control input for the electric utility grid and heat pumps could be used for all scenarios. However, the disadvantage is that the bound would be highly influenced by single outliers resulting in poorer performance and is therefore not used.

5-2-3 Tree-Based Model Predictive Control

Tree-based MPC uses similar reasoning as scenario-based MPC wherein the state distribution is approximated by the generated scenarios. However, in tree-based MPC, these scenarios share a common history up to a branching node as seen in Figure 5-1. For each scenario, a unique control sequence is computed, but the control trajectories are equal for scenarios up to the bifurcation point where they branch from each other. This is done to reduce the large number of decision variables, decreasing the computational complexity of the problem. To ensure that the control trajectories are similar for scenarios up to their branching point, a non-anticipative constraint is introduced

$$\boldsymbol{u}^{\mathrm{i}}(k) = \boldsymbol{u}^{\mathrm{j}}(k), \quad \text{with } k = (1, \ldots, \min(B^{\mathrm{ij}}, N_{\mathrm{p}})),\ \forall i, j \in (1, \ldots, N_{\mathrm{s}}), \tag{5-4}$$

with N_{p} the prediction horizon, $\boldsymbol{u}(k)$ the control inputs at time step k, and B^{ij} the branching point of the scenarios i and j. Furthermore, the control inputs and the stochastic values for all scenarios are the same in the tree root, i.e., the first time step. Therefore, a single control input can be implemented in the closed-loop system. The optimization problem that needs to be solved is almost similar to that of scenario-based MPC as in Eq. (5-3), only multiple different control sequences are considered for the scenarios as

$$\min_{\boldsymbol{u}_1,\ldots,\boldsymbol{u}_{\mathrm{N_s}}} \sum_{\mathrm{i}=1}^{\mathrm{N_s}} J\left(\boldsymbol{x}_{\mathrm{i}},\ \boldsymbol{u}_{\mathrm{i}}\right),$$

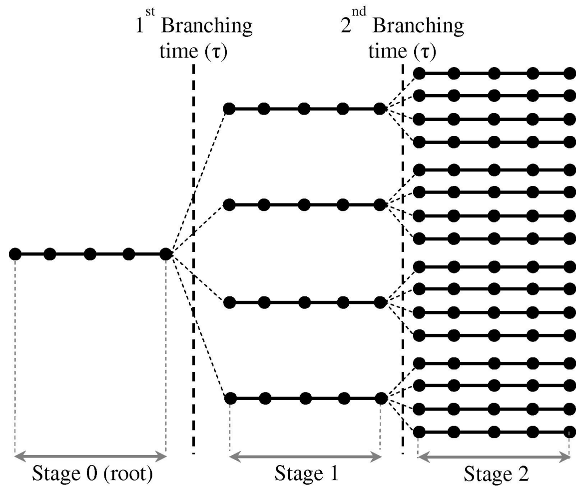

Figure 5-1: An illustrative example of a scenario tree [31].

Tree-based MPC is computationally more complex than scenario-based MPC, but less conservative since the control sequence only has to satisfy the constraints related to the disturbances in its branch.

The same scenarios are used as for scenario-based MPC. The scenarios have to be clustered to generate the tree structure. Many different clustering algorithms can be used as described in [61, 82, 134]. It is chosen to cluster the scenarios based on bounds without a predefined structure, i.e., the scenarios merge if there values lie too close to each other. The following steps are taken to obtain the tree structure from the generated scenarios:

1. For time step $k = 1$, the median value is calculated and is implemented as the root value for all scenarios.
2. A bound Δ is defined wherein scenarios will be merged based on a determined percentage of the average prediction error of the stochastic process.
3. At time step k it is checked if scenarios share a common history, i.e., are still in the same branch at time step k. Multiple clusters are made of scenarios sharing a common history.
4. For each cluster, the median value μ is calculated.
5. If a scenario of cluster n at time step k lays outside the bound $\mu_\mathrm{n} \pm \frac{1}{2}\Delta$, it branches from that cluster. All the branched scenarios from cluster n form a new cluster i.
6. The median is calculated for cluster i and all the scenarios that lie within the bound $\mu_\mathrm{i} \pm \frac{1}{2}\Delta$ are assigned to a new cluster. For the remaining scenarios, this procedure is repeated until all scenarios are assigned to a new cluster.
7. Steps 3–6 are repeated for every time step $1 < k \leq N_\mathrm{p}$.

Since there are multiple stochastic processes in the microgrid, it is chosen to construct two trees, i.e., an electric and thermal tree. The constructed scenarios of the commercial and residential electrical energy consumption are added to the Photovoltaic (PV) power generation,

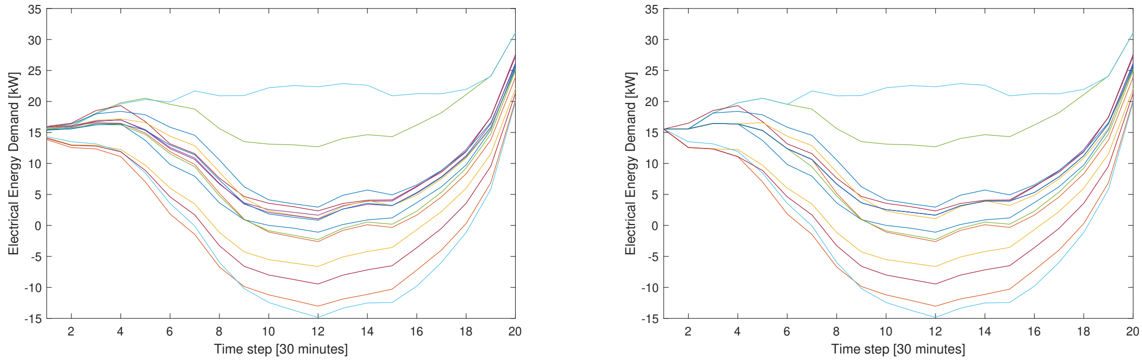

Figure 5-2: An example of 15 electric scenarios used in scenario-based (left) and tree-based model predictive control(right).

and the commercial and residential thermal energy consumption are added to each other. The structures of the trees should be similar to obtain feasibility using the non-anticipative constraint from Eq. (5-4). Therefore, the above described algorithm is used for constructing the electrical energy tree, and the obtained structure is copied to the thermal one. In Figure 5-2, it is seen how this method concludes in a tree structure of the generated scenarios for the electrical energy demand. A recommendation for future work is made in Section 7-3 on how to obtain the optimal trade-off between multiple stochastic trees in tree-based MPC. This optimal trade-off might improve the performance of the microgrid in comparison with copying the structure of one tree to the other, as done in this thesis.

5-3 Objective

A multi-objective optimization problem is defined considering the grid demand J_{gd}, economic J_{eco}, discomfort J_{dis}, and durability J_{dur} objectives. In this section, it is written how the different objectives are constructed that sum up the multi-objective function J as

$$J = \alpha J_{\text{eco}} + \beta J_{\text{dis}} + \gamma J_{\text{dur}} + \lambda J_{\text{gd}},$$

with α, β, γ, and λ being arbitrary predefined weights.

Economic

The economic costs of the microgrid are represented by the energy transfer costs of the microgrid. Operational costs caused by the increase in maintenance can in general be included [107], but is chosen to exclude them due to the difficult assumptions that need to be made to approximate these costs in the future microgrid. If these assumptions were made, they would influence the performance of the microgrid considerably, e.g., the operating costs of hydrogen-based components is currently much higher than these of electric-based ones. Therefore, the economic objective is written down as

$$J_{\text{eco}} = \sum_{\text{k}=1}^{\text{Np}} \left(C^{\text{el}}_{\text{UG}}(k) + C^{\text{gas}}_{\text{UG}}(k) + C^{\text{hyd}}_{\text{UG}}(k) \right),$$

where $C_{\mathrm{UG}}^{\mathrm{el}}$, $C_{\mathrm{UG}}^{\mathrm{gas}}$, and $C_{\mathrm{UG}}^{\mathrm{hyd}}$ are respectively the economic costs of the transferred electrical energy, 'green' gas, and hydrogen.

Discomfort

The discomfort for the consumers in the microgrid will mainly be influenced by the use of demand response. Furthermore, the range anxiety is included by penalizing a lower state of charge of an Electric Vehicle (EV). Another low penalization is placed on the amount of energy in the battery and hydrogen storage tank. This is penalized in a similar way as for the state of charge of the EVs. The discomfort objective can be written as

$$\begin{aligned} J_{\mathrm{dis}} = \sum_{\mathrm{k=1}}^{\mathrm{N_p}} \Bigg(&\rho_{\mathrm{c}}\beta_{\mathrm{c}}(k) + \rho_{\mathrm{r}}^{\mathrm{el}}\beta_{\mathrm{r}}^{\mathrm{el}}(k) + \rho_{\mathrm{r}}^{\mathrm{th}}\beta_{\mathrm{r}}^{\mathrm{th}}(k) + \frac{\rho_{\mathrm{EV}}}{N_{\mathrm{EV}}} \Bigg(\sum_{\mathrm{i=1}}^{\mathrm{N_{BEV}}} \frac{\overline{x}_{\mathrm{BEV,i}} - x_{\mathrm{BEV,i}}(k)}{\overline{x}_{\mathrm{BEV,i}}} \\ &+ \sum_{\mathrm{i=1}}^{\mathrm{N_{FEV}}} \frac{\overline{x}_{\mathrm{FEV,i}} - x_{\mathrm{FEV,i}}(k)}{\overline{x}_{\mathrm{FEV,i}}} \Bigg) + \rho_{\mathrm{bat}} \frac{\overline{x}_{\mathrm{bat}} - x_{\mathrm{bat}}(k)}{\overline{x}_{\mathrm{bat}}} + \rho_{\mathrm{hst}} \frac{\overline{x}_{\mathrm{hst}} - x_{\mathrm{hst}}(k)}{\overline{x}_{\mathrm{hst}}} \Bigg) \end{aligned} \tag{5-5}$$

where ρ_{c}, $\rho_{\mathrm{r}}^{\mathrm{el}}$ and $\rho_{\mathrm{r}}^{\mathrm{th}}$ are the penalty weight on curtailment and rescheduling of the electrical and thermal energy, respectively. The variables ρ_{EV}, ρ_{bat}, and ρ_{hst} are the penalties given on the state of charge of the total number of EVs (N_{EV}), the battery, and the hydrogen storage tank, respectively. The number of battery and fuel cell EVs in the microgrid are respectively noted as N_{BEV} and N_{FEV}

Durability

Frequent use of the EVs in vehicle-to-grid will result in faster degradation of these EVs. Despite fast degradation is partly prevented by the constraint in Eq. (3-2), a penalization is still applied to the use of the EVs in vehicle-to-grid for giving energy to the microgrid, to increase the durability of the EVs, as

$$J_{\mathrm{dur}} = \frac{1}{N_{\mathrm{EV}}} \sum_{\mathrm{k=1}}^{\mathrm{N_p}} \left(\sum_{\mathrm{i=1}}^{\mathrm{N_{BEV}}} \frac{z_{\mathrm{BEV,i}}^{\mathrm{g}}(k)}{\overline{z}_{\mathrm{BEV,i}}^{\mathrm{g}}} + \sum_{\mathrm{i=1}}^{\mathrm{N_{BEV}}} \frac{u_{\mathrm{FEV,i}}^{\mathrm{el}}(k)}{\overline{u}_{\mathrm{FEV,i}}^{\mathrm{el}}} \right), \tag{5-6}$$

where $z_{\mathrm{BEV}}^{\mathrm{g}} = \delta_{\mathrm{BEV}}^{\mathrm{g}} u_{\mathrm{BEV}}$ is chosen as introduced for the mixed logical dynamical modelling in Appendix A, where $\delta_{\mathrm{BEV}}^{\mathrm{g}}$ indicates if the battery EV is in generation mode as explained in Eq. (3-1).

Grid Demand

The maximum value of the electrical energy exchange per time step is penalized to reduce the needed investments in the electrical grid. Therefore, the absolute maximum energy transfer of the electricity is minimized using the weight ρ_{gd}. An auxiliary variable $\zeta_{\mathrm{ug}}^{\mathrm{el}}$ is introduced to maintain the linear objective function using $z_{\mathrm{UG}}^{\mathrm{el}} = \delta_{\mathrm{UG}}^{\mathrm{el}} u_{\mathrm{UG}}^{\mathrm{el}}$ as introduced for the mixed logical dynamical modelling in Appendix A. This results in the grid demand objective as

$$J_{\mathrm{gd}} = \rho_{\mathrm{gd}} \cdot \max_{k} |u^{\mathrm{el}}_{\mathrm{UG}}(k)| = \rho_{\mathrm{gd}} \cdot \zeta^{\mathrm{el}}_{\mathrm{UG}}, \text{ with}$$
$$\zeta^{\mathrm{el}}_{\mathrm{UG}} \geq 2z^{\mathrm{el}}_{\mathrm{UG}}(k) - u^{\mathrm{el}}_{\mathrm{UG}}(k), \quad k = 1, \ \ldots, \ \mathrm{Np}.$$

5-4 Conclusions

An MPC framework will be used to optimize the performance of the microgrid. A nominal MPC structure that considers the point forecasting values is used and a low-level controller is developed to adjust for the errors in the forecast during the optimization. Furthermore, two stochastic MPC methods that consider the uncertainty of the point forecasts, scenario- and tree-based MPC, are implemented. For these stochastic methods, scenarios are generated considering their interdependence structure between time steps in the day and prediction horizon. A tree structure of the scenarios is constructed based on bounds. Moreover, the control objective is described as containing an economic, discomfort, durability, and grid demand component.

Chapter 6

Simulations and Results

In this chapter, simulations are done in different case studies to obtain results to answer the research question of this thesis. The set-up of the case studies is formulated. Three scenarios that consider different levels of penetration of hydrogen in the microgrid are defined. Furthermore, the differences between the case studies and an overview of the performance indices are presented. Specifications of the simulations and assumptions made in this thesis are presented as well. Then, the results of each case study are discussed. Both conclusions on the different performances of the constructed scenarios and on the performance of stochastic Model Predictive Control (MPC) strategies are made.

6-1 Setup of the Case Studies

In this section, firstly, a microgrid is formulated for each scenario. Secondly, the case studies and their differences are presented. Thirdly, the performance indices are formulated. Then, an overview of the main assumptions made in this thesis is presented. Lastly, the details of the simulations are discussed.

6-1-1 Microgrids

The microgrids in the case studies consist of the distributed energy resources listed in Section 2-2. The number of distributed energy resources and their maximum power is partly chosen by making a realistic investment based on the energy demand and partly by obtained ratios from data.

Buildings To estimate the energy demand of the microgrid, the number of buildings in the microgrid is chosen. A ratio of 42:1 for residential to small commercial buildings is calculated based on data in Amsterdam [12]. Therefore, it is chosen to construct a microgrid with 42 residential buildings and one small commercial building. It is chosen not to include more buildings since this will increase the computation time due to an increase of decision variables.

Demand Response In each residential building, a dishwasher, with an energy consumption of 0.78 kWh that is used five times a week, is chosen to participate in the Demand Response (DR) program as rescheduable load. Furthermore, 10% of the real consumed thermal energy demand in residential buildings can be rescheduled and another 10% curtailed.

Electric Distributed Energy Resources Photovoltaic (PV) panels are installed on each building with an average power of 3.34 kW, estimated from the research done in [20]. This yields a 143.62 kW maximum power of solar panels in the microgrid. A district battery with a maximum storage capacity of 500 kWh and a maximum power of 150 kW is considered. It is assumed that the battery does not discharge below 10% of its maximum capacity and has a charging and discharging efficiency of 90%. An electrolyzer is used with a maximum power consumption of 25 kW containing an integrated hydrogen storage system of 500 kg. It is assumed that the storage level does not drop below 5% of the maximum storage. Since an efficiency of the electrolyzer of 70% and a heating value of hydrogen of 39.4 kWh/kg [9] are assumed, the model parameter α_{elc} is estimated to be 0.02 kg/kWh.

Thermal Distributed Energy Resources A hybrid heat pump is installed with a maximum power of 20 kW. The efficiency for the electric part is 400%, assuming similar ground temperatures as in the United Kingdom [55]. The boiler in the hybrid heat pump that burns gas has an efficiency of 90% for both 'green' gas and hydrogen. Furthermore, a 5 kW μ-Combined Heat and Power (CHP) plant is installed with a thermal storage capacity of 70 kWh. The efficiency for the electrical energy and thermal energy are 22.5% and 67.5% for the $\mu-$CHP plant with an internal combustion engine, respectively, and both 45% for the $\mu-$CHP plant with a fuel cell.

Electric Vehicles The current ratio for the number of vehicles per building is 1.09 [32]. In this thesis, it is chosen to lower this ratio for the future scenario and a single Electric Vehicle (EV) per household is considered. Battery EVs with a charging and discharging efficiency of 90% and a maximum battery storage capacity of 100 kWh are used. Their charging or discharging power is set to be a maximum of 16 kW. The fuel cell EVs in the microgrid have a fuel storage of 7 kg of hydrogen with a refilling rate of 2 kg/h. Since this EV operates on partial load in the microgrid, the maximum power is set to be at 15 kW. The model parameters α_{FEV} and β_{FEV} for the fuel cell EVs are based on the model of fuel cell stacks in [113] and are determined to be 0.06 kg/kWh and 0.11 kg/h, respectively [9].

Scenarios

Three scenarios with a different level of penetration of hydrogen in the microgrid are considered. The energy and thermal demand is similar for each scenario. Therefore, a fair comparison can be made about how the introduction of hydrogen to the microgrid will influence the performance. The following three scenarios are considered:

1. **Electric**: In this scenario, no hydrogen is present in the microgrid, excluding the presence of the electrolyzer with an integrated hydrogen storage tank and fuel cell EVs.

The hybrid heat pumps and μ-CHP plant can run on 'green' gas that is imported from the utility grid.

2. **Mixed**: This scenario is based on the expected microgrid assuming the developments explained in Section 2-1-3. Both electric- and hydrogen-based components are present in the microgrid. However, no 'green' gas is considered since hydrogen will be using the current natural gas infrastructure. Using both gases will lead to an extra gas network that is preferred to be avoided since the extra investments needed will probably overrule the potential profit. Therefore, the hybrid heat pumps and μ-CHP plant will contain fuel cells to run on hydrogen instead of the 'green' gas. Furthermore, the electrolyzer with an integrated hydrogen storage tank is included in the microgrid. Both types of EVs are present and a ratio of 1.5:1 for the battery to the fuel cell EVs is used [20].

3. **Hydrogen**: In this scenario, a largely hydrogen-based microgrid is sketched. The microgrid consists of almost the same distributed energy resources as in the mixed scenario, only the battery is excluded from the microgrid. Furthermore, all the battery EVs are replaced by fuel cell EVs.

A schematic overview of the scenarios is found in Appendix G. In Table 6-1, the difference in the fixed investment costs due to the different distributed energy resources in each scenario is presented. These investment costs are based on the specifications presented in Section 2-2. Introducing hydrogen in the microgrid increases the investment costs by 9.15%. This increase is due to including the electrolyzer with an integrated hydrogen storage tank and changing the hybrid heat pumps to run on hydrogen instead of 'green' gas. Especially the investment costs for hydrogen-based hybrid heat pumps are high and contributed to approximately 90% of the increase in investments. For the hydrogen scenario, the battery is excluded, decreasing the investment by 24.36% compared to the mixed scenario. These differences in the fixed investment costs need to be acknowledged when concluding on the scenarios in the case studies.

Table 6-1: Fixed investment costs for the distributed energy resources in the microgrid for the different proposed scenarios in the year 2050.

Scenario	Electric	Mixed	Hydrogen
Investment costs yearly [€]	56,410.70	61,570.70	46,570.70
Investment costs weekly[€]	1,081.85	1,180.81	893.14

6-1-2 Difference in Case Studies

Three case studies are considered that represent different energy demand and generation patterns. A strong difference for the energy demand and PV power generation throughout the year is concluded from the analysis of the stochastic processes in Chapter 4. Therefore, it is chosen to simulate a typical winter and summer week in the Netherlands. These two case studies are analyzed, and it is concluded what type of week the most energy transfer between the microgrid and utility grid is expected. Then, a week with extreme conditions is constructed where the most energy transfer between the microgrid and utility grid is expected. This case study indicates the minimum electrical energy grid investment needed to guarantee the reliability of the microgrid. From these different case studies, an overview of the average costs during the year can be sketched based on the summer and winter case study. Furthermore, the minimum electrical energy grid investments can be obtained by the extreme condition case study.

6-1-3 Performance Indices

The performance of the tertiary control of the microgrid is measured by quantitative and qualitative performance indices. In the quantitative performance indices, the performance is measured in economic costs. The qualitative performance indices are estimated as a ratio between 0 and 1, resembling a better performance with a higher value. An overview of these different performance indices for the simulation time T are:

Quantitative performance indices

- **Electrical grid investment:** The peak of electrical energy transfer is translated to variable economic investments needed to be paid by the energy suppliers following the current prices of Stedin in 2020 [121]. It is assumed that for all the microgrids a 'MS' connection [121] is established with its corresponding fixed investments. Hence, economic costs can be associated with the rise of the peak electrical energy transfer, i.e., €2.4147 per month (T_{m}) per maximum transferred energy in kW. This results in the equation for the electrical grid investment as

$$EGI = 2.4147 \cdot \frac{T}{T_{\mathrm{m}}} \zeta_{\mathrm{UG}}^{\mathrm{el}}$$

- **Energy import costs:** The netted economic costs of the microgrid by purchasing and selling energy is calculated as

$$EIC = \sum_{\mathrm{k}=1}^{\mathrm{T}} \left(C_{\mathrm{UG}}^{\mathrm{el}}(k) + C_{\mathrm{UG}}^{\mathrm{gas}}(k) + C_{\mathrm{UG}}^{\mathrm{hyd}}(k) \right)$$

Qualitative performance indices

- **Comfort level:** The discomfort costs as estimated in the objective function in Eq. (5-5) are rewritten as a normalized comfort level for the consumers. This comfort level is estimated by normalizing Eq. (5-5) by its weights, considering the comfort decrease due to participation in DR, the influence of range anxiety, and battery state of charge. The comfort level is calculated as

$$CL = 1 - \frac{J_{\mathrm{dis}}}{\rho_{\mathrm{c}} + \rho_{\mathrm{r}}^{\mathrm{el}} + \rho_{\mathrm{r}}^{\mathrm{th}} + \rho_{\mathrm{EV}} + \rho_{\mathrm{bat}} + \rho_{\mathrm{hst}}}$$

- **Durability of EV:** The durability of the EVs is influenced by the possible intensive usage in vehicle-to-grid and is also penalized in the objective function as Eq. (5-6). A durability ratio for the EVs is calculated that identifies the ratio of vehicle-to-grid used when not on transportation $\left(\delta^{\mathrm{t}} = 0\right)$. The durability ratio for the EVs is calculated as

$$DEV_{\mathrm{num}} = \sum_{\mathrm{k=1}}^{\mathrm{T}} \left(\sum_{\mathrm{i=1}}^{\mathrm{N_{BEV}}} \left(1 - \delta_{\mathrm{i}}^{\mathrm{t}}(k)\right) \frac{z_{\mathrm{BEV,i}}^{\mathrm{g}}(k)}{\overline{z}_{\mathrm{BEV,i}}^{\mathrm{g}}} + \sum_{\mathrm{i=1}}^{\mathrm{N_{BEV}}} \left(1 - \delta_{\mathrm{i}}^{\mathrm{t}}(k)\right) \frac{u_{\mathrm{FEV,i}}^{\mathrm{el}}(k)}{\overline{u}_{\mathrm{FEV,i}}^{\mathrm{el}}} \right)$$
$$DEV = 1 - \frac{DEV_{\mathrm{num}}}{\sum_{\mathrm{k=1}}^{\mathrm{T}} \sum_{\mathrm{i=1}}^{\mathrm{N_{EV}}} \left(1 - \delta_i^{\mathrm{t}}(k)\right)}$$

- **Electric self-supply:** A microgrid can be rated by the ability to use the generated energy in the microgrid as proposed in [29,30,58], i.e., not selling the energy if there is an abundance. The electric self-supply performance index calculates the ratio between the exported and generated electrical energy in the microgrid, where $(\cdot)^{\mathrm{th}}$ can be presenting hydrogen or 'green' gas in kWh dependent on the scenario, as

$$ESS = 1 - \frac{\sum_{\mathrm{k=1}}^{\mathrm{T}} \left(z_{\mathrm{UG}}^{\mathrm{el}}(k) - u_{\mathrm{UG}}^{\mathrm{el}}(k)\right)}{\sum_{\mathrm{k=1}}^{\mathrm{T}} \left(P_{\mathrm{PV}}(k) + P_{\mathrm{CHP}}(k)\right)}$$

- **Energy independence:** The energy independence of a microgrid can be rated by calculating the ratio of imported energy to the consumed energy [29, 30, 71, 73]. The energy independence is a measure for self reliance of a microgrid. It explains the ability of a microgrid to deal with unexpected excessive demand. Similar to the self-supply performance index, $(\cdot)^{\mathrm{th}}$ can be presenting hydrogen or 'green' gas in kWh dependent on the scenario. Furthermore, the trip costs of the fuel cell EVs are also written in kWh. The energy independence of the microgrid is calculated as

$$EI_{\mathrm{den}} = \sum_{\mathrm{k=1}}^{\mathrm{T}} \Bigg(P_{\mathrm{res}}(k) + P_{\mathrm{com}}(k) + Q_{\mathrm{res}}(k) + Q_{\mathrm{com}}(k)$$
$$+ \sum_{\mathrm{k=1}}^{\mathrm{N_{BEV}}} \left(h_{\mathrm{BEV,i}}(k)\right) + \sum_{\mathrm{k=1}}^{\mathrm{N_{FEV}}} \left(h_{\mathrm{FEV,i}}(k)\right) \Bigg)$$
$$EI = 1 - \frac{\sum_{\mathrm{k=1}}^{\mathrm{T}} \left(z_{\mathrm{UG}}^{\mathrm{el}}(k) + z_{\mathrm{UG}}^{\mathrm{th}}(k)\right)}{EI_{\mathrm{den}}}$$

6-1-4 Assumptions

Different assumptions are made in the simulations in the case studies to simplify the model or as a result of the absence of data. The main assumptions are:

1. Tertiary control optimization is performed in this study and deals with the long-term behaviour of the microgrid. It is assumed that the influences of the fast dynamics in the system are minimal to the performance of the distributed energy resources. Therefore, a steady-state where no loss of accuracy is considered for the distributed energy resources in the microgrid is assumed.

2. A constant ratio between energy and power per time step is assumed due to the constant sampling $\Delta T = T(k+1) - T(k)$.

3. The energy can flow unconditionally throughout the microgrid. The consumers have agreed that the central controller regulates the energy flow to optimize the total performance, even when the performance will locally be decreased.
4. The energy demand of the buildings in the microgrid and the energy generated by the PV panels are available by using the proposed forecasting methods.
5. The central controller can decide the participation in DR actions of the consumers.
6. The specifications of the distributed energy resources in the microgrid related to efficiency are assumed to be similar to current specifications. All the specifications of these distributed energy resources are known by the central controller.
7. Future arrival and departure times of the EVs are known. Therefore, the controller knows when the EVs can be used for vehicle-to-grid operations and if they have enough energy upon departure.
8. The purchasing and sale prices of energy are known and are based on a time-of-use pattern. The electrical energy has a weekly pattern containing different prices at each time step. The prices of 'green' gas and hydrogen are constant throughout the simulation.

6-1-5 Simulations

Each simulation in the case studies consists of eight consecutive days whereof the first day is used for initialization. Thus, the results are based on the last seven days of the simulation. The simulation starts on a Monday and ends on the next Monday. It is chosen to use this order to include the influences of the weekend on the first weekday. Time steps of 30 minutes are taken to get an accurate model, but decreasing the computational complexity compared to smaller time steps. The PV power and thermal energy demand are interpolated to obtain data per 30 minutes. A prediction horizon of eight hours is used since a longer prediction horizon did not improve the results on the performance indices, sometimes even worse, and increased the computational complexity.

In each case study, the scenarios are compared to each other using nominal MPC controllers. A 'perfect' controller is included as well that resembles the best performance possible while assuming point forecasts without errors. Then, the different control strategies are compared for the mixed scenario to conclude if stochastic MPC control strategies could improve the performance of the microgrid. The mixed scenario is chosen since it approaches the expected future microgrid, as sketched in Section 2-1-3. These stochastic MPC control strategies both used 20 scenarios since for a larger number of scenarios the computation time was decided to be too long. The energy flows between the microgrid and the utility grid in each simulation are presented in Appendix H.

The mixed-integer linear programming problem is solved in the Matlab R2020a environment using Gurobi [57]. A HP EliteBook 8570w with a 2.3 GHz Intel Core i7 processor and 4 GB of RAM is used for the simulations. Different computation times are obtained for the controllers in each case study and scenario. In general, the computation time increases with a higher energy demand in the case study. The computation time for the week with extreme conditions are approximately 3 hours, 11 hours, and 78 hours for the nominal, scenario-based, and tree-based MPC, respectively.

6-2 Case Study A: Winter Week

In this case study, an average winter week in the Netherlands is simulated. This week represents a microgrid with a relatively high thermal energy demand due to the cold ambient temperatures and lower PV power generation due to the lower solar irradiation in winter than in summer. Moreover, the electrical energy consumption is higher than in the summer due to the shorter daylight. It is expected that the microgrids show low energy independence, resulting in a large amount of energy transfer between the microgrid and utility grid. First the different results in this case study for the scenarios are discussed. Then, the performances of the stochastic MPC strategies are compared for the mixed scenario.

6-2-1 Scenarios of Hydrogen Penetration

The introduction of hydrogen to the microgrid results in a lower peak of electrical energy transfer and, therefore, lowers the investment costs in the electrical energy grid, as concluded from Table 6-2. The results show a strong decrease in maximal energy transfer of 29.33% and 86.75% while a decrease in electrical energy demand by the replacement of battery to fuel cell EVs of 8.39% and 26.79% is realized for the mixed and hydrogen scenario, respectively. However, the energy import costs increase substantially. The hydrogen-based microgrid have a higher total costs due the higher 80% higher price of hydrogen per kWh than electrical energy. Moreover, more energy is consumed due to reduce the peak of electrical energy transfer and the low efficiency of the fuel cell, resulting in even a higher total costs. Decreasing the price of hydrogen to that of electrical energy only has a marginal effect on the total costs. To reduce the total costs of the hydrogen-based microgrid it is more appealing to increase the efficiency of the fuel cells.

For the mixed scenario, a decrease in comfort level is seen compared to the other scenarios in Table 6-3. From Table 6-5, only a small difference is seen in the use of DR and the decrease of comfort level is mostly due to the lower state of charge of the EVs, battery, and hydrogen storage tank. This decrease in comfort level based on the lower state of charge of the EVs is in line with the decrease in the durability of the EVs for the mixed scenario, i.e., more intensive use of vehicle-to-grid operations.

The electric self-supply of the microgrids is roughly the same for each scenario. The difference between the ‘perfect’ and nominal controller for each scenario is due to the exported energy to adjust for the errors in the forecasts. The high values of the electric self-supply are explained by the fact that the PV power generation is low in the winter and the generated electrical energy can be consumed by the microgrid at all times.

The energy independence of the microgrids shows a negative trend for the introduction of hydrogen, i.e., it decreases with the introduction of more hydrogen in the microgrid. This decrease is partially caused by the lower efficiency of hydrogen to electrical energy in the fuel cells used for driving and vehicle-to-grid operations.

A noteworthy observation is made that the thermal energy demand is for more than 98% satisfied by converting electrical energy to thermal energy for all the scenarios, i.e., almost no ‘green’ gas or hydrogen is consumed to generate thermal energy. Therefore, the μ-CHP plant is not operating much of the time, resulting in the question if it should be excluded in the microgrid resulting in a decrease of investments for the distributed energy resources. This reasoning also applies to the boiler parts of the hybrid heat pumps. An explanation for this unexpected result is the higher price of 'green' gas and hydrogen in the future compared to the current price of natural gas. Furthermore, the high efficiency of the electric heat pump amplifies the difference in economic costs between the gases and electrical energy even more. These developments cause that it is economically more beneficial to consume electrical energy than gas for the generation of thermal energy.

In conclusion, the overall performance of the microgrid in winter decreases with a higher penetration of hydrogen in the microgrid, as seen in Table 6-4. On the other hand, on a purely economic level, the electrical energy grid investment can be substantially reduced against extra import energy costs.

Table 6-2: Results of quantitative performance indices for the scenarios in the winter week.

Scenario	Electric		Mixed		Hydrogen	
Controller	Perfect	Nominal	Perfect	Nominal	Perfect	Nominal
EGI [€]	358.56	338.03	242.47	238.87	45.09	47.50
EIC [€]	383.59	408.70	665.60	711.29	1,103.07	1,114.57
Total costs [€]	743.25	746.73	908.07	950.16	1,148.16	1,162.07

Table 6-3: Results of qualitative performance indices for the scenarios in the winter week.

Scenario	Electric		Mixed		Hydrogen	
Controller	Perfect	Nominal	Perfect	Nominal	Perfect	Nominal
CL	0.6493	0.6379	0.5811	0.5873	0.6583	0.6320
DEV [10^3]	0.7512	0.7554	0.62392	0.6230	0.7367	0.7424
ESS	1.0000	0.8448	1.0000	0.8414	1.0000	0.8660
EI	0.6385	0.5956	0.5573	0.5171	0.4345	0.4075

Table 6-4: Calculated relative objectives of the optimizations in the winter week.

Scenario	Electric		Mixed		Hydrogen	
Controller	Perfect	Nominal	Perfect	Nominal	Perfect	Nominal
Objective	1.0000	1.0272	1.3727	1.4474	1.9742	2.0017

Table 6-5: Residential energy demand used in demand response in the winter week.

Scenario	Electric		Mixed		Hydrogen	
Controller	Perfect	Nominal	Perfect	Nominal	Perfect	Nominal
Electrical rescheduled [kWh]	92.74	90.02	96.56	68.88	43.78	72.89
Thermal rescheduled [kWh]	5.65	14.29	13.67	3.73	48.51	38.00
Thermal curtailed [kWh]	848.23	902.37	874.29	893.29	863.84	898.25

6-2-2 Stochastic Control Strategies

The implementation of stochastic control strategies to the mixed scenario increases the overall performance compared to the nominal MPC strategy, as can be concluded Table 6-8. As expected, tree-based MPC performs better than scenario-based MPC. However, one should remember that the computation time is significantly increased by using tree-based MPC.

A distinction in focus for the different stochastic control strategies is seen from Table 6-6 and 6-7, i.e., while scenario-based MPC tends to focus more on reducing the import costs and increasing the comfort level, tree-based MPC focuses more on reducing the investments of the electrical energy grid investments. Moreover, the scenario-based strategy has an overall increase in economic costs but obtains good results for the comfort level due to the low usage in DR, as seen in Table 6-9. It is seen that compared to nominal MPC, the implementation of scenario-based MPC results in more degradation of the EVs, while tree-based MPC results in less degradation of the EVs.

The electric self-supply and energy independence are both decreased for scenario-based MPC and increased for tree-based MPC, compared to the nominal controller. These lower values for these performance indices indicate lower self-reliance of the scenario-based MPC controller. Note that the energy independence of the microgrids is also partly lowered due to the higher total energy consumption since almost no thermal energy curtailment is realized.

The difference in focus can be explained by the working principle of the different controllers. Scenario-based MPC optimizes a single sequence of decision variables for all the generated scenarios. However, the decision variables representing the behaviour of the electric utility grid are unique for each scenario. Averaging the cost function stimulates to lower the import energy costs and DR since they have a similar effect for each scenario, while the peak of electrical energy transfer changes with a lower relative degree. Thus, these decisions lead to a lower value for the cost function. Tree-based MPC considers multiple scenarios with their own decision variables when branched in the prediction horizon $N_\mathrm{p} > 1$. Therefore, the controller decides to import more energy beforehand, i.e., in the implemented control input for $N_\mathrm{p} = 1$, preventing excessive electrical energy transfer for the higher energy demand scenarios. Hence, more energy is stored and the peak of electrical energy transfer is lowered compared to the nominal controller. However, this results in buying energy sometimes at a higher cost price, explaining the increase in import energy costs compared to the nominal controller.

Table 6-6: Results of quantitative performance indices for the different control strategies for the mixed scenario in the winter week.

Controller	Perfect	Nominal	Scenario	Tree
EGI [€]	242.47	238.87	468.61	193.82
EIC [€]	665.60	711.29	605.83	718.28
Total costs [€]	908.07	950.16	1,074.44	912.10

Table 6-7: Results of qualitative performance indices for the different control strategies for the mixed scenario in the winter week.

Controller	Perfect	Nominal	Scenario	Tree
CL	0.5811	0.5873	0.7241	0.5931
DEV [10^3]	0.6292	0.6230	0.5382	0.6702
ESS	1.0000	0.8414	0.7222	0.9461
EI	0.5573	0.5171	0.4420	0.5191

Table 6-8: Calculated relative objectives of the different control strategies for the mixed scenario in a winter week.

Controller	Perfect	Nominal	Scenario	Tree
Objective	1.0000	1.0544	1.04054	1.0335

Table 6-9: Residential energy demand used in demand response for the different control strategies for the mixed scenario in the winter week.

Controller	Perfect	Nominal	Scenario	Tree
Electrical rescheduled [kWh]	96.56	68.88	58.90	54.68
Thermal rescheduled [kWh]	13.67	3.73	0.00	15.82
Thermal curtailed [kWh]	874.29	893.29	18.11	907.46

6-3 Case Study B: Summer Week

An average summer week in the Netherlands is used to simulate the performance of the different microgrids in a relatively low energy demand environment. Furthermore, a large amount of PV power can be obtained due to the high amount of solar irradiation in the summer, causing potential problems to the electric self-supply of the microgrid, i.e., too much energy is generated to consumer or store in the microgrid. It is expected to see a considerable reduction in the economic costs for the import of energy and investments for the electrical energy grid. First the different results in this case study for the scenarios are discussed. Then, the performances of the stochastic MPC strategies are compared for the mixed scenario.

6-3-1 Scenarios of Hydrogen Penetration

Almost similar behaviour between the scenarios is seen for the summer week compared to the winter week. The introduction of hydrogen lowers the electrical energy grid investments but increases the imported energy costs, as seen in Table 6-10. Therefore, the total economic costs of the microgrid increase with a higher level of penetration of hydrogen in the microgrid. Moreover, this rise in economic costs concludes to a poorer performance of the microgrid, as concluded from Table 6-12.

For all the scenarios, the electrical energy grid investments are higher in the winter case. Therefore, it can be concluded that a lower penalization can potentially be used on the maximum energy transfer in the summer to reduce the other costs. Moreover, it is concluded that the electrical energy grid investments will not be based on extreme conditions in the summer but in the winter.

For the qualitative performance indices in Table 6-11, a similar trend is visible for the comfort level compared to the winter case. The comfort level is mainly based on the stored energy in the EVs and storage system since almost no energy is used in DR, as seen in Table 6-13. Note that no thermal energy is rescheduled or curtailed. For a full hydrogen microgrid, a substantial increase in the durability of the EVs is realized. Furthermore, the energy independence index lowers considerably while using more hydrogen. This large difference is due to the fact that the hydrogen demand of the fuel cell EVs have a large mark on the total energy demand due to the lower energy demand of the buildings. The electric self-supply is almost the same for each scenario. Therefore, it can be concluded that each scenario can cope with the abundance of energy by the PV panels equally well. Similar as to the winter week, almost no 'green' gas or hydrogen is consumed to generate thermal energy.

Table 6-10: Results of quantitative performance indices for the scenarios in the summer week.

Scenario	Electric		Mixed		Hydrogen	
Controller	Perfect	Nominal	Perfect	Nominal	Perfect	Nominal
EGI [€]	280.32	271.31	170.88	172.78	12.09	33.54
EIC [€]	45.95	53.02	190.73	211.45	445.91	510.66
Total costs [€]	326.27	324.33	361.61	384.24	458.00	544.20

Table 6-11: Results of qualitative performance indices for the scenarios in the summer week.

Scenario	Electric		Mixed		Hydrogen	
Controller	Perfect	Nominal	Perfect	Nominal	Perfect	Nominal
CL	0.8901	0.8826	0.7431	0.7432	0.8358	0.8258
DEV [10^3]	0.6705	0.6795	0.6355	0.6349	0.8099	0.8031
ESS	1.0000	0.7973	1.0000	0.8007	1.0000	0.8034
EI	0.7938	0.7073	0.4731	0.3831	0.2481	0.1347

Table 6-12: Calculated relative objectives of the optimizations in the summer week.

Scenario	Electric		Mixed		Hydrogen	
Controller	Perfect	Nominal	Perfect	Nominal	Perfect	Nominal
Objective	1.0000	1.0203	1.5047	1.6320	2.5884	2.8544

Table 6-13: Residential energy demand used in demand response in the summer week.

Scenario	Electric		Mixed		Hydrogen	
Controller	Perfect	Nominal	Perfect	Nominal	Perfect	Nominal
Electrical rescheduled [kWh]	0.00	14.08	0.00	0.00	3.80	22.09

6-3-2 Stochastic Control Strategies

The stochastic control strategies did not improve the overall performance of the microgrid in the mixed scenario compared to nominal MPC, as observed from Table 6-16. Scenario-based MPC originally performed worse but setting constraints on the maximum electrical energy transfer, i.e., a maximum energy transfer per time step of 50% higher than the computed maximal energy transfer of the nominal MPC, improved its performance. This reduced the peak of electrical energy transfer that was computed first but still not enough to provide better results than the nominal controller. The bad performance of the stochastic control strategies could be caused by a high difference in the thermal energy since the probabilistic forecasting in Section 4-5 uses a single cumulative distribution for the entire year. Therefore, the scenarios consider unlikely high thermal demands resulting in a decrease in the performance for the stochastic control strategies. Improvements could be made by considering a different cumulative distribution for the thermal demand in the summer. Another explanation can be that poorer performance for the global objective is obtained since the global objective of the simulation differentiates from the partial objective during the MPC strategy. This can occur since the electrical energy grid investment is based on the peak of electrical energy transfer throughout the whole simulation, but is penalized at each time step. Furthermore, similar trends between scenario-based and tree-based MPC are seen in Table 6-14 and 6-15 compared to the winter week. No energy is rescheduled or curtailed for all the different control strategies.

Table 6-14: Results of quantitative performance indices for the different control strategies for the mixed scenario in the summer week.

Controller	Perfect	Nominal	Scenario	Tree
EGI [€]	170.88	172.78	254.40	156.11
EIC [€]	190.73	211.46	177.22	227.98
Total costs [€]	361.61	384.24	431.62	384.09

Table 6-15: Results of qualitative performance indices for the different control strategies for the mixed scenario in the summer week.

Controller	Perfect	Nominal	Scenario	Tree
CL	0.7431	0.7432	0.7452	0.7404
DEV [10^3]	0.6355	0.6349	0.6710	0.6827
ESS	1.0000	0.8007	0.7347	0.9036
EI	0.4731	0.3831	0.3453	0.3883

Table 6-16: Calculated relative objectives of the different control strategies for the mixed scenario in a summer week.

Controller	Perfect	Nominal	Scenario	Tree
Objective	1.0000	1.0846	1.1087	1.1083

6-4 Case Study C: Week with Extreme Conditions

The overall peak is used to determine the electrical energy grid investments to assure the reliability of the microgrid. As expected and confirmed by the previous case studies, the worst performance and highest peak of electrical energy transfer is found in the winter. Therefore, in this case study, a winter week with extreme conditions for the Netherlands is simulated.

Since the maximum solar irradiance in the winter is low in the Netherlands, it is expected that this will be of significantly less importance compared to the thermal energy demand. Therefore, the focus is on a week with extreme cold temperatures. The week of 30 January 2012 is found as an extremely cold week in the Netherlands with an average daily temperature of -5.9 °C with hourly outliers up to -17.8 °C. The PV power and commercial energy demand are calculated from the historical data of this week. However, for the residential energy demand, only data from the year 2013 is available. It is assumed that the ratio between the same week in 2013 is similar for the residential energy demand as for the commercial energy demand. A ratio is obtained and the residential energy demand for the chosen week in 2012 is calculated.

6-4-1 Scenarios of Hydrogen Penetration

The highest electrical grid investments are obtained for this week with extreme conditions for each scenario and similar trend are obtained as in the previous case studies, as seen in Table 6-17. A reduction in the electrical grid investments of 16.90% and 81.29% is obtained while a decrease in electrical energy demand by the replacement of battery to fuel cell EVs of 8.36% and 26.70% is realized for the mixed and hydrogen scenario, respectively. However, the prevented investments in the electrical grid are not enough to compensate for the increase in energy import costs for the scenarios containing hydrogen. Therefore, it is concluded that only based on economic incentives, the electric scenario performs the best. Moreover, the overall performance is better for the electric scenario as concluded from Table 6-19.

The increase of the electrical grid investments is rather low compared to the rise in the thermal (59.01%) and total energy demand (55.77%) of the microgrid. Therefore, the microgrid can cope with unexpected high energy demand in colder periods and no extra measures need to be applied for such weeks, e.g., emergency generators. Furthermore, still more than 95% of the thermal energy is generated by electrical energy in the scenarios

The qualitative performance indices show a similar underlying relationship between the scenarios compared to the winter case and are presented in Table 6-18 and 6-20. Therefore, similar conclusions are drawn as in Section 6-2-1. The main reason for the increase in the electric self-supply compared to the winter week is due to the percent increase of generated energy by the PV panels. Note that the energy generated by the PV panels is little compared to the total energy demand and has little influence on the performance of the microgrid.

Table 6-17: Results of quantitative performance indices for the scenarios in the week with extreme conditions.

Scenario	Electric		Mixed		Hydrogen	
Controller	Perfect	Nominal	Perfect	Nominal	Perfect	Nominal
EGI [€]	294.57	344.73	309.60	286.44	63.16	64.50
EIC [€]	525.69	547.60	798.74	849.84	1,168.61	1,256.90
Total costs [€]	820.26	892.33	1,108.34	1,136.28	1,231.77	1,321.40

Table 6-18: Results of qualitative performance indices for the scenarios in the week with extreme conditions.

Scenario	Electric		Mixed		Hydrogen	
Controller	Perfect	Nominal	Perfect	Nominal	Perfect	Nominal
CL	0.4536	0.4537	0.4387	0.4306	0.4656	0.4624
DEV [10^3]	0.7607	0.7648	0.6346	0.6450	0.7494	0.7497
ESS	1.000	0.9478	1.0000	0.9402	1.0000	0.9618
EI	0.6942	0.6760	0.6432	0.6081	0.5835	0.5406

Table 6-19: Calculated relative objectives of the optimizations in the week with extreme conditions.

Scenario	Electric		Mixed		Hydrogen	
Controller	Perfect	Nominal	Perfect	Nominal	Perfect	Nominal
Objective	1.0000	1.0662	1.3804	1.4379	1.7416	1.8676

Table 6-20: Residential energy demand used in demand response in the week with extreme conditions.

Scenario	Electric		Mixed		Hydrogen	
Controller	Perfect	Nominal	Perfect	Nominal	Perfect	Nominal
Electrical rescheduled [kWh]	120.22	122.85	120.67	122.11	104.85	98.06
Thermal rescheduled [kWh]	0.00	16.21	0.00	26.16	20.10	37.62
Thermal curtailed [kWh]	2,643.50	2,618.01	2,611.38	2,614.34	2,589.25	2,595.46

6-4-2 Stochastic Control Strategies

The stochastic control strategies for the mixed scenario outperform the nominal one, as concluded from Table 6-23. Similar trends for scenario-based and tree-based MPC as in the winter week are seen in Table 6-21, 6-22, and 6-24. Tree-based MPC shows a better overall performance than scenario-based MPC. Moreover, tree-based MPC lowers the peak of electrical energy transfer while increasing the energy import and discomfort costs for the consumer. Scenario-based MPC focuses more on the reduction of the energy import costs and increases the comfort level, resulting in a higher peak of electrical energy transfer.

Table 6-21: Results of quantitative performance indices for the different control strategies for the mixed scenario in the week with extreme conditions.

Controller	Perfect	Nominal	Scenario	Tree
EGI [€]	309.60	286.44	474.87	225.57
EIC [€]	798.74	849.84	772.55	870.26
Total costs [€]	1,108.34	1,136.28	1,247.42	1,095.83

Table 6-22: Results of qualitative performance indices for the different control strategies for the mixed scenario in the week with extreme conditions.

Controller	Perfect	Nominal	Scenario	Tree
CL	0.4387	0.4306	0.5821	0.4229
DEV [10^3]	0.6346	0.6450	0.5636	0.6568
ESS	1.000	0.9405	0.9477	0.9557
EI	0.6432	0.6081	0.5639	0.6016

Table 6-23: Calculated relative objectives of the different control strategies for the mixed scenario in the week with extreme conditions.

Controller	Perfect	Nominal	Scenario	Tree
Objective	1.0000	1.0416	1.0358	1.0325

Table 6-24: Residential energy demand used in demand response for the different control strategies for the mixed scenario in the week with extreme conditions.

Controller	Perfect	Nominal	Scenario	Tree
Electrical rescheduled [kWh]	120.67	122.11	118.46	116.86
Thermal rescheduled [kWh]	0.00	26.16	16.83	34.81
Thermal curtailed [kWh]	2,611.38	2,614.34	1,440.13	2,770.44

6-5 Conclusions

In this chapter, scenarios with different levels of penetration of hydrogen in the microgrid are sketched and the case studies are defined. Simulations are performed for each case study and it is concluded that the introduction of hydrogen decreases the peak of electrical energy transfer. At the same time, the introduction of hydrogen results in higher total economic costs due to the increase in the energy import costs. Furthermore, a strong decrease in energy independence for the microgrids with more hydrogen is obtained.

Stochastic MPC strategies are implemented in the different case studies and it is concluded that for weeks with high energy demand, i.e., the winter weeks, the stochastic MPC strategies outperform nominal MPC for the mixed scenario. For the summer week, the stochastic MPC strategies did not obtain better performance compared to nominal MPC. Specific trends are identified for the different stochastic control strategies. Scenario-based MPC focuses more on decreasing the energy import costs and increasing the comfort level, where tree-based MPC focuses more on minimizing the peak of electrical energy transfer and durability of the EVs. Tree-based MPC provides better performance than scenario-based MPC but results in a substantially larger computation time.

Chapter 7

Conclusions and Recommendations for Future Work

A summary of the work done in this thesis is presented in this chapter. Then, the research question and the two sub-questions for this thesis are answered. Lastly, recommendations for future work are given.

7-1 Summary

In this thesis, it is investigated how the introduction of hydrogen in a future microgrid influences the peak of electrical energy transfer between the microgrid and utility grid. The motivation behind this research is that in a future microgrid the energy demand is expected to rise, and more uncertainty is added to the microgrid by the introduction of renewable energy sources. These aspects can result in a higher peak of electrical energy transfer, resulting in needed economic investments in the electrical energy grid. Since hydrogen has not yet emerged in the microgrid or only on small scale, a future electric and thermal microgrid with residential and commercial consumers in the year 2050 in the Netherlands is sketched. Furthermore, smart upcoming strategies are implemented in the microgrid, i.e., vehicle-to-grid for the Electric Vehicle (EV) management and direct load control as implemented Demand Response (DR) program.

Different stochastic processes in the microgrid are forecasted, i.e., Photovoltaic (PV) power generation and energy demand of residential and commercial consumers. Multiple point forecasting models are analyzed and the model with the smallest root mean square error for each stochastic process is concluded. With the results of the point forecasting models, distributions of the forecasting errors are obtained by using quantile regression. Scenarios for each stochastic process are generated based on the point forecasting values and distributions of the errors, including the interdependence structure between time steps.

For the control of the microgrid, multiple Model Predictive Control (MPC) controllers are introduced. A nominal MPC controller is introduced and to include the errors of the forecast of the stochastic processes, stochastic MPC controllers are constructed: scenario-based and tree-based MPC. The tree structure of the stochastic processes in tree-based MPC is build up from the same scenarios used in scenario-based MPC, with clustering the scenarios if they appear too similar based on a defined bound. A linear multi-objective function is formulated and the microgrid is modelled as a mixed logic dynamical model, resulting in a mixed-integer linear programming problem that is solved.

Case studies are formulated to answer the research question and the different sub-questions of this thesis. The first two case studies show the results for an average summer and winter week in the Netherlands. From these results, a week with extreme conditions is formulated where the lowest performance of the microgrid is expected, i.e., the highest peak of electrical energy transfer, since the electrical energy grid should be designed for this largest obtained peak. In each case study, three scenarios with different levels of penetration of hydrogen in the microgrid are constructed: electric, mixed, and hydrogen. From these results, it is concluded how the performance of the microgrid changes with different levels of hydrogen penetration. Moreover, for the realistic hydrogen-based scenario in 2050 in the Netherlands, i.e, the mixed scenario, stochastic MPC strategies are compared to a nominal MPC controller to analyze if they improve the performance of the microgrid.

7-2 Conclusions

The effects of hydrogen on the peak of electrical energy transfer has been researched in this thesis. The research question of this thesis is:

> *How does the introduction of hydrogen to the microgrid influence the peak of electrical energy transfer between the microgrid and utility grid?*

To answer this question, the formulated sub-questions are first answered:

1. *What is the difference in the peak of electrical energy transfer for different microgrids with a different level of penetration of hydrogen?*
   This question can be answered from the obtained results of the scenarios of hydrogen penetration in each case study. It is concluded that a general trend is present for each case study between the scenarios. A higher level of hydrogen penetration in the microgrid reduces the peak of electrical energy transfer of the microgrid. However, the total economic costs increase due to the higher energy import costs. These higher energy import costs are mainly due to the more expensive fuel costs for fuel cell EVs compared to battery EVs. The fuel costs are more expensive due to the higher import price of hydrogen compared to electrical energy and the low efficiency in the fuel cells. It must be noted that the expected hydrogen price and low efficiency of the fuel cells influence the results of the optimization substantially and future research should focus on these developments.

   To quantify the reduction of the peak of electrical energy transfer and the total economic costs, the electrical energy grid investments are based on the week with extreme conditions. The energy import costs are calculated by averaging the costs in the typical winter and summer weeks, representing an approximation of the mean costs throughout the year. It is concluded that a reduction in the electrical grid investments is realized of 16.90% and 81.29% for the mixed and hydrogen scenario, respectively. However, the total economic costs are increased for the mixed and hydrogen scenario, respectively, by 16.36% and 6.81%. Excluding the investment costs of the distributed energy resources result in an increase in the economic costs of 29.92% and 52.38% for the mixed and hydrogen scenario, respectively.

The introduction of hydrogen results in lower energy independence of the microgrid, decreasing the self-reliance of the microgrid. This is caused due to the lower efficiency of the fuel cell compared to the battery. Another trend is that for the mixed scenario including both battery and fuel cell EVs, there is more degradation on the vehicles due to the higher use of the EVs in vehicle-to-grid operations. Furthermore, in the mixed scenario, a lower comfort level is obtained due to the lower state of charge of the EVs. No clear differences are concluded for the self-supply of the microgrids between the scenarios.

2. *Can stochastic MPC strategies improve the performance of the microgrid and will it reduce the peak of electrical energy transfer?*
   It is concluded that in the winter weeks, comprising the winter and extreme conditions case study, stochastic MPC strategies improve the performance of the microgrid. In the summer, no better performance is obtained using stochastic MPC strategies. Tree-based MPC performs better than scenario-based MPC, but increases the computation time by approximately 700%.

   A different focus on the objectives in the multi-objective optimization for the different stochastic MPC strategies is concluded. Implementation of scenario-based MPC increases the electrical energy grid investment costs but reduces the import energy costs. It results in overall higher economic costs compared to nominal MPC. The comfort level is higher in scenario-based MPC compared to the other controller, and there is a significant reduction in the use of DR in the winter weeks. Tree-based MPC lowers the electrical energy grid investments against higher energy import costs. This decision leads to lower total economic costs compared to nominal MPC. In conclusion, tree-based MPC reduces the peak of electrical energy transfer with a better overall performance of the microgrid in the winter weeks.

With the two sub-questions answered, an answer is formulated on the research question of this thesis. The introduction of hydrogen in the microgrid reduces the peak of electrical energy transfer against higher energy import costs. Therefore, the total economic costs of the microgrid and the overall performance increase with the introduction of hydrogen. Furthermore, the introduction of hydrogen in the microgrid shows a clear decrease in the energy independency of the microgrid. In a microgrid containing both battery and fuel cell EVs, it is concluded that more vehicle-to-grid operations are used compared to the microgrids including only one type of EV. Stochastic MPC methods improve the overall performance of a hydrogen-based microgrid in winter weeks, but do not lead to better overall performance compared to a microgrid without hydrogen. Tree-based MPC reduces the peak of electrical energy transfer compared to nominal MPC.

7-3 Recommendations for Future Work

Suggestions for future work on the continuation of this thesis and different problems encountered in the construction of this thesis are:

1. **Larger microgrids:** The fixed economic investments for the electrical energy grid rise considerably after reaching a certain threshold, e.g., for a peak higher than 1,500 kW [121]. Microgrids around this turning point can potentially obtain large economic benefits by introducing hydrogen. Therefore, the influence of hydrogen on these larger microgrids should be evaluated. Moreover, it should be analyzed if their performance alters compared to the considered microgrid in this thesis to conclude on the scalability of the microgrid.

2. **Decreasing computation time:** For the implementation of smaller time steps to improve the performance of the microgrid, or larger microgrids, the computation time for the MPC strategies can exceed the sampling time. Therefore, the effects of methods as distributed MPC, parameterized MPC, or by using a hybrid control scheme on the problem in this thesis should be analyzed. These methods will decrease the computation time against expected lower performance. Furthermore, these methods could provide the solution to implement the MPC controllers in real-time.

3. **Composition of future microgrid:** In the study, it was shown that with the implementation of hybrid heat pumps, almost no gas was consumed to satisfy the thermal energy demand in the microgrid. This raises the question of how the performance of the microgrid will be if only electric heat pumps are considered, reducing the investment costs for the heat pumps and removing the investments costs for the μ-Combined Heat and Power (CHP). Using only the electric heat pumps could change the performance in tertiary control, but the influences on the primary or secondary control of the microgrid should also be analyzed.

4. **Including operational costs:** Due to the hard prediction of the operational costs in the future microgrid, the operational costs are not included in the objective function in this thesis. However, including these operational costs will influence the economic costs of the microgrid substantially. Therefore, it can result in a different performance of the microgrid and potentially changes the preferred composition of the future microgrid. Research should be done to approximate these expected operational costs in the future microgrid and analyze their influence on a hydrogen-based microgrid.

5. **Stochastic arrival and departure times of EVs:** An important assumption made in this thesis is that the arrival and departure times of the EVs are known beforehand. By considering unknown departure times, forecasting models should be developed to predict the behaviour of this stochastic process. Furthermore, it is expected that different (lower) performance will be obtained for the microgrid that should be analyzed.

6. **Heat from fuel cells:** Heat is produced when hydrogen converts to electrical energy in the fuel cell. This heat can be transferred to the buildings to supply their thermal energy demand. It should be analyzed how this heat can be captured and used in the microgrid, causing an increase in the energy independence of the microgrid.

7. **Hydrogen price and efficiency:** Extensive research on the future price of imported hydrogen and the future efficiency of the fuel cells needs to be done. These specifications influence the performance of the microgrid considerably and can lead to lower energy import costs for the hydrogen-based microgrids.

8. **Multiple stochastic trees:** In this thesis, two different trees are considered in tree-based MPC. It is chosen to project the tree structure of one stochastic process to the other. However, probably better performance of the microgrid can be obtained if an optimal trade-off in the structure generation of the different trees is computed. Constructing an algorithm to define this trade-off can improve the performance in fields where multiple stochastic processes are present.

9. **Memorizing the peak of electrical energy transfer:** The optimization penalizes the maximum electrical energy transfer for the prediction horizon for every moment in the simulation. However, only the peak in the whole simulation is considered. Therefore, better performance of the microgrid could be obtained by memorizing the obtained highest peak of the electrical energy transfer in the closed-loop optimization of the microgrid and not penalizing the energy transfer for future lower values. This method was tried in the process of this thesis, but it resulted in an unreliable comparison due to the high influence on the time in which, during the simulation, the peak was obtained. A robust method should be constructed to prevent this problem.

Appendix A

Mixed Logic Dynamical Models

In this appendix, mixed logic dynamical models are explained and it is clarified how to derive a mixed logic dynamical form of the model. Moreover, an example is given of the derivation of a battery in mixed logic dynamical form.

A-1 Intermediate Steps in Deriving a Mixed Logic Dynamical Model

Mixed logic dynamical models can easily be derived from the insightful piecewise affine models. To derive to a mixed logic dynamical model, binary logic variables $\boldsymbol{\delta}$ are introduced to indicate to each mode from the piecewise affine model. Through this method, the system can be described by a single equation containing continuous and binary variables. The dynamics of the system changes in these different modes, so a link between the continuous and the logical variables needs to be established. Consider the statement that $\delta = 1 \iff f(x) \leq 0$, with $f : \mathbb{R}^n \longrightarrow \mathbb{R}$ is linear and $x \in \mathbb{X}$. The maximum and minimum of the function $f(x)$ are given as

$$\begin{aligned} M &\triangleq \max_{x \in \mathbb{X}} f(x) \\ m &\triangleq \min_{x \in \mathbb{X}} f(x) \end{aligned}.$$

Then, the statement can be transformed into two linear inequalities as

$$\delta = 1 \iff f(x) \leq 0 \text{ is true iff } \begin{cases} f(x) \leq M(1-\delta) \\ f(x) \geq \epsilon + (m - \epsilon)\delta \end{cases},$$

where ϵ is a small tolerance. This tolerance is needed to transform the constraint of the form $f(x) < 0$ to $f(x) \leq 0$, since only nonstrict inequalities are handled by mixed-integer linear or quadratic solvers [107]. These constraints are written as mixed-integer linear inequalities, i.e., inequalities containing both continuous and logical binary variables.

Nonlinearities can occur due to the multiplication of binary variables, and of binary and continuous variables. These nonlinearities can be transformed to linear inequalities by introducing auxiliary variables as in [19]. For example, a new variable is defined to account for a nonlinear equation in the model $z(x) = u(x)\delta(x)$ with

$$\begin{aligned} M &\triangleq \max_{x \in \mathbb{X}} u(x), \\ m &\triangleq \min_{x \in \mathbb{X}} u(x). \end{aligned}$$

This nonlinear statement is expressed by linear inequalities as

$$\begin{aligned} z(x) &\leq M\delta(x), \\ z(x) &\geq m\delta(x), \\ z(x) &\leq u(x) - m(1 - \delta(x)), \\ z(x) &\leq u(x) - M(1 - \delta(x)). \end{aligned}$$

The dynamics of the system and corresponding constraints can than be transformed in an easily linear standard mixed logical dynamical model as

$$\begin{aligned} x(k+1) &= Ax(k) + B_1 u(k) + B_2 \delta(k) + B_3 z(k) + B_4, \\ y(k) &= Cx(k) + D_1 u(k) + D_2 \delta(k) + D_3 z(k), \\ E_1 x(k) + E_2 u(k) &+ E_3 \delta(k) + E_4 z(k) \leqslant g_5. \end{aligned} \tag{A-1}$$

A-2 Example: Battery as Mixed Logic Dynamical Model

The dynamics of the battery can be described as explained in Section 3-1-1 with $\underline{x}_{\text{bat}} \leq x_{\text{bat}}(k) \leq \overline{x}_{\text{bat}}$ and $\underline{u}_{\text{bat}} \leq u_{\text{bat}}(k) \leq \overline{u}_{\text{bat}}$:

$$x_{\text{bat}}(k+1) = \begin{cases} x_{\text{bat}}(k) + \eta_{\text{bat}}^{\text{c}} u_{\text{bat}}(k), & \text{if } \delta_{\text{bat}}(k) = 1 \\ x_{\text{bat}}(k) + \frac{1}{\eta_{\text{bat}}^{\text{d}}} u_{\text{bat}}(k), & \text{if } \delta_{\text{bat}}(k) = 0 \end{cases}, \tag{A-2}$$

where the binary auxiliary variable δ_{bat} is to indicate whether the battery is charging ($\delta_{\text{bat}}(k) = 1$) or discharging ($\delta_{\text{bat}}(k) = 0$) at time step k. Therefore, the transferred energy $u_{\text{bat}}(k)$ at time step k to the battery can be defined as $\delta_{\text{bat}} = 1 \iff u_{\text{bat}}(k) \geq 0$.

A continuous auxiliary variable $z_{\text{bat}}(k) = u_{\text{bat}}(k)\delta_{\text{bat}}(k)$ is introduced to write the dynamics of the battery in Eq. (A-2) as a single equation:

$$x_{\text{bat}}(k+1) = x_{\text{bat}}(k) + \frac{1}{\eta_{\text{bat}}^{\text{d}}} u_{\text{bat}}(k) + \left(\eta_{\text{bat}}^{\text{c}} - \frac{1}{\eta_{\text{bat}}^{\text{d}}} \right) z_{\text{bat}}(k).$$

The extra constraints that will be added to the model to explain that $z_{\text{bat}}(k) = u_{\text{bat}}(k)\delta_{\text{bat}}(k)$ at time step k are

$$
\begin{aligned}
-\overline{u}_{\text{bat}+} z_{\text{bat}}(k) &\leq 0, \\
\underline{u}_{\text{bat}-} z_{\text{bat}}(k) &\leq 0, \\
-u_{\text{bat}}(k) - \underline{u}_{\text{bat}+} z_{\text{bat}}(k) &\leq -\underline{u}_{\text{bat}}, \\
u_{\text{bat}}(k) + \overline{u}_{\text{bat}-} z_{\text{bat}}(k) &\leq \overline{u}_{\text{bat}}.
\end{aligned}
$$

To tackle the degradation, as explained in Section 3-4-1, the following constraint is added:

$$
\begin{aligned}
&\delta_{\text{bat}}(k+1) - \delta_{\text{bat}}(k) - \delta_{\text{bat}}(\tau) \leq 0, \quad \tau = k+2, \ldots, t + T_{\text{C}_{\text{bat}}}, \\
&\delta_{\text{bat}}(k) - \delta_{\text{bat}}(k+1) + \delta_{\text{bat}}(\tau) \leq 1, \quad \tau = k+2, \ldots, t + T_{\text{D}_{\text{bat}}},
\end{aligned}
$$

where $T_{\text{C}_{\text{bat}}}$ and $T_{\text{D}_{\text{bat}}}$ are the minimum time the battery should be in charging or discharging mode, respectively.

The dynamics and constraints of the battery can be described in a standard mixed logical dynamic model as written in Eq. (A-1). This results in the equation:

$$
\begin{aligned}
x_{\text{bat}}(k+1) &= A x_{\text{bat}}(k) + B_1 u_{\text{bat}}(k) + B_3 z_{\text{bat}}(k), \\
E_1 x_{\text{bat}}(k) + E_2 u_{\text{bat}}(k) &+ E_3 \delta_{\text{bat}}(k) + E_4 z_{\text{bat}}(k) \leqslant g_5.
\end{aligned}
$$

Appendix B

Long Short-Term Memory Recurrent Artificial Neural Network

In this appendix, the mathematical description of the long short-term memory recurrent Artificial Neural Network (ANN) is presented. Then, different gradient descent algorithms are presented that can be used to train the ANN.

B-1 Mathematical Description of the Artificial Neural Network

A long short-term memory recurrent ANN computes a mapping from the input sequence $X = (x_1, \ldots, x_\mathrm{T})$ to an ouput sequence $Y = (y_1, \ldots, y_\mathrm{T})$. These are calculated iteratively from $t = (1, \ldots, T)$ using the equation [76, 114]:

$$\begin{aligned} i_t &= \sigma\left(W_{\mathrm{ix}} x_t + W_{im} m_{t-1} + b_i\right) \\ f_t &= \sigma\left(W_{fx} x_t + W_{fm} m_{t-1} + b_f\right) \\ c_t &= f_t \odot c_{t-1} + i_t \odot g\left(W_{cx} x_t + b_c\right) \\ o_t &= \sigma\left(W_{ox} x_t + W_{om} m_{t-1} + b_o\right) \\ m_t &= o_t \odot h\left(c_t\right) \\ y_t &= \phi\left(W_{ym} m_t + b_y\right) \end{aligned},$$

where W is the weight matrix, e.g., W_{ix} is the weight matrix from the input gate to the input. Furthermore, σ, b, i, f, c, m, and o are respectively the logistic sigmoid function, bias vectors, input gate, forget gate, cell activation vectors, cell output activation vector, and output gate. The functions g, h, and ϕ denote the cell input, cell output, and network output activation functions, respectively. Deep long short-term memory recurrent ANNs can be built up by multiple of these layers between the input and ouput [114].

B-2 Gradient Descent

The gradient descent is an algorithm for training shallow and deep ANN [54]. It optimizes the cost function with respect to the weights matrices W_i from one to the next layer for each time step k, with i the number of layers. Three different variants can be described for the gradient descent with cost function J based on the input vector X and desired output Y [54]:

1. **Batch gradient descent:** Computes the weight vectors for the next time step for each layer by using the entire training set as

$$W_\mathrm{i}(k+1) = W_\mathrm{i} - \frac{\partial J(X, Y)}{\partial W_\mathrm{i}(k)}.$$

2. **Stochastic gradient descent:** This algorithm is faster and more useful for the training of large data sets. However, this method results in a frequent update of the parameters that often results in a high variance that causes the cost function to fluctuate a lot. This method computes the weight vectors for the next time step for each layer by using one training example:

$$W_\mathrm{i}(k+1) = W_\mathrm{i} - \frac{\partial J(X(k), Y(k))}{\partial W_\mathrm{i}(k)}.$$

3. **Mini-batch gradient descent:** Uses a trade-off between the batch and stochastic gradient descent. Therefore, it is a lot faster than the batch gradient descent, but it reduces the variance of the parameter update resulting in a more stable convergence state. This method computes the weight vectors for the next time step for each layer by using n training examples for a parameter update:

$$W_\mathrm{i}(k+1) = W_\mathrm{i} - \frac{\partial J(X(k:k+n), Y(k:k+n))}{\partial W_\mathrm{i}(k)}.$$

Appendix C

Linear Quantile Regression

In this appendix, the algorithm used for the linear quantile regression is presented. The linear quantile regression is based on the method described in [83]. A linear relationship is assumed between the predictand y and the predictors $\boldsymbol{x}$ as

$$y = \boldsymbol{\beta x} + \epsilon,$$

where $\boldsymbol{\beta}$ is the vector of optimized parameters and ϵ a random error term. In this method, the quantiles of the error distribution are estimated by applying asymmetric weights to the mean absolute error. A quantile loss function is used with τ representing the quantile probability level as

$$\rho_\tau(u) = \begin{cases} \tau u & \text{if } u \geq 0 \\ (\tau - 1)u & \text{if } u < 0 \end{cases} .$$

Therefore, the estimated quantity of the quantile τ is calculated as $\hat{y}_\tau = \boldsymbol{\hat{\beta}_\tau x}$. $\boldsymbol{\hat{\beta}_\tau}$ is obtained by optimizing the minimization problem:

$$\boldsymbol{\hat{\beta}}_\tau = \underset{\beta}{\operatorname{argmin}} \sum_{\mathrm{i}=1}^{\mathrm{N}} \rho_\tau \left(y_{\mathrm{i}} - \boldsymbol{\beta x}_{\mathrm{i}} \right).$$

Due to the fact that every quantile is computed separately, it is possible that the quantile regression curves may intersect, i.e., $\hat{y}^1_\tau > \hat{y}^2_\tau$ while $\tau^1 < \tau^2$ [83]. A rearrangement method can be used to avoid this problem as described in [34].

Appendix D

Supportive Figures and Tables for Analyzing of Stochastic Processes

In this appendix, supportive figures and tables used in analyzing of the different stochastic processes of Chapter 4 are given.

D-1 Solar Irradiance

The autocorrelation of the clear sky index is presented in Figure D-1. In Table D-1, the correlation coefficients between the clear sky index and multiple exogenous inputs are presented.

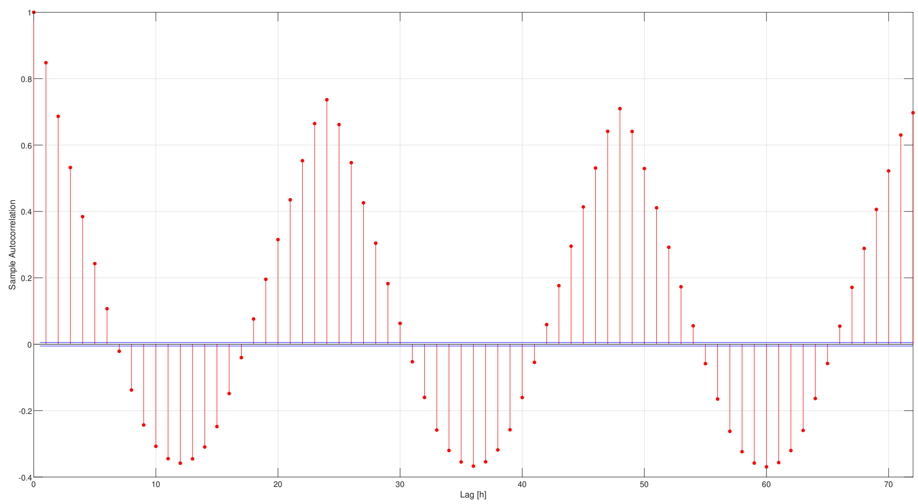

Figure D-1: Autocorrelation of the clear sky index.

Table D-1: Correlation coefficients of exogenous variables with respect to the clear sky index.

Variable	Correlation coefficient
Humidity	-0.5958
Rainfall	-0.0952
Snow	-0.42
Temperature	0.3769
Wind speed	0.0888

D-2 Ambient Temperature

The autocorrelation of the ambient temperature is presented in Figure D-2. In Table D-2, the correlation coefficients between the ambient temperature and multiple exogenous inputs are presented. Furthermore, in Figure D-3, the distribution of the ambient temperature is given throughout the day.

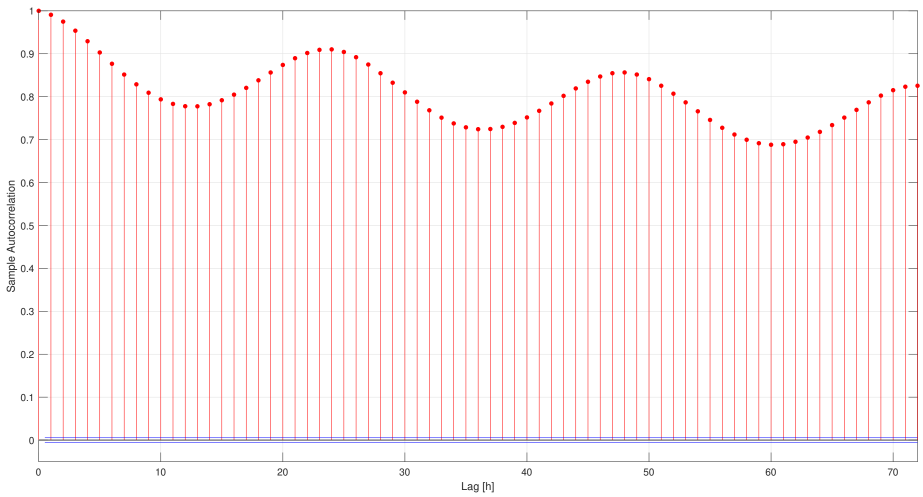

Figure D-2: Autocorrelation of the ambient temperature.

Table D-2: Correlation coefficients of exogenous variables with respect to the ambient temperature.

Variable	Correlation coefficient
Air pressure	-0.0320
Humidity	-0.4624
Rainfall	0.0107
Solar irradiance	0.5066
Wind speed	0.0399

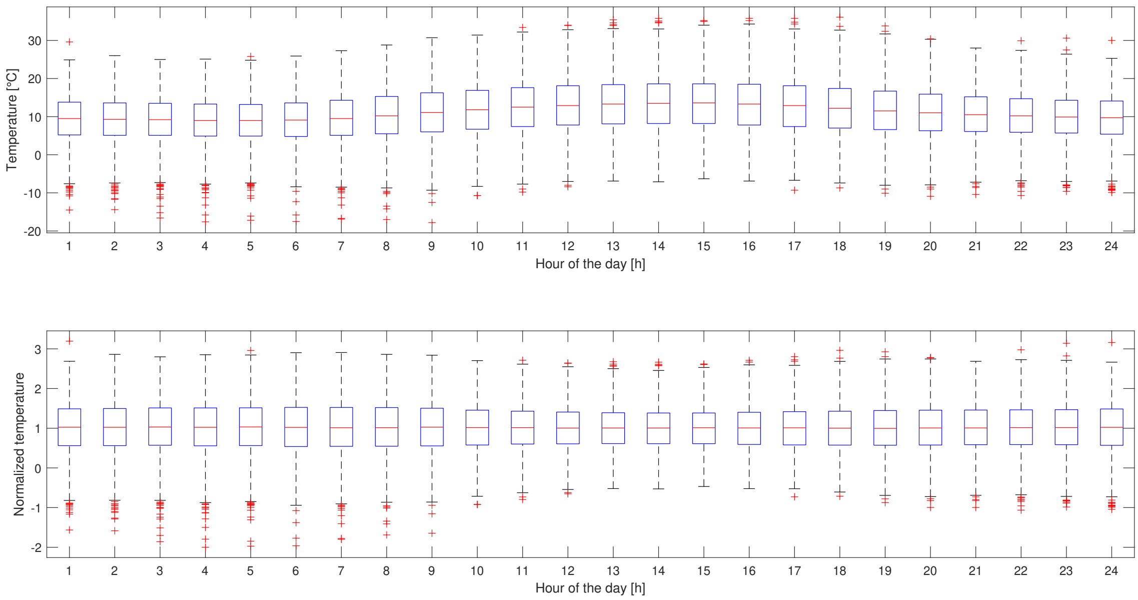

Figure D-3: Boxplot of the ambient temperature during the day. The upper graph shows the distribution of the measured ambient temperature and the lower graph the normalized ambient temperature by its mean per hour during the day.

D-3 Residential Energy Demand

The autocorrelations of the residential energy demands are presented in Figure D-4. In Table D-3, the correlation coefficients between the residential energy demands and multiple exogenous inputs are presented. Furthermore, in Figure D-5, the distribution of the residential energy demands are given throughout the day.

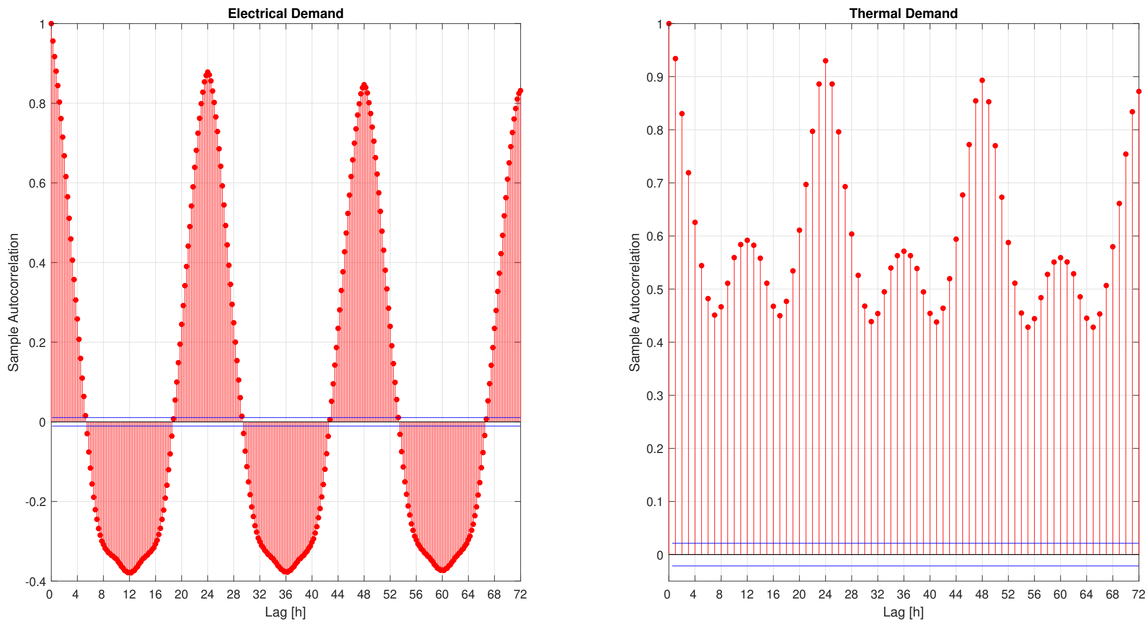

Figure D-4: Autocorrelation of the electrical and thermal energy demand of residential buildings.

Table D-3: Correlation coefficients of exogenous variables with respect to the energy demands of residential buildings

Variable	Correlation coefficient	
	Electrical demand	Thermal demand
Air presssure	-0.0116	-0.1326
Humidity	-0.1480	-0.0097
Rainfall	0.0341	-0.0059
Snowfall	0.0337	0.2192
Solar irradiance	0.0152	-0.1544
Temperature	-0.1022	-0.6765
Windspeed	0.1460	0.1850

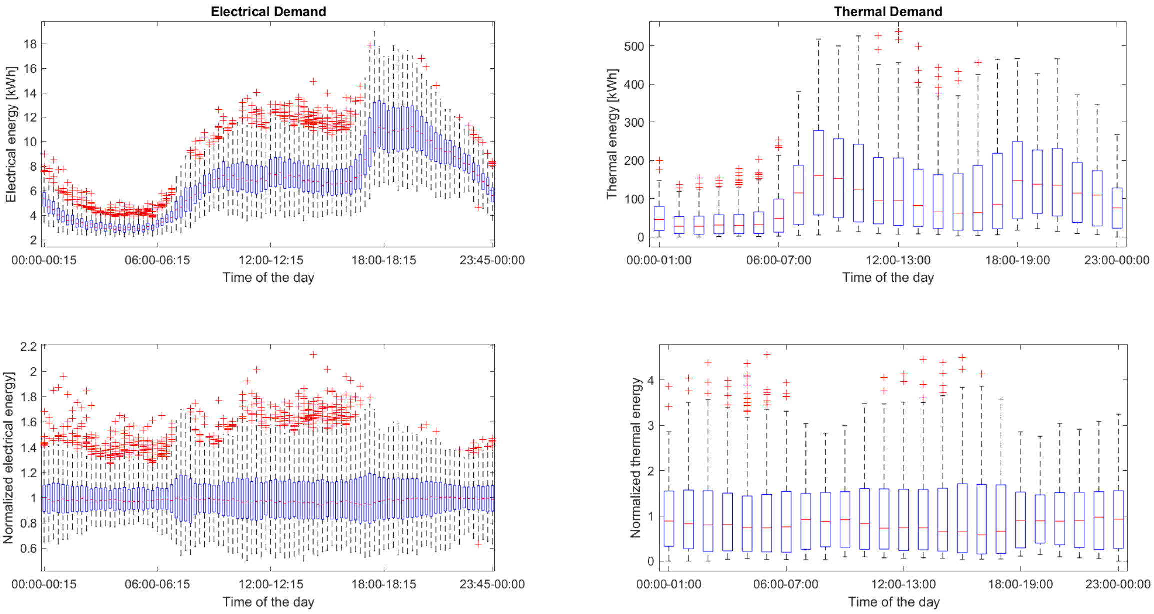

Figure D-5: Boxplots of the energy demand of residential buildings during the day. The upper graphs show the distribution of the measured residential energy demands and the lower graphs the normalized energy demands by their mean per quarter or hour during the day.

D-4 Commercial Energy Demand

The autocorrelations of the commercial energy demands are presented in Figure D-6. In Table D-4, the correlation coefficients between the commercial energy demands and multiple exogenous inputs are presented. Furthermore, in Figure D-7, the distribution of the commercial energy demands are given throughout the day.

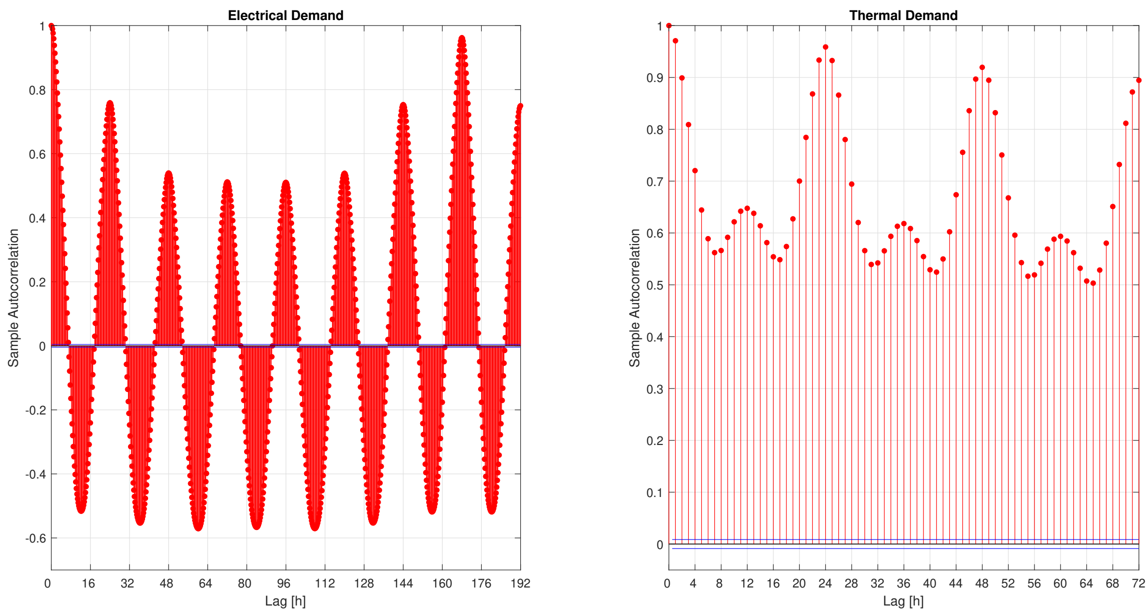

Figure D-6: Autocorrelation of the electrical and thermal energy demand of commercial buildings.

Table D-4: Correlation coefficients of exogenous variables with respect to the energy demand of commercial buildings.

Variable	Correlation coefficient	
	Electrical demand	Thermal demand
Air presssure	0.0002	-0.0115
Humidity	-0.3079	0.0804
Rainfall	-0.0058	-0.0234
Snowfall	0	0
Solar irradiance	0.4589	-0.1647
Temperature	0.1094	-0.7028
Windspeed	0.2022	0.1542

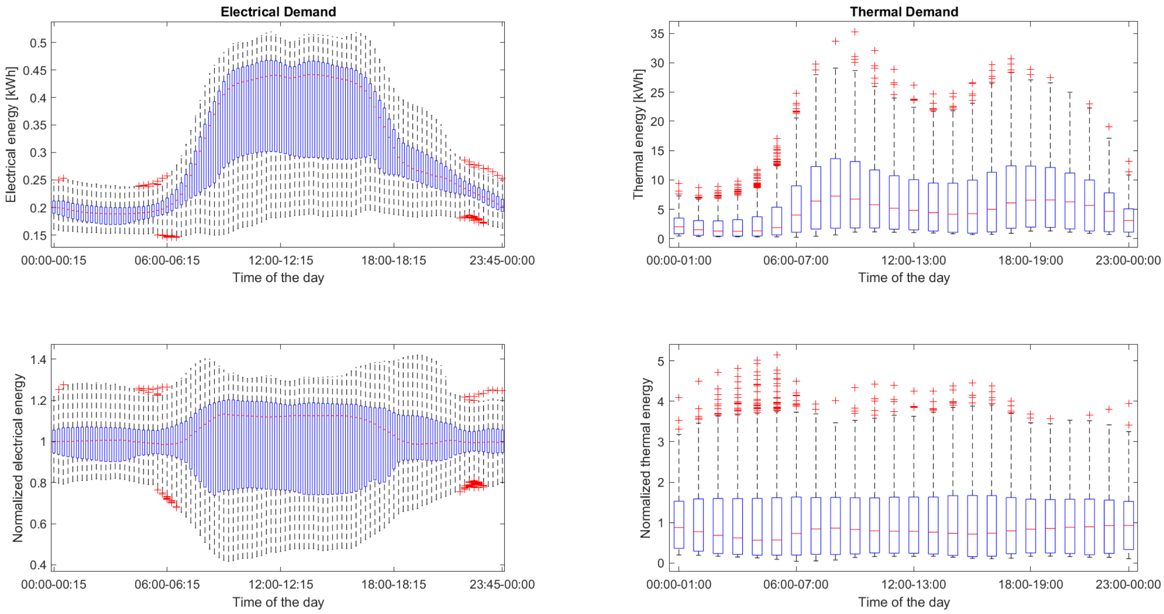

Figure D-7: Boxplots of the energy demand of commercial buildings during the day. The upper graphs show the distribution of the measured commercial energy demands and the lower graphs the normalized energy demands by their mean per quarter or hour during the day.

Appendix E

Capturing Interdependencies of Prediction Errors in Scenario Generation

In this appendix, the algorithm that captures the interdependencies of the prediction errors is presented. Furthermore, it is explained how scenarios are generated using these captured interdependencies of the prediction errors.

The interdependencies of the prediction errors that are needed for scenario generation are captured using the method described in [109]. This method assumes that the interdependence of the prediction errors can be made Gaussian by applying a transformation. Then, a covariance matrix is constructed containing these interdependencies. In the algorithm, at a time of the day t, with a look-ahead time of k, a random uniformly distributed variable Y is introduced. This variable depends on the estimated cumulative distribution $\hat{F}$ and a measured value of the stochastic value from the training data set s as

$$Y_{\mathrm{k}}^{\mathrm{t}} = \hat{F}_{\mathrm{t+k}}(s_{\mathrm{t+k}}).$$

Using the probit function for a Gaussian distribution with 'erf' the error function

$$\Phi^{-1}(p) = \sqrt{2}\,\mathrm{erf}^{-1}(2p-1),$$

a random variable X is obtained that is a distributed Gaussian with zero mean and unit standard deviation as

$$X_{\mathrm{k}}^{\mathrm{t}} = \Phi^{-1}(Y_{\mathrm{k}}^{\mathrm{t}}). \tag{E-1}$$

This random variable X is configured for each look ahead time k at different time steps during the day t using the training data set. A covariance for each time step during the day in the prediction horizon N_{p} can be obtained by

$$\Sigma_t^{\mathrm{i,j}} = \mathrm{Cov}\left(X_{\mathrm{i}}^{\mathrm{t}}, X_{\mathrm{j}}^{\mathrm{t}}\right),$$

with $i, j \in 1, \ldots, N_{\mathrm{p}}$. A large covariance matrix is constructed for each time step during the day containing all the covariance in the prediction horizon.

Scenario Generation

Using the calculated covariance matrices for each time step during the day, scenarios can be generated following the steps:

1. A multivariate Gaussian random number generator with zero mean and using the estimated covariance matrix for that time step during the day configures a number of realizations N_s of the random variable X.
2. For each look-ahead time k, N_s realizations of the uniformly variable Y are obtained using the inverse probit function from Eq. (E-1) as

$$Y_{\mathrm{k}}^{\mathrm{t}} = \Phi(X_{\mathrm{k}}^{\mathrm{t}}).$$

3. The forecasted value for each scenario is then produced as putting the obtained uniformly variable in the inverse cumulative distribution function as

$$\hat{s}_{\mathrm{k}}^{\mathrm{t}} = \hat{F}_{\mathrm{t+k}}^{-1}\left(Y_{\mathrm{k}}^{\mathrm{t}}\right).$$

Appendix F

Low-Level Controller

In this appendix, the low-level controller that is implemented in the microgrid is presented. This controller is implemented to guarantee saturation of the power balance. It is first checked if the thermal rescheduled or curtailed energy exceeds the maximum possible using the actual thermal demand. The new curtailed and thermal energy is updated and a thermal difference due to the difference in thermal load ($\Delta_{\text{th,dr}}$) is computed as

$$\begin{aligned}
Q_{\text{c}}^{\text{new}}(1) &= \max\left(D_{\text{c}}(1), Q_{\text{c}}(1)\right)\\
Q_{\text{r}}^{\text{new}}(1) &= \max\left(D_{\text{r}}^{\text{th}}(1), Q_{\text{r}}(1)\right)\\
\Delta_{\text{th,dr}} &= Q_{\text{c}}^{\text{new}}(1) - Q_{\text{c}}(1) + Q_{\text{r}}(1) - Q_{\text{r}}^{\text{new}}(1)
\end{aligned}$$

The thermal imbalance Δ_{th} is calculated by adding the calculated thermal difference in the above equation to the thermal difference between the forecasted and real value of the thermal energy of buildings $\Delta_{\text{th,b}}$ as $\Delta_{\text{th}} = \Delta_{\text{th,l}} + \Delta_{\text{th,dr}}$. The electric imbalance Δ_{el} is equal to the error of the forecasted values for the electrical residential energy, electrical commercial energy, and the generated Photovoltaic (PV) power. A rule-based algorithm is used to act as low-level controller to compensate for those imbalances as seen in Algorithm 1.

The difference in thermal energy is compensated by using the heat pumps. Firstly, it is checked if it can be compensated by using gas since this option can react the fastest and has the least impact on the peak of electrical energy transfer. If that is not possible, it is assumed that by consuming electrical energy the difference can be compensated as well in the thermal demand. The utility grid is exclusively used to compensate for the difference in the electrical energy demand. Another source that could have been used is the battery. However, this could potentially lead to poorer results due to the change in energy stored in the battery compared to the initial optimization.

Algorithm 1: Low-level controller in the microgrid.

Input: A calculated electric (Δ_{el}) and thermal difference (Δ_{th}). Moreover, the results of the variables out of the optimization for time step $k = 1$. The amount of heat pumps in the microgrid N_{HP}. Furthermore, a logic binary variable is chosen as F to indicate whether the low-level controller has already succeeded to provide for the thermal energy difference.

Output: The actual produced energy, imported energy, and costs where $(\cdot)^{\text{el}}$ and $(\cdot)^{\text{th}}$ are the electric and thermal part, respectively.

$F \leftarrow 0,\ \Delta_{\text{HP,el}} \leftarrow 0$
if $\Delta_{\text{th}} \leq 0$ **then**
  for $i \leftarrow 1$ **to** N_{HP} **do**
    if $Q^{\text{i}}_{\text{HP}} - \underline{Q}^{\text{th,i}}_{\text{HP}} > \Delta_{\text{th}}$ & $\delta^{\text{th,i}}_{\text{HP}} = 1$ **then**
      $Q^{\text{i}}_{\text{HP}} = Q^{\text{i}}_{\text{HP}} + \Delta_{\text{th}}$
      $u^{\text{th,i}}_{\text{UG}} = u^{\text{th,i}}_{\text{UG}} + \eta^{\text{th,i}}_{\text{HP}} \Delta_{\text{th}}$
      $C^{\text{th}}_{\text{UG}} = C^{\text{th}}_{\text{UG}} + c^{\text{P,th}} \cdot \eta^{\text{th,i}}_{\text{HP}} \Delta_{\text{th}}$
      $F = 1$
  for $i \leftarrow 1$ **to** N_{HP} **do**
    if $Q^{\text{i}}_{\text{HP}} - \underline{Q}^{\text{th,i}}_{\text{HP}} > \Delta_{\text{th}}$ & $\delta^{\text{el,i}}_{\text{HP}} = 1$ & $F = 0$ **then**
      $Q^{\text{i}}_{\text{HP}} = Q^{\text{i}}_{\text{HP}} + \Delta_{\text{th}}$
      $\Delta_{\text{HP,el}} = \eta^{\text{el}}_{\text{HP}} \Delta_{\text{th}}$
      $F = 1$
else if $\Delta_{\text{th}} > 0$ **then**
  for $i \leftarrow 1$ **to** N_{HP} **do**
    if $\overline{Q}^{\text{th,i}}_{\text{HP}} - Q^{\text{i}}_{\text{HP}} \geq \Delta_{\text{th}}$ & $\delta^{\text{th,i}}_{\text{HP}} = 1$ **then**
      $Q^{\text{i}}_{\text{HP}} = Q^{\text{i}}_{\text{HP}} + \Delta_{\text{th}}$
      $u^{\text{th,i}}_{\text{UG}} = u^{\text{th,i}}_{\text{UG}} + \eta^{\text{th,i}}_{\text{HP}} \Delta_{\text{th}}$
      $C^{\text{th}}_{\text{UG}} = C^{\text{th}}_{\text{UG}} + c^{\text{P,th}} \eta^{\text{th}}_{\text{HP}} \Delta_{\text{th}}$
      $F = 1$
  for $i \leftarrow 1$ **to** N_{HP} **do**
    if $Q^{\text{i}}_{\text{HP}} - \underline{Q}^{\text{th,i}}_{\text{HP}} > \Delta_{\text{th}}$ & $\delta^{\text{el,i}}_{\text{HP}} = 1$ & $F = 0$ **then**
      $Q^{\text{i}}_{\text{HP}} = Q^{\text{i}}_{\text{HP}} + \Delta_{\text{th}}$
      $\Delta_{\text{HP,el}} = \eta^{\text{el}}_{\text{HP}} \Delta_{\text{th}}$
      $F = 1$
$\Delta_{\text{el}} = \Delta_{\text{el}} + \Delta_{\text{HP,el}}$
$u^{\text{el}}_{\text{UG}} = u^{\text{el}}_{\text{UG}} \Delta_{\text{el}}$
if $\Delta_{\text{el}} \leq 0$ **then**
  $C^{\text{el}}_{\text{UG}} = C^{\text{th}}_{\text{UG}} + c^{\text{S,el}} \Delta_{\text{el}}$
else if $\Delta_{\text{el}} > 0$ **then**
  $C^{\text{el}}_{\text{UG}} = C^{\text{th}}_{\text{UG}} + c^{\text{P,el}} \Delta_{\text{el}}$

Appendix G

Microgrid Build-Up for the Scenarios in the Case Studies

In this appendix, a schematic overview of the different microgrids used in the case studies is presented. The three scenarios with a different level of penetration of hydrogen in the microgrid, as explained in Section 6-1-1, are:

1. **Electric**: In this scenario, no hydrogen is present in the microgrid, excluding the presence of the electrolyzer with an integrated hydrogen storage tank and fuel cell Electric Vehicle (EV)s. The hybrid heat pumps and μ-Combined Heat and Power (CHP) plant can run on 'green' gas that is imported from the utility grid.
2. **Mixed**: This scenario is based on the expected microgrid assuming the developments explained in Section 2-1-3. Both electric- and hydrogen-based components are present in the microgrid. However, no 'green' gas is considered since hydrogen will be using the current natural gas infrastructure. Using both gases will lead to an extra gas network that is preferred to be avoided since the extra investments needed will probably overrule the potential profit. Therefore, the hybrid heat pumps and μ-CHP plant will contain fuel cells to run on hydrogen instead of the 'green' gas. Furthermore, the electrolyzer with an integrated hydrogen storage tank is included in the microgrid. Both types of EVs are present and a ratio of 1.5:1 for the battery to the fuel cell EVs is used [20].
3. **Hydrogen**: In this scenario, a largely hydrogen-based microgrid is sketched. The microgrid consists of almost the same distributed energy resources as in the mixed scenario, only the battery is excluded from the microgrid. Furthermore, all the battery EVs are replaced by fuel cell EVs.

In Figure G-1, a schematic overview is given of these different microgrids. An overview of the different distributed energy resources present in each scenario can be obtained. Moreover, the four different types of energy flows are given: hydrogen, 'green' gas, electrical energy, and thermal energy. These flows are based on the behaviour of the distributed energy resources and the power balance written in Eq. (3-3).

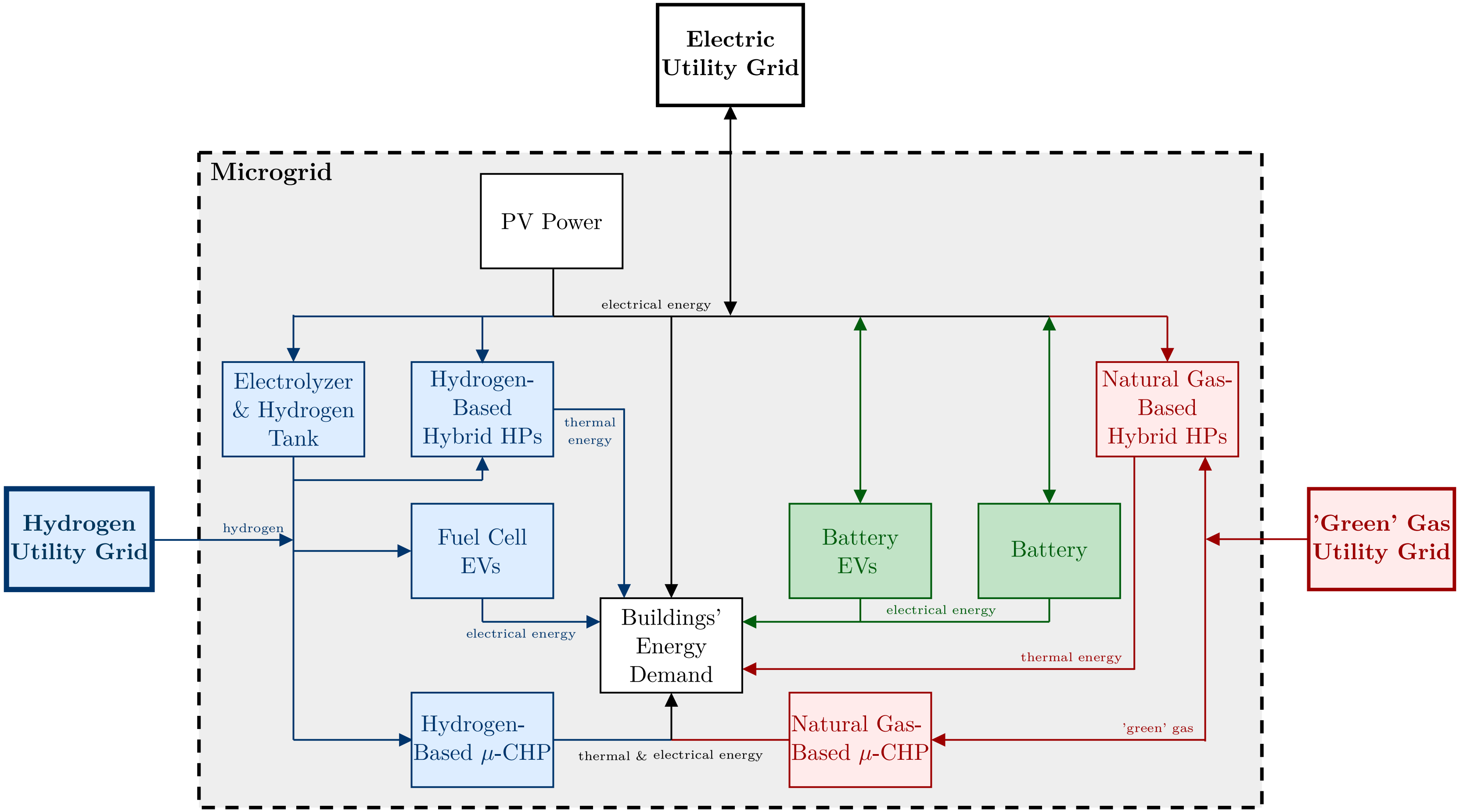

Figure G-1: Visualization of the scenarios considered in the case studies, with Electric Vehicles (EVs), Photovoltaic (PV) power, Heat Pumps (HP), and micro-Combined Heat and Power (μ-CHPs) plants. The white boxes are included in each scenario. The electric scenario is constructed by adding the red and green parts, the mixed scenario by adding the blue part and green parts, and the hydrogen scenario by only including the blue part.

Appendix H

Supportive Figures of Simulations in Case Studies

In this Appendix, figures are presented of the energy transfer between the microgrid and the utility grid in the different simulations in the case studies.

H-1 Case Study A: Winter Week

In this section, an overview is given of the energy transfer between the microgrid and utility grid for the scenarios in the typical winter week. In Figure H-1, the energy transfer for the electric scenario is presented. In Figure H-2, the energy transfer for the mixed scenario is presented. Lastly, in Figure H-3, the energy transfer for the hydrogen scenario is presented.

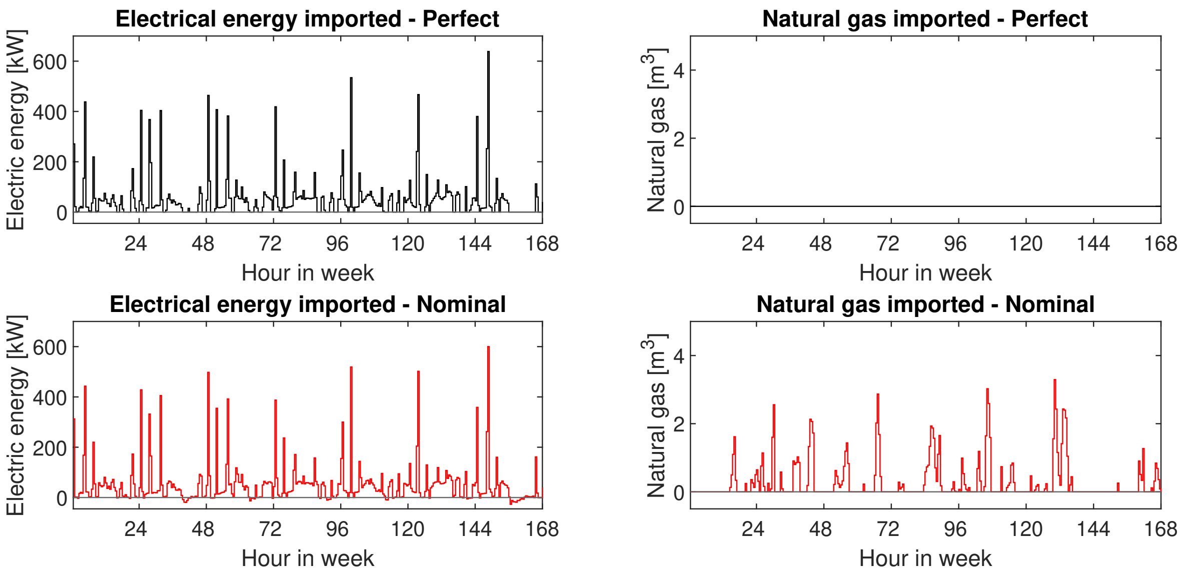

Figure H-1: Energy transfer between the microgrid and utility grid for the electric scenario in the winter week case study.

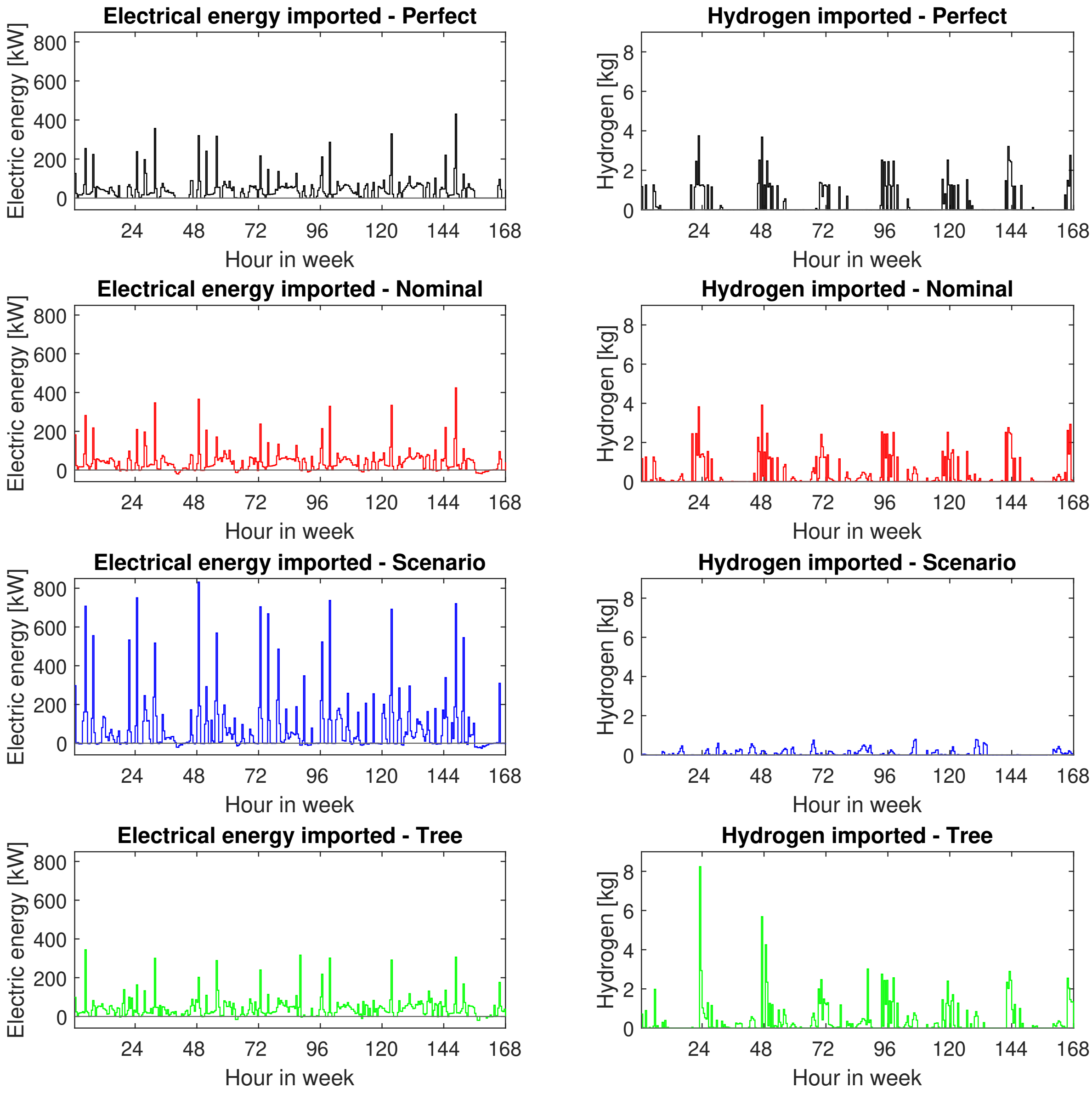

Figure H-2: Energy transfer between the microgrid and utility grid for the mixed scenario in the winter week case study.

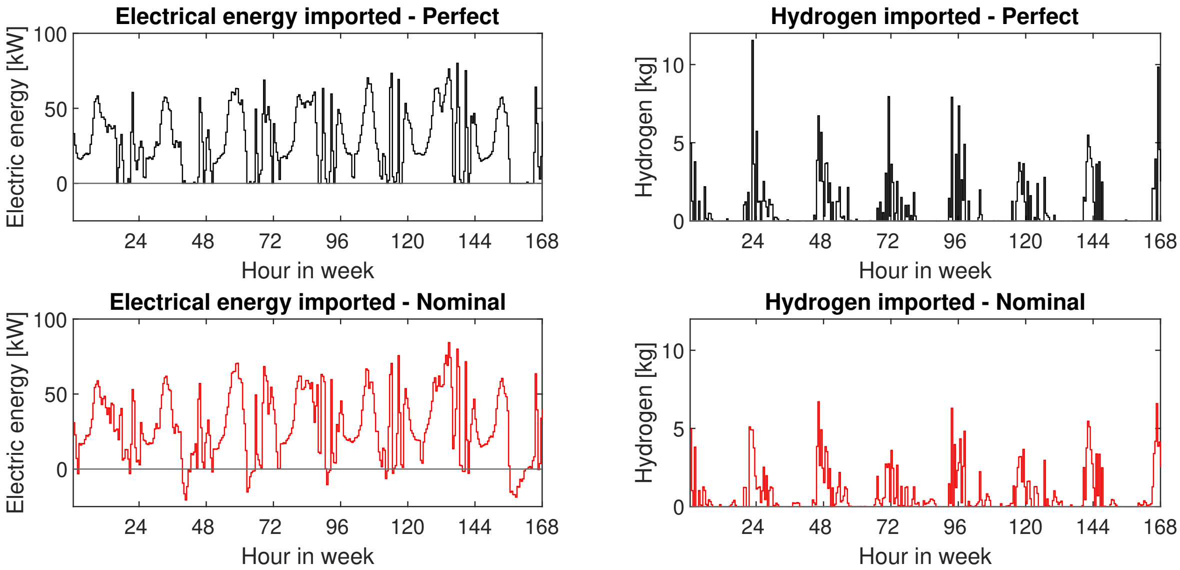

Figure H-3: Energy transfer between the microgrid and utility grid for the hydrogen scenario in the winter week case study.

H-2 Case Study B: Summer Week

In this section, an overview is given of the energy transfer between the microgrid and utility grid for the scenarios in the typical summer week. In Figure H-4, the energy transfer for the electric scenario is presented. In Figure H-5, the energy transfer for the mixed scenario is presented. Lastly, in Figure H-6, the energy transfer for the hydrogen scenario is presented.

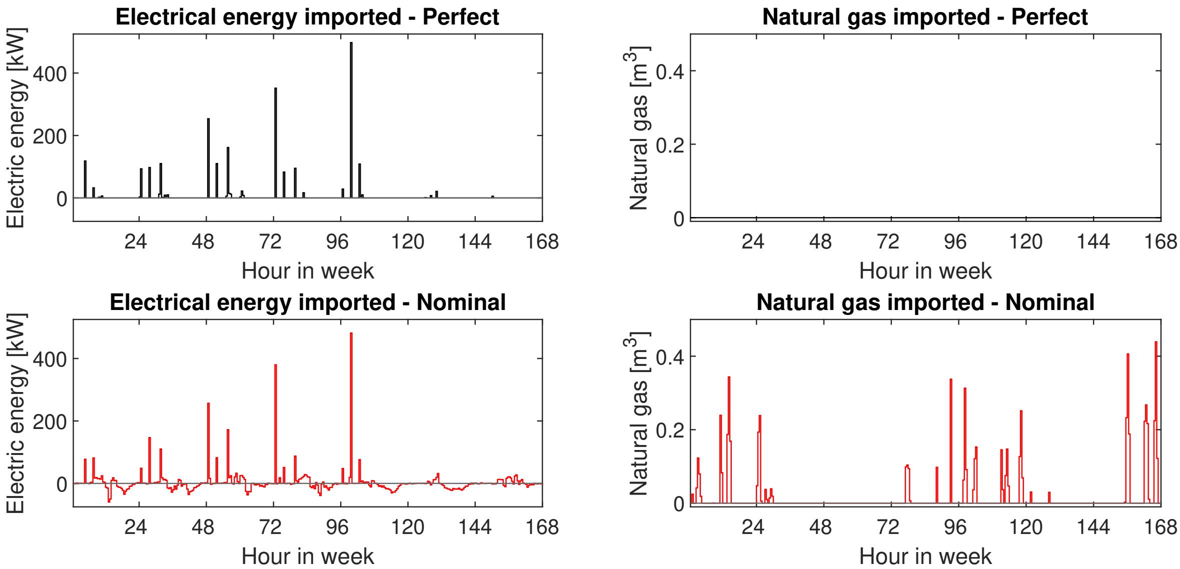

Figure H-4: Energy transfer between the microgrid and utility grid for the electric scenario in the summer week case study.

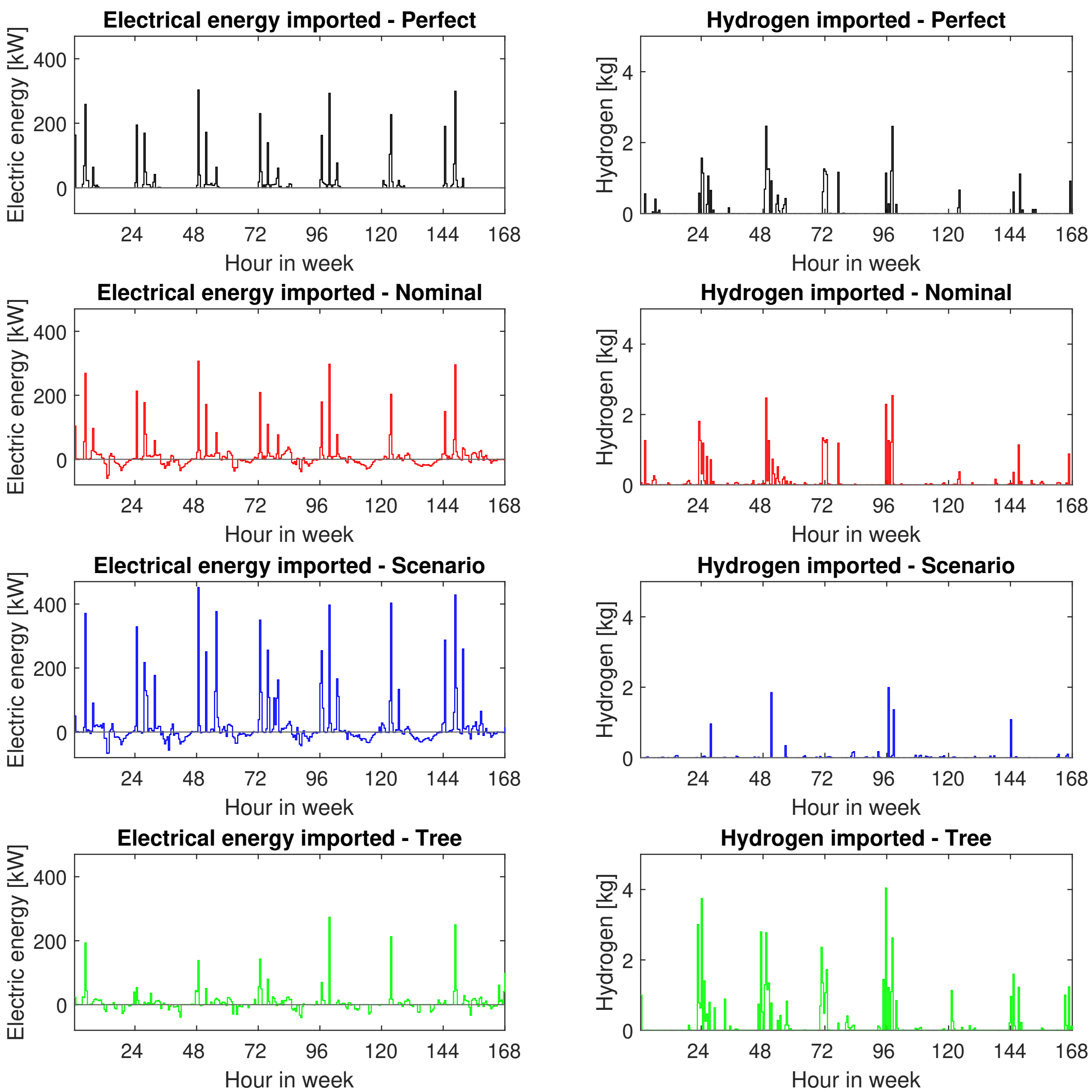

Figure H-5: Energy transfer between the microgrid and utility grid for the mixed scenario in the summer week case study.

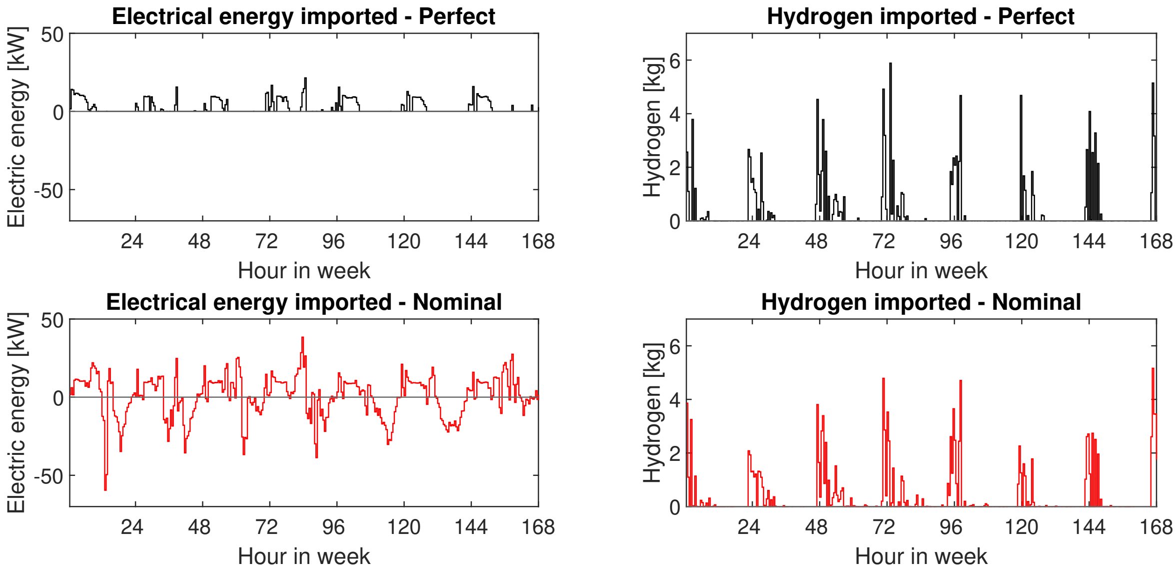

Figure H-6: Energy transfer between the microgrid and utility grid for the hydrogen scenario in the summer week case study.

H-3 Case Study C: Week with Extreme Conditions

In this section, an overview is given of the energy transfer between the microgrid and utility grid for the scenarios in the week with extreme conditions. In Figure H-7, the energy transfer for the electric scenario is presented. In Figure H-9, the energy transfer for the mixed scenario is presented. Lastly, in Figure H-8, the energy transfer for the hydrogen scenario is presented.

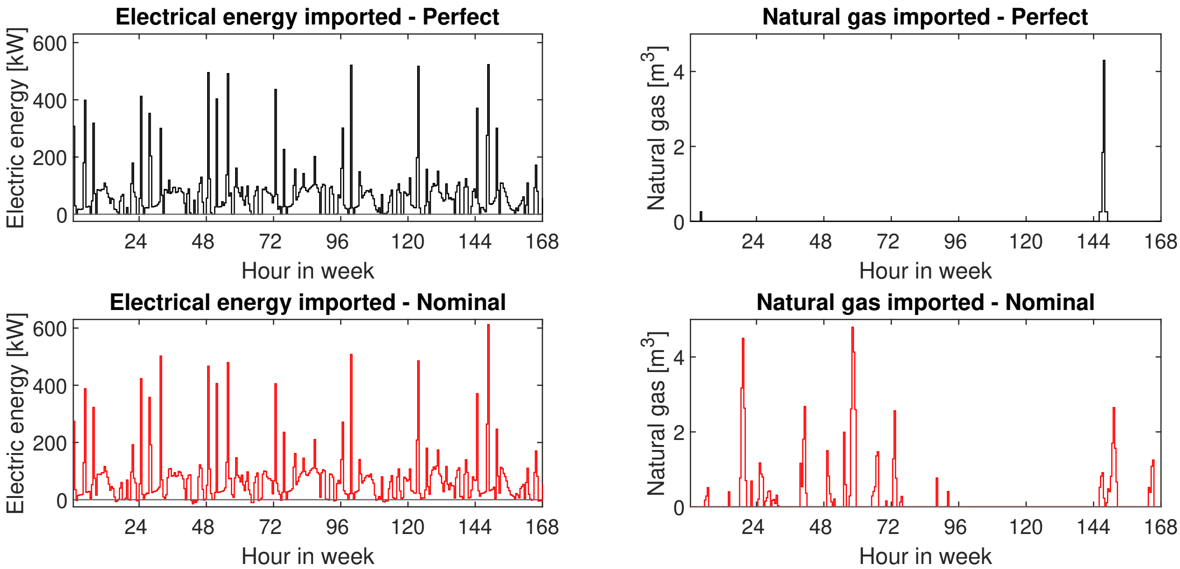

Figure H-7: Energy transfer between the microgrid and utility grid for the electric scenario in the week with extreme conditions case study.

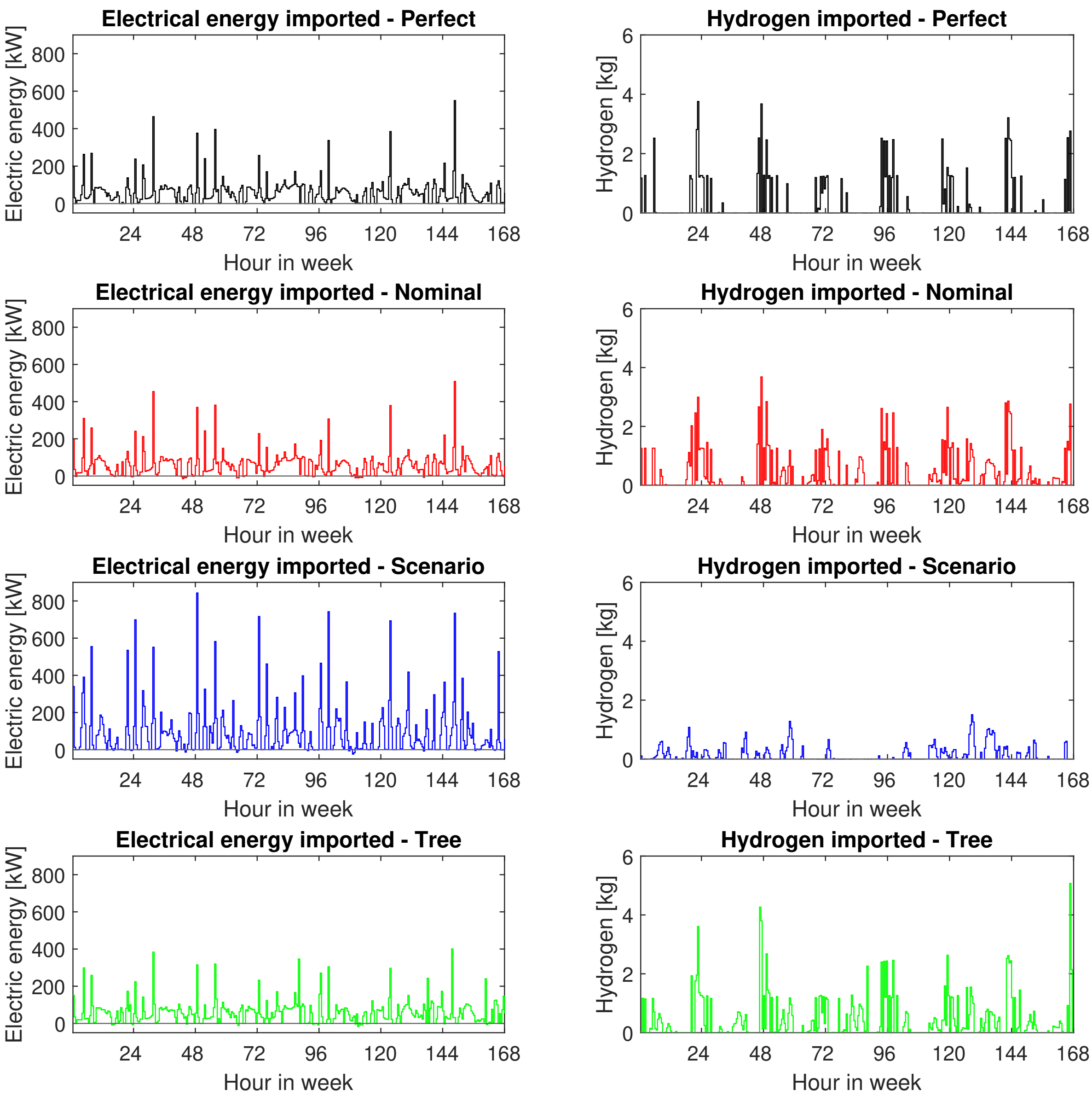

Figure H-8: Energy transfer between the microgrid and utility grid for the hydrogen scenario in the week with extreme conditions case study.

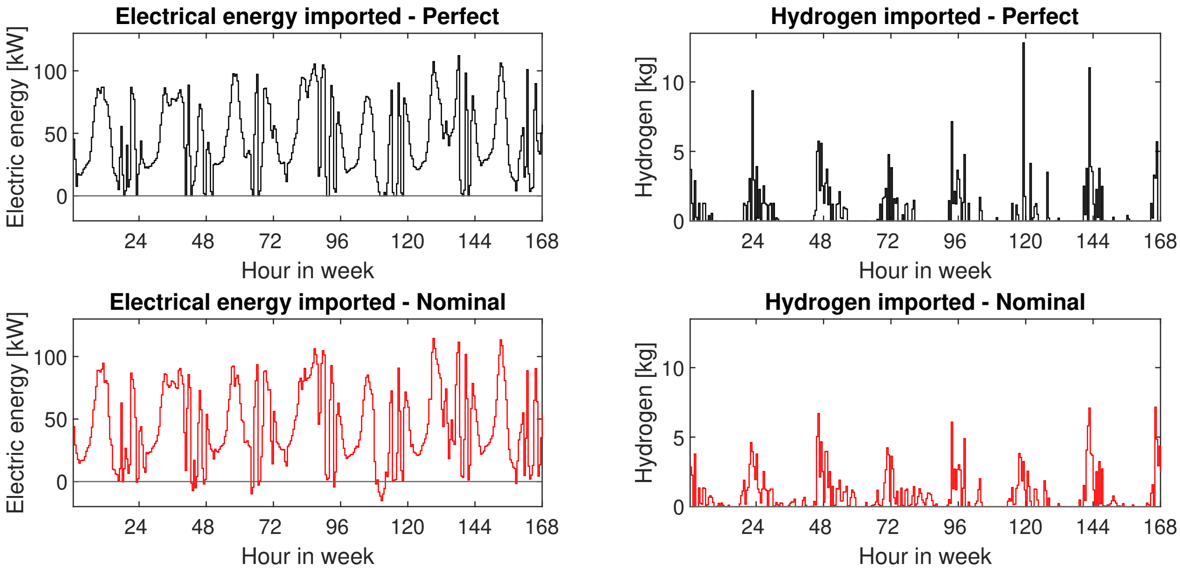

Figure H-9: Energy transfer between the microgrid and utility grid for the mixed scenario in the week with extreme conditions case study.

Appendix I

Paper draft

In this appendix, a draft version of a paper describing the results for the nominal Model Predictive Control (MPC) controller for the scenarios in the different case studies is attached.

Influences of Hydrogen on the Grid Investments for a Future Microgrid with Model Predictive Control

Emiel Bartels, Tomas Pippia, Bart De Schutter, *Senior Member, IEEE*

***Abstract*—Electrification of the heat network in buildings and rise in popularity of the Electric Vehicle (EV) will result in needed investments made in the electrical energy infrastructure preventing congestion at the transformer. This paper concludes on the influence of hydrogen in smart future microgrids on these investments. Moreover, smart control strategies as EV management and Demand Response (DR) programs are used to lower the peak of electrical energy demand resulting in the prevention of these investments. The performance of microgrids with different level of hydrogen penetration are discussed. It is shown that a higher level of penetration of hydrogen does reduce the needed electrical grid investments against a higher total costs due to the increase of energy import costs.**

***Index Terms*—demand response, electric vehicles, hydrogen, microgrid, model predictive control**

I. Introduction

IN 2015, 195 governments signed an agreement for a long-term goal of keeping the increase of the global average temperature this century below two degrees and aiming for an increase of a maximum of one and a half degrees, the Paris agreement. To prevent exceeding this maximum of two degrees rising of the global average temperature, scientists have determined that human society needs to reduce the electricity produced by burning fossil fuels from 70% in 2010 to 20% in 2050 [1]. Therefore, more energy needs to be produced by renewable energy sources, because they have no emission of greenhouse gases. However, due to the intermittent nature of these renewable energy resources, there is a need for more flexibility in the energy grid [2] and a rise of complexity for the energy management [3].

The implementation of microgrids seems to be a possible key solution to the integration of these renewable energy resources in the energy grid [4]. Microgrids consist of interconnected loads, distributed energy resources, and energy storage systems. These microgrids can be seen as a miniature version of the larger utility grid. A connection to the utility grid is sometimes available, but in other cases, the microgrid needs to be self-supplied and operate in an islanded mode [5]. Due to the distribution of the energy resources by implementing a microgrid, improved reliability, power quality, and reduced distribution loss are realized [6], [7].

Furthermore, changes are happening in the transport sector as well to reduce the emission of greenhouse gases by replacing the internal combustion engine vehicle with an Electric Vehicle (EV). The increased use of EVs has a strong effect on the demand of energy for the grid due to their relatively high consumption of energy [7]. This increase in energy demand in the microgrid results in needed economic investments in the infrastructure of the energy grid since during large consuming times the current infrastructure will not be able to cope with the rising energy demand [8]. Therefore, in future microgrids, the focus should be on the peak of electrical energy transfer between the microgrid and utility grid.

In these future microgrids, smart strategies can be used to create a framework where renewable energy sources can be implemented and reduce the peak of electrical energy transfer to prevent unnecessary investments in the energy grid. The impact of the increasing energy demand by the addition of EVs in the microgrid can be reduced by using smart charging strategies where the EVs can be charged when there is an abundance, or less shortage, of energy in the microgrid. Moreover, EVs can contribute to mitigate the problem for energy distribution in the microgrid while being used as a power plant or energy storage system to provide energy at times of high energy demand in the microgrid [9], [7], [10]. Another strategy is the use of Demand Response (DR) programs where the consumption pattern of the consumers in the microgrid is altered. The use of DR programs has proven to generate more flexibility in the grid and reduce the electrical energy transfer peak [6], [11].

A new source of energy is emerging in both the energy and transport sector, hydrogen [12]. The popularity of hydrogen is expected to increase in the next years due to its storing capabilities and cheap transport of energy. Furthermore, it can be produced without the emission of greenhouse gases [13]. Hydrogen offers a great solution to the distribution of generated renewable energy, e.g., when generated on offshore wind farms. Fuel cell EVs are emerging due to some beneficial specifications compared to the nowadays more used battery EVs, e.g., greater range and faster refueling [12], [14]. This introduction of hydrogen to the microgrid can alter its behaviour. Therefore, different performance regarding the peak electrical energy transfer of the microgrid could be obtained.

In this study, the microgrids will be controlled with a nominal Model Predictive Control (MPC) framework that has proven to provide good performance on the energy management of a microgrid [9], [15], [16], [17]. For the control of the microgrid, different stochastic processes in the microgrid are forecasted, i.e., the energy demand of the buildings and power generation by renewable energy sources.

In this paper, future microgrids are constructed based on the year 2050 in the Netherlands where hydrogen has widely emerged in the energy infrastructure. Different levels of penetration of hydrogen in the microgrid are compared to reduce the electrical grid investments. The mixed logical dynamical framework is used in this paper to describe the model of the microgrid. A multi-objective mixed-integer linear programming problem is solved using an MPC framework.

The remainder of this papers is organized as follows. In Section II the key features of the microgrid are given and how the microgrid is modelled. In Section III, the different forecasting models are given that are used to forecast the stochastic processes in the microgrid. For each stochastic process, it is concluded which model obtains the smallest error. Then, the control objective is presented and the nominal MPC framework in Section IV. Scenarios with different level of hydrogen penetration are compared and discussed. Some final conclusions and suggestions for future work are given in Section VI

II. Microgrid Modelling

In this section, we describe the key features of the microgrid, which comprises continuous-time dynamics of the distributed energy resources and energy flows. We remark that a constant ratio between energy and power per time step is assumed due to the constant sampling $\Delta T = T_{\mathrm{k+1}} - T_{\mathrm{k}}$. A future microgrid is constructed based on future predictions in the Dutch energy infrastructure in 2050 [18]. In this future microgrid, a level of penetration of hydrogen can be considered, resulting in a relatively vast share of hydrogen-based components in the microgrid. Therefore, an electrolyzer with hydrogen storage tank and fuel cell EVs are present. Furthermore, 'green' gas that will be used in the future to satisfy the thermal demand, could be replaced by hydrogen resulting in fuel cells in the thermal devices. A microgrid with residential and small commercial consumers is considered with a high use of Photovoltaic (PV) panels.

A. Components in the microgrid

1) Battery: The dynamics to determine the stored energy in a battery x_{bat} at the next time step $k+1$ depends on the different mode the battery is in, i.e., the battery is charging or discharging. If the binary variable $\delta_{\mathrm{bat}}(k) = 1$, the battery is charging and if $\delta_{\mathrm{bat}}(k) = 0$, the battery is discharging. It is necessary to model the battery using this binary variable due to the difference in charging and discharging efficiency. Therefore, the battery can be described by the following equation:

$$x_{\mathrm{bat}}(k+1) = \begin{cases} x_{\mathrm{bat}}(k) + \eta_{\mathrm{c}} u_{\mathrm{bat}}(k), & \text{if } \delta_{\mathrm{bat}}(k) = 1 \\ x_{\mathrm{bat}}(k) + \frac{1}{\eta_{\mathrm{d}}} u_{\mathrm{bat}}(k), & \text{if } \delta_{\mathrm{bat}}(k) = 0 \end{cases}, \tag{1}$$

where u_{bat} is the exchanged electrical energy, η_{c} the charging efficiency, and η_{d} the discharging efficiency. The state of the battery and the electrical energy exchanged to or from the battery cannot exceed their minimal and maximal bounds. Therefore, the equations $\underline{x}_{\mathrm{bat}} \leq x_{\mathrm{bat}}(k) \leq \overline{x}_{\mathrm{bat}}$ and $\underline{u}_{\mathrm{bat}} \leq u_{\mathrm{bat}}(k) \leq \overline{u}_{\mathrm{bat}}$ apply to these variables. Moreover, an extra constraint on the energy transfer is set to distinguish if energy is coming in or leaving the battery, i.e., if the battery is in charging or discharging mode. Therefore, $\delta_{\mathrm{bat}}(k) = 1 \iff u_{\mathrm{bat}}(k) \geq 0$.

2) Hydrogen storage tank: The model of the hydrogen storage tank is quite similar to that of the battery. However, since no charging and discharging efficiency are considered, the model becomes more simple without using a logic binary variable. Therefore, the amount of hydrogen stored in the tank x_{hst} at time step $k+1$ can be modelled as

$$x_{\mathrm{hst}}(k+1) = x_{\mathrm{hst}}(k) + u_{\mathrm{hst}}(k),$$

where u_{hst} is the exchanged hydrogen. Similar to the battery, bounds are set on the amount of stored and exchanged hydrogen, i.e., $\underline{x}_{\mathrm{hst}} \leq x_{\mathrm{hst}} \leq \overline{x}_{\mathrm{hst}}$ and $\underline{u}_{\mathrm{hst}} \leq u_{\mathrm{hst}} \leq \overline{u}_{\mathrm{hst}}$.

3) Electrolyzer: The electrolyzer converts the consumed electrical energy u_{elc} into hydrogen H_{elc} when the system is on. When the system is off, the electrolyzer will not produce any hydrogen. Therefore, using the logic variable δ_{elc}, the system at time step k can be described as on or off, i.e., $\delta_{\mathrm{elc}}(k) = 1$ or $\delta_{\mathrm{elc}}(k) = 0$, respectively. The electrolyzer can be written as

$$H_{\mathrm{elc}}(k) = \begin{cases} \alpha_{\mathrm{elc}} u_{\mathrm{elc}}(k), & \text{if } \delta_{\mathrm{elc}}(k) = 1 \\ 0, & \text{if } \delta_{\mathrm{elc}}(k) = 0 \end{cases},$$

where α_{elc} is the model parameter related to the specifications of the system as proposed in [9]. The amount of electrical energy that is consumed is constrained by $0 \leq u_{\mathrm{elc}}(k) \leq \overline{u}_{\mathrm{elc}}$. If the electrolyzer is turned off, the consumed electrical energy needs to be zero as well, i.e., $\delta_{\mathrm{elc}}(k) = 0 \iff u_{\mathrm{elc}}(k) = 0$.

4) PV Power: The power coming from the PV panels is calculated by the obtained solar irradiance and ambient temperature as

$$\begin{aligned} P_{\mathrm{PV}}(k) &= P_{\mathrm{STC}} \frac{G_{\mathrm{c}}(k)}{G_{\mathrm{STC}}} \left[1 + \alpha \left(T_{\mathrm{c}}(k) - T_{\mathrm{STC}}\right)\right], \quad \text{with} \\ T_{\mathrm{c}}(k) &= T_{\mathrm{amb}}(k) + (\mathrm{NOCT} - 20) \frac{G_{\mathrm{c}}(k)}{800}. \end{aligned} \tag{2}$$

The nominal power P_{STC}, the global irradiance G_{STC}, and the cell temperature T_{STC} are under standard test conditions of $(1000W/m^2,\ 25C)$. The air mass coefficient that is commonly used to characterize the performance of solar cells under standardized conditions is assumed to be AM1.5. This is almost universal when characterizing terrestrial PV panels [19]. Furthermore, α is the negative power temperature coefficient, and NOCT the nominal operating cell temperature. These values are commonly given by the manufactures of the PV panels. The global irradiance G_{c} and ambient temperature T_{amb} at time step k are estimated to calculate the cell temperature T_{c} and generated PV power P_{PV}. This equation describes the ratio between the produced PV power and the different variables, where the total effective area of the PV panel is included in the value of the nominal power to be used.

5) Hybrid Heat Pump: The hybrid heat pump can produce thermal energy Q_{HP} by consuming electrical energy $u^{\mathrm{el}}_{\mathrm{HP}}$ or gas $u^{\mathrm{th}}_{\mathrm{HP}}$. Therefore, two logic binary variables are introduced to represent if at time step k the hybrid heat pump is running on electrical energy $\delta^{\mathrm{el}}_{\mathrm{HP}}(k) = 1$, on thermal energy $\delta^{\mathrm{th}}_{\mathrm{HP}}(k) = 1$, or if the system is off $\delta^{\mathrm{el}}_{\mathrm{HP}}(k) = \delta^{\mathrm{th}}_{\mathrm{HP}}(k) = 0$. Therefore, the hybrid heat pump can be modelled as:

$$Q_{\mathrm{HP}}(k)=\begin{cases}\eta^{\mathrm{el}}_{\mathrm{HP}}u^{\mathrm{el}}_{\mathrm{HP}}(k), & \text{if } \delta^{\mathrm{el}}_{\mathrm{HP}}(k)=1 \text{ and } \delta^{\mathrm{th}}_{\mathrm{HP}}(k)=0\\ \eta^{\mathrm{th}}_{\mathrm{HP}}u^{\mathrm{th}}_{\mathrm{HP}}(k), & \text{if } \delta^{\mathrm{el}}_{\mathrm{HP}}(k)=1 \text{ and } \delta^{\mathrm{th}}_{\mathrm{HP}}(k)=0\\ 0, & \text{if } \delta^{\mathrm{el}}_{\mathrm{HP}}(k)=\delta^{\mathrm{th}}_{\mathrm{HP}}(k)=0\end{cases}$$

where $\eta^{\mathrm{el}}_{\mathrm{HP}}$ is the electrical efficiency and $\eta^{\mathrm{th}}_{\mathrm{HP}}$ the efficiency of burning gases such as hydrogen. The maximal consumed energy is constrained by the equations $0 \leq u^{\mathrm{el}}_{\mathrm{HP}}(k) \leq \overline{u}^{\mathrm{el}}_{\mathrm{HP}}$ and $0 \leq u^{\mathrm{th}}_{\mathrm{HP}}(k) \leq \overline{u}^{\mathrm{th}}_{\mathrm{HP}}$. The consumption of energy, electrical or gas, will be zero if that mode is off, i.e., $\delta^{\mathrm{el}}_{\mathrm{HP}}(k)=0 \iff u^{\mathrm{el}}_{\mathrm{HP}}(k)=0$ and $\delta^{\mathrm{th}}_{\mathrm{HP}}(k)=0 \iff u^{\mathrm{th}}_{\mathrm{HP}}(k)=0$. Since the hybrid heat pump will not consume electrical energy and uses the boiler at simultaneous time, a constraint is added that the logical binary variables cannot both be equal to one at time step k, i.e., $\delta^{\mathrm{el}}_{\mathrm{HP}}(k)+\delta^{\mathrm{th}}_{\mathrm{HP}}(k) \leq 1$.

6) Micro-combined heat and power plant: The micro-combined heat and power (μ-CHP) plant produces electrical P_{CHP} and thermal energy Q_{CHP} simultaneously. Moreover, a thermal storage unit is integrated with an amount of energy stored x_{CHP}. The production of energy depends on the amount of consumed gas u_{CHP}. Similarly to the hybrid heat pump, two logic binary variables are introduced to indicate whether the CHP system is turned on or off, i.e., $\delta_{\mathrm{CHP}}(k)=1$ or $\delta_{\mathrm{CHP}}(k)=0$ at time step k, respectively. The system of a μ-CHP plant can therefore be described by

$$P_{\mathrm{CHP}}(k)=\begin{cases}\eta^{\mathrm{el}}_{\mathrm{CHP}}u_{\mathrm{CHP}}(k), & \text{if } \delta_{\mathrm{CHP}}(k)=1\\ 0, & \text{if } \delta_{\mathrm{CHP}}(k)=0\end{cases}$$

$$x_{\mathrm{CHP}}(k+1)=\begin{cases}x_{\mathrm{CHP}}(k)+\eta^{\mathrm{th}}_{\mathrm{CHP}}u_{\mathrm{CHP}}(k)-Q_{\mathrm{CHP}}(k),\\ \text{if } \delta_{\mathrm{CHP}}(k)=1\\ x_{\mathrm{CHP}}(k)-Q_{\mathrm{CHP}}(k),\\ \text{if } \delta_{\mathrm{CHP}}(k)=0\end{cases}$$

where $\eta^{\mathrm{el}}_{\mathrm{CHP}}$ and $\eta^{\mathrm{th}}_{\mathrm{CHP}}$ are the electrical and thermal efficiency of the plant. The consumed energy and stored energy are bounded by $0 \leq u_{\mathrm{CHP}}(k) \leq \overline{u}_{\mathrm{CHP}}$ and $\underline{x}_{\mathrm{CHP}} \leq x_{\mathrm{CHP}}(k) \leq \overline{x}_{\mathrm{CHP}}$. The minimum stored thermal energy needs to be higher than a determined threshold $\underline{x}_{\mathrm{CHP}} > 0$. Furthermore, the consumed energy is zero if the system is turned off at time step k, i.e., $u_{\mathrm{CHP}}(k)=0 \iff \delta_{\mathrm{CHP}}(k)=0$.

B. Electric vehicles

Smart EV management can be implemented in a microgrid where smart charging or refueling of the EV is done and the EV can be used as an energy storage system or power plant when parked. Due to these strategies, a microgrid can be more flexible and self-sustainable, i.e., less power exchange with the utility grid will be needed [9], [20], [21], [22]. Moreover, the EV can provide energy in times of great demand for energy, reducing the peak of electrical energy demand [20]. In this study, vehicle-to-grid is chosen since a microgrid is considered with a large amount of EVs and the assumption is made that in a future scenario, the implementation of it will be possible. Moreover, this strategy can provide the most beneficial results for the microgrid [22], [21].

1) Battery EV: The battery EV dynamics are based on the dynamics of the battery but includes more modes since the EV can be in transportation. The EV can be refilled with electrical energy, generate electrical energy to the microgrid, be in transportation, and arrive after its trip. The amount of electrical energy stored in the battery EV x_{BEV} is based on the electrical energy u_{BEV} transferred and the energy costs of a trip h_{BEV}. The model of the battery EV can be written down as

$$x_{\mathrm{bev}}(k+1)=\begin{cases}x_{\mathrm{bev}}(k)+\eta^{\mathrm{c}}_{\mathrm{bev}}u_{\mathrm{bev}}(k), & \text{if refilling}\\ x_{\mathrm{bev}}(k), & \text{if no generation}\\ x_{\mathrm{bev}}(k)+\frac{1}{\eta^{\mathrm{d}}_{\mathrm{bev}}}u_{\mathrm{bev}}(k), & \text{if generation}\\ x_{\mathrm{bev}}(k), & \text{if transportation}\\ x_{\mathrm{bev}}(k)-h_{\mathrm{bev}}(k), & \text{if arrival.}\end{cases}$$

where $\eta^{\mathrm{c}}_{\mathrm{bev}}$ and $\eta^{\mathrm{d}}_{\mathrm{bev}}$ are the charging and discharging efficiencies, respectively. Constraints are set on the total energy storage of the battery $\underline{x}_{\mathrm{bev}} \leq x_{\mathrm{bev}}(k) \leq \overline{x}_{\mathrm{bev}}$ as well as on the transferred energy $\underline{u}_{\mathrm{bev}} \leq u_{\mathrm{bev}}(k) \leq \overline{u}_{\mathrm{bev}}$. The value of the transferred energy is managed in a similar way as in the battery: $u_{\mathrm{bev}}(k) \geq 0 \iff$ refilling mode, and $u_{\mathrm{bev}}(k) < 0 \iff$ generation mode.

2) Fuel cell EV: The fuel cell EV is modelled in similar way as the battery EV to estimate the amount of hydrogen x_{fev} in the tank. However, a difference is that the refilled energy $u^{\mathrm{hyd}}_{\mathrm{fev}}$ and trip cost h_{fev} are expressed in hydrogen, while in generation mode electrical energy $u^{\mathrm{el}}_{\mathrm{fev}}$ is produced. Furthermore, the dynamics of the battery in the battery EV are replaced by the dynamics of a fuel cell to get the model for a fuel cell EV [9]:

$$x_{\mathrm{fev}}(k+1)=\begin{cases}x_{\mathrm{fev}}(k)+u^{\mathrm{hyd}}_{\mathrm{fev}}(k), & \text{if refilling}\\ x_{\mathrm{fev}}(k), & \text{if no generation}\\ x_{\mathrm{fev}}(k) \\ \quad -\left(\alpha_{\mathrm{fev}}u^{\mathrm{el}}_{\mathrm{fev}}(k)+\beta_{\mathrm{fev}}\right), & \text{if generation}\\ x_{\mathrm{fev}}(k), & \text{if transportation}\\ x_{\mathrm{fev}}(k)-h_{\mathrm{fev}}(k), & \text{if arrival.}\end{cases}$$

where α_{fev} and β_{fev} are the model parameters of the fuel cell in the EV. These model parameters are based on the specifications of the fuel stack in the EV as described in [23], [24]. Constraints are set on the hydrogen storage, transferred hydrogen, and the electrical energy transferred, i.e., $\underline{x}_{\mathrm{fev}} \leq x_{\mathrm{fev}}(k) \leq \overline{x}_{\mathrm{fev}}$, $0 \leq u^{\mathrm{hyd}}_{\mathrm{fev}}(k) \leq \overline{u}^{\mathrm{hyd}}_{\mathrm{fev}}$, and $0 \leq u^{\mathrm{el}}_{\mathrm{fev}}(k) \leq \overline{u}^{\mathrm{el}}_{\mathrm{fev}}$, respectively. The maximum generated electrical energy is based on the fact the fuel cell will operate at partial load when in generation mode. Furthermore, constraints are introduced to prevent the fuel cell EV from being in different modes simultaneously.

3) Trip charactersitcs: A stochastic part for the EV modelling is the trip pattern as well as the fuel costs of these trips. Assumptions need to be made to model these stochastic processes. For real data on the arrival and departure time of EVs, a data set of charging patterns of EVs in the Netherlands form ElaadNL has been obtained. These charging sessions can be clustered into three groups by the method described in [25]: charge-near-home, park-to-charge, and charge-near work. In this method, the charging sessions are clustered based on the duration of charging and the time of the day. Furthermore, it is concluded in [25] that the arrivals are earlier in the summer and spring than in the autumn and winter. Moreover, people stay out of home longer during weekends resulting in later arrival times compared to the weekdays. The obtained data set is clustered and the charge-near-home data are used to describe different arrival and departure time patterns for the EVs in the microgrid.

The energy cost per trip is calculated based on the average kilometres driven per year. It is assumed that the driving behaviour will not change when switching form internal combustion engine vehicles to EVs, and that the average kilometres driven per trip is 35.57 in the Netherlands. From [25], it is estimated that 54.4% of the charging sessions are charge-near-home sessions. Therefore, not all the energy for the EV will be refilled in the microgrid, but also at work or in public charging poles elsewhere. It is assumed that 19.35 kilometres worth of fuel is the average energy cost per trip for the EVs in the microgrid. Since different vehicles will have different driving patterns, a multivariate random Gaussian sampling is used to obtain different trip costs for different EVs.

C. Demand response

Direct load control is implemented in the microgrid as DR program since it can provide good performance on lowering the peak of electrical energy transfer and is suitable for the low consumption consumers considered in the microgrid. It is assumed that only residential consumers are willing to participate in the DR program.

1) Curtailable load: Curtailable load D_{c} can temporarily be lowered or switched off. The variable $\beta_{\mathrm{c}}(k)$ with $0 \leq \beta_{\mathrm{c}}(k) \leq 1$ shows the percentage of preferred power level to be curtailed at time step k. Thus, if no curtailment is allowed, $\beta_{\mathrm{c}}(k) = 0$ at time step k [16]. In the model it is assumed that the thermal energy can only be lowered during the day against the discomfort costs, i.e., that the temperature in the building becomes lower than preferred (or higher in hot climates). Note that only a fraction of the thermal energy demand will be considered to be able to curtail. The curtailed load Q_{c} is expressed by

$$Q_{\mathrm{c}}(k) = \beta_{\mathrm{c}}(k) D_{\mathrm{c}}(k).$$

2) Rescheduable load: Rescheduable loads D_{r} can be shifted in time, but in contrast to the curtailable loads, they have to be fulfilled after a certain time. These loads are divided into two different subcategories: uninterruptible and interruptible loads. In this thesis, only uninterruptible loads are considered. However, the smart charging of EVs due to the implementation of the EV management strategies can be considered as an interruptible load in the microgrid.

Both fractions of the electrical and thermal energy are considered to be rescheduable. The only electric devices that are considered to be rescheduable are dishwashers. These devices are chosen due to their regular consumption pattern and their time of use. Dishwashers are used in the evening where, in general, large peaks of electrical energy demand are visible. Similar as to the curtailable load, a variable $\beta_{\mathrm{r}}(k)$ with $0 \leq \beta_{\mathrm{r}}(k) \leq 1$ is introduced to indicate the percentage of preferred level to be rescheduled at time step k. This results in the equation of rescheduled load for electrical and thermal demand:

$$\begin{aligned} P_{\mathrm{r}}(k) &= \beta_{\mathrm{r}}^{\mathrm{el}}(k) D_{\mathrm{r}}^{\mathrm{el}}(k) \\ Q_{\mathrm{r}}(k) &= \beta_{\mathrm{r}}^{\mathrm{th}}(k) D_{\mathrm{r}}^{\mathrm{th}}(k) \end{aligned},$$

where P_{r} and Q_{r} are the rescheduled electrical and thermal load, respectively. These rescheduled loads have to be consumed at other time steps. Since these loads are uninterruptible ones, they have to be satisfied in consecutive time steps. The amount of load that is consumed at each time step is a constant denotes as $D_{\mathrm{rc}}^{\mathrm{el}}$ or $D_{\mathrm{rc}}^{\mathrm{th}}$ for the electrical and thermal energy, respectively. A binary variable δ_{rc} is introduced to determine if the rescheduled load is consumed ($\delta_{\mathrm{rc}}(k) = 1$) or not ($\delta_{\mathrm{rc}}(k) = 0$) at time step k. This leads to the following constraint of the consumed rescheduled load per time step:

$$\begin{aligned} P_{\mathrm{rc}}(k) &= D_{\mathrm{rc}}^{\mathrm{el}} \delta_{\mathrm{rc}}^{\mathrm{el}}(k) \\ Q_{\mathrm{rc}}(k) &= D_{\mathrm{rc}}^{\mathrm{th}} \delta_{\mathrm{rc}}^{\mathrm{th}}(k) \end{aligned},$$

where $P_{\mathrm{rc}}(k)$ and $Q_{\mathrm{rc}}(k)$ are the consumed electrical and thermal energy at time step k. That this energy is uninterruptedly consumed, is assured using the constraint

$$\begin{aligned} \delta_{\mathrm{rc}}^{\mathrm{el}}(k) - \delta_{\mathrm{rc}}^{\mathrm{el}}(k-1) &\leq \delta_{\mathrm{rc}}^{\mathrm{el}}(\tau), \\ \delta_{\mathrm{rc}}^{\mathrm{th}}(k) - \delta_{\mathrm{rc}}^{\mathrm{th}}(k-1) &\leq \delta_{\mathrm{rc}}^{\mathrm{th}}(\tau), \end{aligned}$$

with $\tau = k+1, \ldots, k+T_{\mathrm{cr}}^{\mathrm{el}} - 1$ for the electrical energy or $\tau = k+1, \ldots, k+T_{\mathrm{cr}}^{\mathrm{th}} - 1$ for the thermal. $T_{\mathrm{cr}}^{\mathrm{el}}$ and $T_{\mathrm{cr}}^{\mathrm{th}}$ are the time needed for the unsatisfied rescheduled electrical $l_{\mathrm{r}}^{\mathrm{el}}$ and thermal load $l_{\mathrm{r}}^{\mathrm{th}}$ to be fully consumed, respectively. To estimate how much electrical and thermal load still needs to be consumed at time step k, it is updated following:

$$\begin{aligned} l_{\mathrm{r}}^{\mathrm{el}}(k) &= \sum_{i=1}^{k-1} P_{\mathrm{r}}(i) - \sum_{i=1}^{k} P_{\mathrm{rc}}(i) \\ l_{\mathrm{r}}^{\mathrm{th}}(k) &= \sum_{i=1}^{k-1} Q_{\mathrm{r}}(i) - \sum_{i=1}^{k} Q_{\mathrm{rc}}(i) \end{aligned}.$$

The rescheduled load has to be consumed before reaching a defined time step F. For example, a dishwasher can be rescheduled in the evening to a later time step, but one wants that the program is done by the coming morning. Therefore, no unsatisfied load should be present at that time step, i.e., $l_{\mathrm{r}}^{\mathrm{el}}(F_{\mathrm{el}}) = 0$ and $l_{\mathrm{r}}^{\mathrm{th}}(F_{\mathrm{th}}) = 0$.

D. Connection to utility grid

The microgrid remains connected to the utility grid at all times. Therefore, it is able to import or export electrical energy, hydrogen, or 'green' gas at a certain price. To model the utility grid, a binary logic variable δ_{UG} is introduced to determine if energy u_{UG} is bought ($\delta_{\mathrm{UG}}(k) = 1$) or sold ($\delta_{\mathrm{UG}}(k) = 0$) to the utility grid at time step k with $u_{\mathrm{UG}}(k) \geq 0 \iff \delta_{\mathrm{UG}}(k) = 1$. The economic cost C_{UG} for the microgrid, from the imported and exported energy with the utility grid, is modelled as

$$C_{\mathrm{UG}}(k)=\begin{cases} c^{\mathrm{P}}(k)u_{\mathrm{UG}}(k), & \text{if } \delta_{\mathrm{UG}}(k)=1 \\ c^{\mathrm{S}}(k)u_{\mathrm{UG}}(k), & \text{if } \delta_{\mathrm{UG}}(k)=0 \end{cases},$$

where $c^{\mathrm{P}}(k)$ and $c^{\mathrm{S}}(k)$ are the purchase and sale price of energy at time step k, respectively. The transferred energy is constrained by the maximum allowed energy transfer between the microgrid and the utility grid, i.e., $\underline{u}_{\mathrm{UG}}(k) \leq u_{\mathrm{UG}}(k) \leq \overline{u}_{\mathrm{UG}}(k)$.

For the purchase and sale price of electricity, a time-of-use price is computed. The electrical energy price varies greatly throughout the day and shows strong weekly patterns. Therefore, a weekly import price is computed for every time step during the week based on the national data of the Netherlands. A 20% increase in this price is added due to rising electrical energy price [18]. The purchasing price of hydrogen and 'green' gas is fixed throughout the day based on the data of [18]. The sale price of energy is assumed to be equal to the net import price, i.e., excluding taxes and transportation costs.

E. Operational constraints

Multiple operational constraints are presented in this section that are used in the microgrid.

1) Degradation: To tackle the problem of fast degradation for multiple components in the microgrid, a constraint is added as introduced in [16]. A constraint is set on the minimum time the system is turned on or off, i.e., T_{ON} and T_{OFF}, respectively. In this constraint, the introduced binary logic variables are used to define if the system is on ($\delta=1$) or off ($\delta=0$). Note that in the previous section, these modes were respectively the charging and discharging mode of the battery and battery EV. The constraint is expressed without resorting to any additional variable as

$$\begin{aligned}&\delta(k)-\delta(k-1)\leq\delta(\tau),\ \text{(off–on switch)}\\ &\delta(k-1)-\delta(k)\leq 1-\delta(\tau),\ \text{(on-off switch)}\end{aligned}$$

with $\tau=k+1,\ldots,k+T_{\mathrm{ON}}-1$ if the constraints for the ON time are considered or $\tau=k+1,\ldots,k+T_{\mathrm{OFF}}-1$ otherwise. The first line in this equation ensures the system satisfies the minimal 'on time' and the second line the minimal 'off time'. This constraint is used to prevent fast switching between modes in the battery, electrolyzer, $\mu-$CHP, hybrid heat pump, and both types of EVs. For the hybrid heat pumps, both for thermal energy generated by electrical energy consumption and by gas, the constraint is added. Moreover, for the EVs, this constraint is introduced for both the modes refilling and generation.

2) Range anxiety: The use of EV management strategies results in fear of the users that the EV will not be sufficiently charged upon departure, i.e., range anxiety [10]. In the model, it is chosen that it is not necessary that the EV should be fully charged upon departure since this will lead to conservative results and the exact departure time is generally not known in real life. However, the following constraint is introduced to ensure a certain state of charge $\underline{x}^{\mathrm{t}}_{\mathrm{EV}}$ is reached when the vehicle turns into transportation mode $\delta^{\mathrm{t}}_{\mathrm{EV}}$:

$$x_{\mathrm{EV}}(k)\geq \underline{x}^{\mathrm{t}}_{\mathrm{EV}}\delta^{\mathrm{t}}_{\mathrm{EV}}(k),$$

where $x_{\mathrm{EV}}(k)$ is the fuel storage of the EV at time step k. Since not all trips are known beforehand, one wants to ensure as well that enough fuel is in the EV before the EV will be generating electricity to the microgrid. Therefore, another constraint is added that assures a minimal state of charge $\underline{x}^{\mathrm{g}}_{\mathrm{EV}}$ in the EV is set before the EV can be in generation mode $\delta^{\mathrm{g}}_{\mathrm{EV}}$:

$$x_{\mathrm{EV}}(k)\geq \underline{x}^{\mathrm{g}}_{\mathrm{EV}}\delta^{\mathrm{g}}_{\mathrm{EV}}(k),$$

where $\underline{x}^{\mathrm{g}}_{\mathrm{EV}} < \underline{x}^{\mathrm{t}}_{\mathrm{EV}}$.

3) Power balance: The different types of energies in the microgrid have to be balanced at every time step. A constant ratio between energy and power at each time interval is due to the constant sampling time [16]. In the microgrid, different types of energies are considered: electrical energy, thermal energy, hydrogen, and 'green' gas. The power balances are given using the variables introduced in the previous section, respectively:

$$\begin{aligned}&u^{\mathrm{el}}_{\mathrm{UG}}(k)+P_{\mathrm{PV}}(k)+P_{\mathrm{CHP}}(k)+u^{\mathrm{el}}_{\mathrm{fev}}(k)=P_{\mathrm{res}}(k)\\ &+P_{\mathrm{com}}(k)+P_{\mathrm{rc}}(k)-P_{\mathrm{r}}(k)\\ &+u_{\mathrm{bat}}(k)+u_{\mathrm{bev}}(k)+u_{\mathrm{elc}}(k)+u^{\mathrm{el}}_{\mathrm{HP}}(k)\\ &Q_{\mathrm{CHP}}(k)+Q_{\mathrm{HP}}(k)=Q_{\mathrm{res}}(k)+Q_{\mathrm{com}}(k)+Q_{\mathrm{rc}}(k)\\ &-Q_{\mathrm{r}}(k)-Q_{\mathrm{c}}(k)\\ &u^{\mathrm{gas}}_{\mathrm{UG}}(k)=u^{\mathrm{gas}}_{\mathrm{CHP}}(k)+u^{\mathrm{gas}}_{\mathrm{HP}}(k)\\ &u^{\mathrm{hyd}}_{\mathrm{UG}}(k)+H_{\mathrm{elc}}(k)=u^{\mathrm{hyd}}_{\mathrm{CHP}}(k)+u^{\mathrm{hyd}}_{\mathrm{HP}}(k)+u^{\mathrm{hyd}}_{\mathrm{fev}}(k).\end{aligned}\tag{3}$$

In above equations, $(\cdot)^{\mathrm{el}}$, $(\cdot)^{\mathrm{gas}}$, and $(\cdot)^{\mathrm{hyd}}$ represent the energy that is generated or consumed as electricity, gas, and hydrogen, respectively. For almost all the power balances a connection to the utility grid that can act as an infinite buffer is present. The net imbalance of the microgrid can be compensated by importing or exporting more energy from the utility grid. The thermal power balance does not have this connection. However, since the generation of thermal energy is more of a conversion of other types of energy to thermal energy, the connections to the utility grid in the other power balances act indirectly as an infinity buffer for the thermal power balance.

III. Stochastic processes

The different stochastic processes in the microgrid, i.e., PV power, electrical and thermal energy demand of residential buildings, and electrical and thermal energy demand of commercial buildings, need to be forecasted to control the model described in previous section. This section comprises an overview of the different point forecasting models for each stochastic process. Real data is used based on meteorological measurements and energy consumption patterns in the Netherlands.

A. Background literature

An overview is presented of the different point forecasting models compared in this study.

1) Persistence approach: The persistence approach is a naive approach that assumes that the forecast values are the same as past observed values, e.g., for PV power generation, the solar irradiance during the day is similar to that of the previous day for each time step. For the energy demand of buildings, an assumption can be made that the value for next time steps are similar to the previous time step. However, increasing the forecasting horizon will significantly reduce the accuracy of the model [26]. For day-ahead forecasting, a day-to-day persistence method can be used [27]. Due to its naive approach and simplicity, the model is generally used as a benchmark model.

2) Linear regression: Linear regressions are widely used to forecast simple models that have an underlying linear correlation structure in the time series. This model is often used due to its simplicity. When nonlinear relationships describe the correlations in the time series better, a more complex estimation method should be used [28]. The forecasted values are based on the measured values of previous time steps and can include seasonality. Exogenous influences can be added as a linear time series to the model. Drawbacks of this method are the worse performance compared to smarter forecasting models for complex processes and the fact that data should be stationary to use the model. The model is trained by using historic data to calculate the coefficients for the constructed linear regression model.

3) Autoregressive Moving Average: A conventional statistical approach model used for forecasting is the autoregressive moving average model based on the Box-Jenkins method [29]. This model shows reliable predictions when there exists an underlying linear correlation structure in the time series. Furthermore, a favorable aspect of the model is its flexibility, since it can represent multiple types of time series by using different orders [26]. A main difference with the linear regression model is that it includes the moving average. Therefore, unobserved errors of previous forecasts are included for predicting the value of the next time steps. With the autoregressive moving average model, one assumes that the data show no characteristics of non-stationarity [30]. When non-stationarity data are considered, a generalization of the model can be used by creating an autoregressive integrated moving average model. Inherent seasonal effects of the data can be added to the model by adding seasonality to the model. Lastly, exogenous inputs with a high correlation to the forecasting data can be added to improve the performance of the model. Considering all extensions, a seasonal autoregressive integrated moving average model can be constructed as

$$\varphi_p(L)\Phi_P(L^s)\nabla^d\nabla_s^D X_t = \theta_q(L)\Theta_Q\left(L^s\right)\varepsilon_t + \beta_k x'_{k,t}.$$

In the above equation, the P, D, and Q are the seasonal autoregressive order, seasonal difference order, and seasonal moving average order, respectively. The quantity $\phi_p(L)$ is the regular autoregressive polynomial of order p and $\theta_q(L)$ the regular moving average polynomial of order q, while $\Phi_P(L^s)$ is the seasonal autoregressive polynomial of order P and $\Theta_Q(L^s)$ the seasonal moving average polynomial of order Q. Furthermore, L is the lag operator, X_t represents the forecast variable, ∇^d the differentiating operator, ∇_s^D the seasonal differentiating operator, and ε_t white noise. The exogenous part in the equation is $\beta_k x'_{k,t}$, where $x'_{k,t}$ is the exogenous input and β_k the coefficient value of the exogenous input of the k^{th} exogenous input variable.

4) Artificial neural network: An Artificial Neural Network (ANN) is a series of algorithms inspired by the neural network in a biological brain. It is trained by using a historical data set where it computes nonlinear relationships between the in- and outputs of the model. In general, an ANN consists of an input layer, output layer, and multiple hidden layers that make the connection between the input and output layer. Each layer is composed of one or more neurons where an activation function in the neurons determines the nonlinear mapping characteristics across the ANN [31]. This approach is widely used since it does not require mathematical expressions, it is self-learning, easy to implement, and short online computation time is needed. This approach is especially used for detecting complex nonlinear relations between the input and output [32]. However, drawbacks of the model are that it needs a significant amount of historical data to be properly trained and overfitting may occur [30].

The ANN has many different structures and applications. For forecasting time series, supervised learning algorithms are used to train the ANN. In this thesis, a long short-term memory recurrent ANN, as first introduced in [33], is used to forecast the stochastic processes. Recurrent networks are fundamentally different from the traditional feedforward neural network since they can establish a temporal correlation between previous information and current circumstances [34]. Therefore, decisions made at a previous time step influences the decision for coming time steps in the ANN. These recurrent ANNs are trained by the popular back-propagation through time. Due to the gradient vanishing or exploring in the training of the ANN, long-range dependencies are difficult to learn. This problem can be overcome by using long short-term recurrent ANNs that uses a memory cell to capture these long-range dependencies [34], [33]. The long short-term recurrent ANNs used in this thesis are modelled with multiple layers using a mini-batch gradient descent. This is done to increase the training speed of the ANN compared to the batch gradient descent, but preventing the regularizing effect of using a stochastic gradient descent where a batch size of one is used.

B. PV power

For the PV power, two stochastic processes needed to be forecasted as determined from (2), i.e., the solar irradiance and ambient temperature. Both stochastic processes are forecasted in time steps of one hour.

1) Solar irradiance: A clear sky model is sued where the global horizontal solar irradiance is computed as if it is a clear sky day $G_{\mathrm{c}}^{\mathrm{cs}}$, i.e., without any clouds [35], [36]. Therefore, the stochastic component is excluded and a clear sky global horizontal solar irradiance can be obtained for every hour in the year. With these values, the clear sky index τ can be computed as the normalization of the measured solar irradiance $G_{\mathrm{c}}(k)$:

$$\tau(k) = \frac{G_{\mathrm{c}}}{G_{\mathrm{c}}^{\mathrm{cs}}}. \tag{4}$$

The clear sky model is obtained from the used data, and absent data are computed using a statistical smoothing technique based on weighted quantile regressions as in [35]. In general, a limiting factor of developing clear sky data is the absence or quality of the data [37], i.e., in the winter there are not many clear sky observations to train the model and this increases the error of the quantile regression. This problem is partly solved by using data of the past 20 years.

It is decided from the autocorrelation of the the clear sky index that the prediction models will use data of one hour and 24 hours before. Different exogenous inputs can be considered based on the geographical location [30], [38] and from the data it is concluded the highest correlation coefficients for the solar irradiance are obtained with the temperature, presence of snow, and humidity. With these exogenous inputs, it is concluded that an ANN model provides the smallest error.

2) Ambient Temperature: The autocorrelation is analyzed and it is chosen to use the data from one to five and 24 hours before for the forecasting. It is concluded that solar irradiance and humidity have the strongest correlation for temperature, but are still low. Using a seasonal autoregressive integrated moving average model provided the smallest error, i.e., without the use of exogenous inputs.

C. Residential energy demand

The energy of residential consumers is characterized by the distinctive pattern during the day, having a peak consumption in the early evening. This peak is often the creating the general peak in the microgrid where the electrical energy grid investments are based upon. In this section, both the electrical and thermal energy demand are forecasted in the sampling time of 15 minutes and one hour, respectively. Since data of only one year is available and used, the ANN did not have enough training data to construct a proper model.

1) Electrical energy demand: From the autocorrelation, it is chosen that for the electrical energy demand, data of the previous 45 minutes and of 23:45-24:15 hours before is used. No exogenous inputs did improve the models of for the residential electrical energy demand. A seasonal autoregressive integrated moving average obtained the smallest error and is used in this study.

2) Thermal energy demand: Time series data of the previous two hours and of of 23 - 25 hours before is used, as concluded from the autocorrelation. A high correlation coefficient between the thermal energy demand and the ambient temperature is calculated, and the temperature is used as an exogenous input in the forecasting models. The smallest error is obtained using the seasonal autoregressive integrated moving average model.

D. Commercial energy demand

The commercial energy demand show great differences in the consumption pattern between weekdays and the weekend. This is based on their opening hours, i.e., small stores are more often closed in the weekend in the Netherlands. In this section, both the electrical and thermal energy demand are forecasted in the sampling time of 15 minutes and one hour, respectively.

1) Electrical energy demand: From the autocorrelation, it is chosen that for the electrical energy demand, data of the previous 30 minutes and of 168 hours before (week) is used. No exogenous inputs did improve the models of for the commercial electrical energy demand. The ANN obtained the best performance, i.e., smallest error in the point forecasts.

2) Thermal energy demand: Time series data of the previous hour and of 23 - 25 hours before is used, as concluded from the autocorrelation. A high correlation coefficient between the thermal energy demand and the ambient temperature is calculated, and the temperature is used as an exogenous input in the forecasting models. The smallest error is obtained using the ANN model.

IV. CONTROL

This section comprises the objective function of the optimization in the microgrid and the MPC strategy used.

A. Objective function

The objective function considers the economic profitability of lowering the peak of electrical energy demand (J_{gd}) as well as the energy import costs (J_{eco}). Discomfort penalties (J_{dis}) and the durability of the EVs (J_{dur}) are included as well, concluding on a multi-objective function as

$$J = \alpha J_{\mathrm{eco}} + \beta J_{\mathrm{dis}} + \gamma J_{\mathrm{dur}} + \lambda J_{\mathrm{gd}},$$

with α, β, γ, and λ being arbitrary predefined weights.

1) Economic objective: The economic objective is based on the import costs of the different energy sources from the utility grid in the prediction horizon N_{p}, i.e., electricity ($C_{\mathrm{UG}}^{\mathrm{el}}$), 'green' gas $C_{\mathrm{UG}}^{\mathrm{gas}}$, and hydrogen $C_{\mathrm{UG}}^{\mathrm{hyd}}$. Operational costs as the increase in maintenance and startup and shut-down costs as in [16] are not considered due to the difficult assumptions that need to be made to approximate these costs in the future microgrid. Therefore, the economic objective is written as

$$J_{\mathrm{eco}} = \sum_{\mathrm{k=1}}^{\mathrm{Np}} \left(C_{\mathrm{UG}}^{\mathrm{el}}(k) + C_{\mathrm{UG}}^{\mathrm{gas}}(k) + C_{\mathrm{UG}}^{\mathrm{hyd}}(k) \right).$$

2) Discomfort objective: The discomfort for the consumers in the microgrid will mainly be influenced by the usage of demand response. Furthermore, the range anxiety is included by penalizing a lower state of charge of an EV. Another low discomfort is placed on the amount of energy in the battery and hydrogen storage tank. This is penalized in a similar way as for the state of charge of the EVs. The discomfort objective can be written as

$$
\begin{aligned}
J_{\mathrm{dis}} = &\sum_{\mathrm{k=1}}^{\mathrm{N_p}} \Big(\rho_{\mathrm{c}}\beta_{\mathrm{c}}(k) + \rho_{\mathrm{r}}^{\mathrm{el}}\beta_{\mathrm{r}}^{\mathrm{el}}(k) + \rho_{\mathrm{r}}^{\mathrm{th}}\beta_{\mathrm{r}}^{\mathrm{th}}(k) \\
&+ \frac{\rho_{\mathrm{EV}}}{N_{\mathrm{EV}}}\left(\sum_{\mathrm{i=1}}^{\mathrm{N_{bev}}} \frac{\overline{x}_{\mathrm{bev,i}} - x_{\mathrm{bev,i}}(k)}{\overline{x}_{\mathrm{bev,i}}}\right. \\
&+ \left.\sum_{\mathrm{i=1}}^{\mathrm{N_{fev}}} \frac{\overline{x}_{\mathrm{fev,i}} - x_{\mathrm{fev,i}}(k)}{\overline{x}_{\mathrm{fev,i}}}\right) \\
&+ \rho_{\mathrm{bat}}\frac{\overline{x}_{\mathrm{bat}}(k) - x_{\mathrm{bat}}}{\overline{x}_{\mathrm{bat}}} + \rho_{\mathrm{hst}}\frac{\overline{x}_{\mathrm{hst}} - x_{\mathrm{hst}}(k)}{\overline{x}_{\mathrm{hst}}}\Big)
\end{aligned}
$$

where ρ_{c}, $\rho_{\mathrm{r}}^{\mathrm{el}}$ and $\rho_{\mathrm{r}}^{\mathrm{th}}$ are the penalty weight on curtailment and rescheduling of the electrical and thermal energy, respectively. ρ_{EV}, ρ_{bat}, and ρ_{hst} are the penalty given on the state of charge of the total number of EVs (N_{EV}), the battery, and the hydrogen storage tank, respectively.

3) Durability objective: Frequent use of the EVs in vehicle-to-grid, will result in faster degradation of these EVs. Despite the degradation is tackled up to a certain degree using the operation constraints, a penalization is still applied to the usage of the EVs in vehicle-to-grid for giving energy to the microgrid to increase its durability as

$$
J_{\mathrm{dur}} = \frac{1}{N_{\mathrm{EV}}}\sum_{\mathrm{k=1}}^{\mathrm{N_p}}\left(\sum_{\mathrm{i=1}}^{\mathrm{N_{bev}}}\frac{z_{\mathrm{bev,i}}^{\mathrm{g}}(k)}{\overline{z}_{\mathrm{bev,i}}^{\mathrm{g}}} + \sum_{\mathrm{i=1}}^{\mathrm{N_{bev}}}\frac{u_{\mathrm{fev,i}}^{\mathrm{el}}(k)}{\overline{u}_{\mathrm{fev,i}}^{\mathrm{el}}}\right),
$$

where $z_{\mathrm{bev}}^{\mathrm{g}} = \delta_{\mathrm{bev}}^{\mathrm{g}}u_{\mathrm{bev}}$ is chosen as introduced for the mixed logical dynamical modelling, where $\delta_{\mathrm{bev}}^{\mathrm{g}}$ indicates if the battery EV is in generation mode.

4) Grid demand objective: The maximum value of the electrical energy exchange per time step is penalized since this study wants to reduce the increase in energy infrastructure. Therefore, the absolute maximum energy transfer of the electricity needs to be minimized using the weight ρ_{GD}. An auxiliary variable $\zeta_{\mathrm{ug}}^{\mathrm{el}}$ is introduced to maintain the linear objective function using $z_{\mathrm{UG}}^{\mathrm{el}} = \delta_{\mathrm{UG}}^{\mathrm{el}}u_{\mathrm{UG}}^{\mathrm{el}}$ as introduced for the mixed logical dynamical modelling. This results in the objective as

$$
\begin{aligned}
&J_{\mathrm{gd}} = \rho_{\mathrm{GD}}\cdot\max_{k}|u_{\mathrm{UG}}^{\mathrm{el}}(k)| = \rho_{\mathrm{GD}}\cdot\zeta_{\mathrm{ug}}^{\mathrm{el}},\ \text{with} \\
&\zeta_{\mathrm{ug}}^{\mathrm{el}} \geq 2z_{\mathrm{UG}}^{\mathrm{el}}(k) - u_{\mathrm{UG}}^{\mathrm{el}}(k), \quad k = 1,\ \ldots,\ \mathrm{Np}.
\end{aligned}
$$

B. Nominal MPC

There has been a vast amount of literature on nominal MPC for discrete-time systems where the known states $\boldsymbol{x}$ and inputs $\boldsymbol{u}$ are constrained, described as

$$
\begin{aligned}
&\boldsymbol{x}^{+} = f(\boldsymbol{x},\ \boldsymbol{u}), \quad \boldsymbol{y} = h(\boldsymbol{x}), \boldsymbol{x}\in\mathbb{X},\ \boldsymbol{u}\in\mathbb{U}, \\
&f\in\mathbb{R}^{n}\times\mathbb{R}^{m}\to\mathbb{R}^{n},\ \boldsymbol{y}\in\mathbb{R}^{b},\ \text{and}\ h\in\mathbb{R}^{n},
\end{aligned}
\tag{5}
$$

with $\boldsymbol{x}^{+}$ representing the successor states and $\boldsymbol{y}$ the outputs of the system. In this system, the state is assumed to be observable. At each event of the state or time, the optimal control problem is solved while simulating future states in a receding horizon fashion. The length of the finite-horizon, wherein these future states lie, is called the prediction horizon. For this prediction horizon, a control sequence is computed with the length of the control horizon. The first control of the computed sequence is implemented in the system and the process is repeated for the next control step. Due to this method, future output in the chosen prediction horizon can be considered while choosing the control input. Increasing the control horizon can improve the performance of the optimal control problem, but increases the computation time.

The use of MPC on hybrid systems is not as extensively researched as standard linear processes with linear constraints [39]. The main drawback of hybrid systems is the computational burden due to the introduction of the integer variables in the optimization. The complexity is NP-hard and to test if a new feasible solution improves the best one so far is an NP problem [39]. Another drawback is the loss of convexity and it is therefore not known if a feasible solution is the global optimum.

No constraints satisfaction nor recursive feasibility can be guaranteed by using the nominal MPC due to the errors in the point forecasts, i.e., violations of the constraints can occur [40]. A low-level controller is implemented in the microgrid to compensate for the discrepancies the microgrid during the optimization.

V. Case study

In this chapter, simulations are done in different case studies. The set-up of the case studies is formulated. Three scenarios that consider different levels of penetration of hydrogen in the microgrid are defined to be tested in the case studies. From these results, the question how hydrogen influences the peak of electrical energy transfer of the microgrid is answered.

A. Setup

The number of distributed energy resources and their maximum power is partly chosen by making a realistic investment based on the energy demand and partly by obtained ratios from data.

a) Buildings: To estimate the energy demand of the microgrid, the number of buildings in the microgrid is chosen. A ratio of 42:1 for residential to small commercial buildings is calculated based on data in Amsterdam. Therefore, it is chosen to construct a microgrid with 42 residential buildings and one small commercial building. It is chosen not to include more buildings since this will increase the computation time due to an increase of decision variables.

b) Demand Response: In each residential building, a dishwasher, with an energy consumption of 0.78 kWh that is used five times a week, is chosen to participate in the DR program as rescheduable load. Furthermore, 10% of the real consumed thermal energy demand in residential buildings can be rescheduled and another 10% curtailed.

c) Electric Distributed Energy Resources: PV panels are installed on each building with an average power of 3.34 kW, estimated from the research done in [18]. This yields a 143.62 kW maximum power of solar panels in the microgrid. A district battery with a maximum storage capacity of 500 kWh and a maximum power of 150 kW is considered. It is assumed that the battery does not discharge below 10% of its maximum capacity and has a charging and discharging efficiency of 90%. An electrolyzer is used with a maximum power consumption of 25 kW containing an integrated hydrogen storage system of 500 kg. It is assumed that the storage level does not drop below 5% of the maximum storage. Since an efficiency of the electrolyzer of 70% and a heating value of hydrogen of 39.4 kWh/kg [9] are assumed, the model parameter α_{elc} is estimated to be 0.02 kg/kWh.

d) Thermal Distributed Energy Resources: A hybrid heat pump is installed with a maximum power of 20 kW. The efficiency for the electric part is 400%. The boiler in the hybrid heat pump that burns gas has an efficiency of 90% for both 'green' gas and hydrogen. Furthermore, a 5 kW μ-CHP plant is installed with a thermal storage capacity of 70 kWh. The efficiency for the electrical energy and thermal energy are 22.5% and 67.5% for the $\mu-$CHP plant with an internal combustion engine, respectively, and both 45% for the $\mu-$CHP plant with a fuel cell.

e) Electric Vehicles: A ratio of a single EV per household is considered. Battery EVs with a charging and discharging efficiency of 90% and a maximum battery storage capacity of 100 kWh are used. Their charging or discharging power is set to be a maximum of 16 kW. The fuel cell EVs in the microgrid have a fuel storage of 7 kg of hydrogen with a refilling rate of 2 kg/h. Since this EV operates on partial load in the microgrid, the maximum power is set to be at 15 kW. The model parameters α_{FEV} and β_{FEV} for the fuel cell EVs are based on the model of fuel cell stacks in [23] and are determined to be 0.06 kg/kWh and 0.11 kg/h, respectively [9].

B. Scenarios

Three scenarios with a different level of penetration of hydrogen in the microgrid are considered. The energy and thermal demand is similar for each scenario. Therefore, a fair comparison can be made about how the introduction of hydrogen to the microgrid will influence the performance. The following three scenarios are considered:

1) **Electric**: In this scenario, no hydrogen is present in the microgrid, excluding the presence of the electrolyzer with an integrated hydrogen storage tank and fuel cell EVs. The hybrid heat pumps and μ-CHP plant can run on 'green' gas that is imported from the utility grid.
2) **Mixed**: This scenario is based on the expected microgrid in the Netherlands in 2050 [18]. Both electric- and hydrogen-based components are present in the microgrid. However, no 'green' gas is considered since hydrogen will be using the current natural gas infrastructure. Using both gases will lead to an extra gas network that is preferred to be avoided since the extra investments needed will probably overrule the potential profit. Therefore, the hybrid heat pumps and μ-CHP plant will contain fuel cells to run on hydrogen instead of the 'green' gas. Furthermore, the electrolyzer with an integrated hydrogen storage tank is included in the microgrid. Both types of EVs are present and a ratio of 1.5:1 for the battery to the fuel cell EVs is used [18].
3) **Hydrogen**: In this scenario, a largely hydrogen-based microgrid is sketched. The microgrid consists of almost the same distributed energy resources as in the mixed scenario, only the battery is excluded from the microgrid. Furthermore, all the battery EVs are replaced by fuel cell EVs.

C. Performance Indices

The performance of the tertiary control of the microgrid is measured by quantitative and qualitative performance indices. In the quantitative performance indices, the performance is measured in economic costs. The qualitative performance indices are estimated as a ratio between 0 and 1, resembling a better performance with a higher value. An overview of these different performance indices for the simulation time T are:

Quantitative performance indices

- **Electrical grid investment:** The peak of electrical energy transfer is translated to variable economic investments needed to be paid by the energy suppliers following the current prices in the Netherlands. Hence, economic costs can be associated with the rise of the peak electrical energy transfer, i.e., €2.4147 per month (T_{m}) per maximum transferred energy in kW. This results in the equation for the electrical grid investment as

$$EGI = 2.4147 \cdot \frac{T}{T_{\mathrm{m}}} \zeta_{\mathrm{ug}}^{\mathrm{el}}$$

- **Energy import costs:** The netted economic costs of the microgrid by purchasing and selling energy is calculated as

$$EIC = \sum_{\mathrm{k}=1}^{\mathrm{T}} \left(C_{\mathrm{UG}}^{\mathrm{el}}(k) + C_{\mathrm{UG}}^{\mathrm{gas}}(k) + C_{\mathrm{UG}}^{\mathrm{hyd}}(k) \right)$$

Qualitative performance indices

- **Comfort level:** The discomfort costs in the microgrid are rewritten as a normalized comfort level for the consumers. This comfort level is estimated by considering the comfort decrease due to participation in DR, the influence of range anxiety, and battery state of charge. The comfort level is calculated as the discomfort objective divided by its weights as

$$CL = 1 - \frac{J_{\mathrm{dis}}}{\rho_{\mathrm{c}} + \rho_{\mathrm{r}}^{\mathrm{el}} + \rho_{\mathrm{r}}^{\mathrm{th}} + \rho_{\mathrm{EV}} + \rho_{\mathrm{bat}} + \rho_{\mathrm{hst}}}$$

- **Durability of EV:** The durability of the EVs is influenced by the possible intensive usage in vehicle-to-grid and is also penalized in the objective function. A durability ratio for the EVs is calculated that identifies the ratio of vehicle-to-grid used when not on transportation ($\delta^{\mathrm{t}} = 0$). The durability ratio for the EVs is calculated as

$$DEV_{\mathrm{n}} = \sum_{\mathrm{k=1}}^{\mathrm{T}} \left(\sum_{\mathrm{i=1}}^{\mathrm{N_{BEV}}} \left(1 - \delta_{\mathrm{i}}^{\mathrm{t}}(k)\right) \frac{z_{\mathrm{BEV,i}}^{\mathrm{g}}(k)}{\overline{z}_{\mathrm{BEV,i}}^{\mathrm{g}}} + \sum_{\mathrm{i=1}}^{\mathrm{N_{BEV}}} \left(1 - \delta_{\mathrm{i}}^{\mathrm{t}}(k)\right) \frac{u_{\mathrm{FEV,i}}^{\mathrm{el}}(k)}{\overline{u}_{\mathrm{FEV,i}}^{\mathrm{el}}} \right.$$

$$DEV = 1 - \frac{DEV_{\mathrm{n}}}{\sum_{\mathrm{k=1}}^{\mathrm{T}} \sum_{\mathrm{i=1}}^{\mathrm{N_{EV}}} \left(1 - \delta_{i}^{\mathrm{t}}(k)\right)}$$

- **Electric self-supply:** A microgrid can be rated by the ability to use the generated energy in the microgrid as proposed in [41], [42], [43], i.e., not selling the energy if there is an abundance. The electric self-supply performance index calculates the ratio between the exported and generated electrical energy in the microgrid, where $(\cdot)^{\mathrm{th}}$ can be presenting hydrogen or ‘green’ gas in kWh dependent on the scenario, as

$$ESS = 1 - \frac{\sum_{\mathrm{k=1}}^{\mathrm{T}} \left(z_{\mathrm{UG}}^{\mathrm{el}}(k) - u_{\mathrm{UG}}^{\mathrm{el}}(k)\right)}{\sum_{\mathrm{k=1}}^{\mathrm{T}} \left(P_{\mathrm{PV}}(k) + P_{\mathrm{CHP}}(k)\right)}$$

- **Energy independence:** The energy independence of a microgrid can be rated by calculating the ratio of imported energy to the consumed energy [41], [44], [42], [45]. The energy independence is a measure for self reliance of a microgrid. It explains the ability of a microgrid to deal with unexpected excessive demand. Similar to the self-supply performance index, $(\cdot)^{\mathrm{th}}$ can be presenting hydrogen or ‘green’ gas in kWh dependent on the scenario. Furthermore, the trip costs of the fuel cell EVs are also written in kWh. The energy independence of the microgrid is calculated as

$$EI_{\mathrm{d}} = \sum_{\mathrm{k=1}}^{\mathrm{T}} \left(P_{\mathrm{res}}(k) + P_{\mathrm{com}}(k) + Q_{\mathrm{res}}(k) + Q_{\mathrm{com}}(k) + \sum_{\mathrm{k=1}}^{\mathrm{N_{BEV}}} \left(h_{\mathrm{BEV,i}}(k)\right) + \sum_{\mathrm{k=1}}^{\mathrm{N_{FEV}}} \left(h_{\mathrm{FEV,i}}(k)\right) \right)$$

$$EI = 1 - \frac{\sum_{\mathrm{k=1}}^{\mathrm{T}} \left(z_{\mathrm{UG}}^{\mathrm{el}}(k) + z_{\mathrm{UG}}^{\mathrm{th}}(k)\right)}{EI_{\mathrm{d}}}$$

D. Simulation weeks

Three different weeks are simulated, each representing a different energy demand and generation patterns. A strong difference for the energy demand and PV power generation throughout the year is concluded from the analysis of the stochastic processes. Therefore, it is chosen to simulate a typical winter and summer week in the Netherlands. These two weeks are analyzed, and it is concluded what type of week the most energy transfer between the microgrid and utility grid is expected. Then, a week with extreme conditions is constructed where the most energy transfer between the microgrid and utility grid is expected. This week indicates the minimum electrical energy grid investment needed to guarantee the reliability of the microgrid. A week with extreme cold temperatures in the winter is chosen to present this week. Therefore, there is a high thermal energy demand and low PV power due to the low solar irradiance in the winter. From these different weeks, an overview of the average costs during the year can be sketched based on the summer and winter case study. Furthermore, the minimum electrical energy grid investments can be obtained by the week with extreme conditions.

Each simulation in the different microgrids consists of eight consecutive days whereof the first day is used for initialization. Thus, the results are based on the last seven days of the simulation. The simulation starts on a Monday and ends on the next Monday. It is chosen to use this order to include the influences of the weekend on the first weekday.

The mixed-integer linear programming problem is solved in the Matlab R2020a environment using Gurobi. A HP EliteBook 8570w with a 2.3 GHz Intel Core i7 processor and 4 GB of RAM is used for the simulations. Different computation times are obtained for the controllers in each case study and scenario. In general, the computation time increases with a higher energy demand in the case study. The computation time for the week with extreme conditions are approximately 3 hours.

E. Results

In Table I the system performance is presented. It is concluded that a general trend is present for each week between the scenarios. A higher level of hydrogen penetration in the microgrid reduces the peak of electrical energy transfer of the microgrid. However, the total economic costs increase due to the higher energy import costs. These higher energy import costs are mainly due to the more expensive fuel costs for fuel cell EVs compared to battery EVs. The fuel costs are more expensive due to the higher import price of hydrogen compared to electrical energy and the low efficiency in the fuel cells. It must be noted that the expected hydrogen price and low efficiency of the fuel cells influence the results of the optimization substantially and future research should focus on these developments.

To quantify the reduction of the peak of electrical energy transfer and the total economic costs, the electrical energy grid investments are based on the week with extreme conditions. The energy import costs are calculated by averaging the costs in the typical winter and summer weeks, representing an approximation of the mean costs throughout the year. It is concluded that a reduction in the electrical grid investments is realized of 16.90% and 81.29% for the mixed and hydrogen scenario, respectively. However, the total economic costs are increased for the mixed and hydrogen scenario, respectively, by 29.92% and 52.38%.

The introduction of hydrogen results in lower energy independence of the microgrid, decreasing the self-reliance of the microgrid. This is caused due to the lower efficiency of the fuel cell compared to the battery. Another trend is that for the mixed scenario including both battery and fuel cell EVs, there is more degradation on the vehicles due to the higher use of the EV in vehicle-to-grid operations. Furthermore, in the mixed scenario, a lower comfort level is obtained due to the lower state of charge of the EVs. No clear differences are concluded for the self-supply of the microgrids.

TABLE I
THE RESULTS ON THE PERFORMANCE INDICES FOR THE SCENARIOS IN THE DIFFERENT WEEKS.

Week	Scenario	EGI [€]	EIC [€]	Total costs [€]	CL	DEV [10^3]	ESS	EI
Winter	Electric	338	409	747	0.6379	0.7554	0.8448	0.5956
	Mixed	239	711	950	0.5873	0.6230	0.8414	0.5171
	Hydrogen	48	1,115	1,163	0.6320	0.7424	0.8660	0.4075
Summer	Electric	271	53	324	0.8826	0.6795	0.7973	0.7073
	Mixed	173	211	384	0.7432	0.6349	0.8007	0.3831
	Hydrogen	34	511	545	0.8258	0.8031	0.8034	0.1347
Extreme conditions	Electric	345	548	893	0.4537	0.7648	0.9478	0.6760
	Mixed	286	850	1,136	0.4306	0.6450	0.9402	0.6081
	Hydrogen	64	1,257	1,321	0.4624	0.7497	0.9618	0.5406

VI. CONCLUSIONS

In this paper, the influence of hydrogen to the peak of electrical energy transfer of a microgrid is analyzed. A simulation-based case study is performed where scenarios with different levels of hydrogen are compared. It is concluded that the introduction of hydrogen in the microgrid reduces the peak of electrical energy transfer against higher energy import costs. Therefore, the total economic costs of the microgrid and the overall performance increase with the introduction of hydrogen. Furthermore, the introduction of hydrogen in the microgrid show a clear decrease in the energy indecency of the microgrid. In a microgrid containing both battery and fuel cell EVs, it is concluded that more vehicle-to-grid operations are used compared to the microgrids including only one type of EV.

In this study, the arrival and departure times of the EVs are assumed to be known. By considering unknown departure times, forecasting models should be developed to predict the behaviour of this stochastic process. Furthermore, it is expected that different (lower) performance will be obtained for the microgrid and this should be analyzed.

Scaling the size of the microgrid could influence the performance of the microgrid. Therefore, the influence of hydrogen on these smaller or larger microgrids should be evaluated. Since the computational complexity rises when increasing the size of the microgrid, alternative techniques as distributed MPC or parameterized MPC could be considered.

REFERENCES

[1] A. Hirsch, Y. Parag, and J. Guerrero, "Microgrids: A review of technologies, key drivers, and outstanding issues," *Renewable and Sustainable Energy Reviews*, vol. 90, pp. 402–411, 2018.

[2] S. S. Farahani, R. van der Veen, V. Oldenbroek, F. Alavi, E. H. P. Lee, N. van de Wouw, A. van Wijk, B. De Schutter, and Z. Lukszo, "A hydrogen-based integrated energy and transport system: The design and analysis of the car as power plant concept," *IEEE Systems, Man, and Cybernetics Magazine*, vol. 5, no. 1, pp. 37–50, 2019.

[3] J. Lago, K. De Brabandere, F. De Ridder, and B. De Schutter, "Short-term forecasting of solar irradiance without local telemetry: A generalized model using satellite data," *Solar Energy*, vol. 173, pp. 566–577, 2018.

[4] A. Zakariazadeh, S. Jadid, and P. Siano, "Smart microgrid energy and reserve scheduling with demand response using stochastic optimization," *International Journal of Electrical Power & Energy Systems*, vol. 63, pp. 523–533, 2014.

[5] C. D. Korkas, S. Baldi, I. Michailidis, and E. B. Kosmatopoulos, "Occupancy-based demand response and thermal comfort optimization in microgrids with renewable energy sources and energy storage," *Applied Energy*, vol. 163, pp. 93–104, 2016.

[6] H. S. V. S. K. Nunna and S. Doolla, "Demand response in smart distribution system with multiple microgrids," *IEEE Transactions on Smart Grid*, vol. 3, no. 4, pp. 1641–1649, 2012.

[7] J. C. Mukherjee and A. Gupta, "A review of charge scheduling of electric vehicles in smart grid," *IEEE Systems Journal*, vol. 9, no. 4, pp. 1541–1553, 2014.

[8] B. Yildiz, J. I. Bilbao, and A. B. Sproul, "A review and analysis of regression and machine learning models on commercial building electricity load forecasting," *Renewable and Sustainable Energy Reviews*, vol. 73, pp. 1104–1122, 2017.

[9] F. Alavi, E. P. Lee, N. van de Wouw, B. De Schutter, and Z. Lukszo, "Fuel cell cars in a microgrid for synergies between hydrogen and electricity networks," *Applied Energy*, vol. 192, pp. 296–304, 2017.

[10] J. Geske and D. Schumann, "Willing to participate in vehicle-to-grid (V2G)? Why not!" *Energy Policy*, vol. 120, pp. 392–401, 2018.

[11] P. Siano, "Demand response and smart grids - A survey," *Renewable and Sustainable Energy Reviews*, vol. 30, pp. 461–478, 2014.

[12] Y. Manoharan, S. E. Hosseini, B. Butler, H. Alzhahrani, B. T. F. Senior, T. Ashuri, and J. Krohn, "Hydrogen fuel cell vehicles; Current status and future prospect," *Applied Sciences*, vol. 9, no. 11, p. 2296, 2019.

[13] J. S. Lai and M. W. Ellis, "Fuel cell power systems and applications," *Proceedings of the IEEE*, vol. 105, no. 11, pp. 2166–2190, 2017.

[14] C. E. Thomas, "Fuel cell and battery electric vehicles compared," *International Journal of Hydrogen Energy*, vol. 34, no. 15, pp. 6005–6020, 2009.

[15] P. Velarde, L. Valverde, J. M. Maestre, C. Ocampo-Martínez, and C. Bordons, "On the comparison of stochastic model predictive control strategies applied to a hydrogen-based microgrid," *Journal of Power Sources*, vol. 343, pp. 161–173, 2017.

[16] A. Parisio, E. Rikos, and L. Glielmo, "A model predictive control approach to microgrid operation optimization," *IEEE Transactions on Control Systems Technology*, vol. 22, no. 5, pp. 1813–1827, 2014.

[17] L. Bartolucci, S. Cordiner, V. Mulone, and M. Santarelli, “Hybrid renewable energy systems: Influence of short term forecasting on model predictive control performance,” *Energy*, vol. 172, pp. 997–1004, 2019.

[18] Berenschot and Kalavasta, “Klimaatneutrale energiescenario’s 2050,” [Online]. Available: https://www.rijksoverheid.nl/documenten/rapporten/2020/03/31/klimaatneutrale-energiescenarios-2050, accessed: 04-May-2020.

[19] C. Riordan and R. Hulstron, “What is an air mass 1.5 spectrum? (Solar cell performance calculations),” in *IEEE Conference on Photovoltaic Specialists*. IEEE, 1990, pp. 1085–1088.

[20] C. Liu, K. T. Chau, D. Wu, and S. Gao, “Opportunities and challenges of vehicle-to-home, vehicle-to-vehicle, and vehicle-to-grid technologies,” *Proceedings of the IEEE*, vol. 101, no. 11, pp. 2409–2427, 2013.

[21] M. Van Der Kam and W. van Sark, “Smart charging of electric vehicles with photovoltaic power and vehicle-to-grid technology in a microgrid; a case study,” *Applied Energy*, vol. 152, pp. 20–30, 2015.

[22] C. Corchero, M. Cruz-Zambrano, F. J. Heredia *et al.*, “Optimal energy management for a residential microgrid including a vehicle-to-grid system,” *IEEE Transactions on Smart Grid*, vol. 5, no. 4, pp. 2163–2172, 2014.

[23] P. Rodatz, G. Paganelli, A. Sciarretta, and L. Guzzella, “Optimal power management of an experimental fuel cell/supercapacitor-powered hybrid vehicle,” *Control Engineering Practice*, vol. 13, no. 1, pp. 41–53, 2005.

[24] F. Alavi, N. van de Wouw, and B. De Schutter, “Min-max control of fuel-cell-car-based smart energy systems,” in *European Control Conference*. IEEE, 2016, pp. 1223–1228.

[25] N. Refa and N. Hubbers, “Impact of smart charging on EVs charging behaviour assessed from real charging events,” *32nd Electric Vehicle Symposium*, 2019.

[26] C. Wan, J. Zhao, Y. Song, Z. Xu, J. Lin, and Z. Hu, “Photovoltaic and solar power forecasting for smart grid energy management,” *CSEE Journal of Power and Energy Systems*, vol. 1, no. 4, pp. 38–46, 2015.

[27] G. Santamaría-Bonfil, A. Reyes-Ballesteros, and C. Gershenson, “Wind speed forecasting for wind farms: A method based on support vector regression,” *Renewable Energy*, vol. 85, pp. 790–809, 2016.

[28] L. Hernandez, C. Baladron, J. M. Aguiar, B. Carro, A. J. Sanchez-Esguevillas, J. Lloret, and J. Massana, “A survey on electric power demand forecasting: Future trends in smart grids, microgrids and smart buildings,” *IEEE Communications Surveys & Tutorials*, vol. 16, no. 3, pp. 1460–1495, 2014.

[29] G. E. P. Box, G. M. Jenkins, and G. C. Reinsel, *Time Series Analysis, Forecasting and Control*. Holden Day, 1976.

[30] U. K. Das, K. S. Tey, M. Seyedmahmoudian, S. Mekhilef, M. Y. I. Idris, W. Van Deventer, B. Horan, and A. Stojcevski, “Forecasting of photovoltaic power generation and model optimization: A review,” *Renewable and Sustainable Energy Reviews*, vol. 81, pp. 912–928, 2018.

[31] P. Gou and J. Yu, “A nonlinear ANN equalizer with mini-batch gradient descent in 40Gbaud PAM-8 IM/DD system,” *Optical Fiber Technology*, vol. 46, pp. 113–117, 2018.

[32] J. Jung and R. P. Broadwater, “Current status and future advances for wind speed and power forecasting,” *Renewable and Sustainable Energy Reviews*, vol. 31, pp. 762–777, 2014.

[33] S. Hochreiter and J. Schmidhuber, “Long short-term memory,” *Neural Computation*, vol. 9, no. 8, pp. 1735–1780, 1997.

[34] W. Kong, Z. Y. Dong, Y. Jia, D. J. Hill, Y. Xu, and Y. Zhang, “Short-term residential load forecasting based on LSTM recurrent neural network,” *IEEE Transactions on Smart Grid*, vol. 10, no. 1, pp. 841–851, 2017.

[35] P. Bacher, H. Madsen, and H. A. Nielsen, “Online short-term solar power forecasting,” *Solar energy*, vol. 83, no. 10, pp. 1772–1783, 2009.

[36] B. Elsinga and W. G. J. H. M. van Sark, “Short-term peer-to-peer solar forecasting in a network of photovoltaic systems,” *Applied Energy*, vol. 206, pp. 1464–1483, 2017.

[37] J. Antonanzas, N. Osorio, R. Escobar, R. Urraca, F. J. Martinez-de Pison, and F. Antonanzas-Torres, “Review of photovoltaic power forecasting,” *Solar Energy*, vol. 136, pp. 78–111, 2016.

[38] A. Agüera-Pérez, J. C. Palomares-Salas, J. J. G. de la Rosa, and O. Florencias-Oliveros, “Weather forecasts for microgrid energy management: Review, discussion and recommendations,” *Applied Energy*, vol. 228, pp. 265–278, 2018.

[39] E. F. Camacho, D. R. Ramírez, D. Limón, D. M. De La Peña, and T. Alamo, “Model predictive control techniques for hybrid systems,” *Annual Reviews in Control*, vol. 34, no. 1, pp. 21–31, 2010.

[40] D. Q. Mayne, “Model predictive control: Recent developments and future promise,” *Automatica*, vol. 50, no. 12, pp. 2967–2986, 2014.

[41] R. Carli, G. Cavone, T. Pippia, B. De Schutter, and M. Dotoli, “A robust MPC energy scheduling strategy for multi-carrier microgrids,” in *International Conference on Automation Science and Engineering*. IEEE, 2020, pp. 152–158.

[42] R. Carli, M. Dotoli, J. Jantzen, M. Kristensen, and S. B. Othman, “Energy scheduling of a smart microgrid with shared photovoltaic panels and storage: The case of the Ballen marina in Samsø,” *Energy*, vol. 198, p. 117188, 2020.

[43] R. Hanna, M. Ghonima, J. Kleissl, G. Tynan, and D. G. Victor, “Evaluating business models for microgrids: Interactions of technology and policy,” *Energy Policy*, vol. 103, pp. 47–61, 2017.

[44] M. Kim, S. Parkt, J. K. Choi, and J. Lee, “Energy independence of energy trading system in microgrid,” in *Innovative Smart Grid Technologies*. IEEE, 2017, pp. 1–4.

[45] H. Karimi and S. Jadid, “Optimal energy management for multi-microgrid considering demand response programs: A stochastic multi-objective framework,” *Energy*, vol. 195, p. 116992, 2020.

Bibliography

[1] H. A. Aalami and A. Khatibzadeh. Regulation of market clearing price based on nonlinear models of demand bidding and emergency demand response programs. *International Transactions on Electrical Energy Systems*, 26(11):2463–2478, 2016.

[2] H. A. Aalami, M. P. Moghaddam, and G. R. Yousefi. Modeling and prioritizing demand response programs in power markets. *Electric Power Systems Research*, 80(4):426–435, 2010.

[3] A. Abdulaal, R. Moghaddass, and S. Asfour. Two-stage discrete-continuous multi-objective load optimization: An industrial consumer utility approach to demand response. *Applied Energy*, 206:206–221, 2017.

[4] J. Aghaei and M. I. Alizadeh. Demand response in smart electricity grids equipped with renewable energy sources: A review. *Renewable and Sustainable Energy Reviews*, 18:64–72, 2013.

[5] J. Aghaei and M. I. Alizadeh. Multi-objective self-scheduling of CHP (combined heat and power)-based microgrids considering demand response programs and ESSs (energy storage systems). *Energy*, 55:1044–1054, 2013.

[6] G.R. Aghajani, H.A. Shayanfar, and H. Shayeghi. Presenting a multi-objective generation scheduling model for pricing demand response rate in micro-grid energy management. *Energy Conversion and Management*, 106:308–321, 2015.

[7] A. Agüera-Pérez, J. C. Palomares-Salas, J. J. G. de la Rosa, and O. Florencias-Oliveros. Weather forecasts for microgrid energy management: Review, discussion and recommendations. *Applied Energy*, 228:265–278, 2018.

[8] A. Ahmadian, M. Sedghi, A. Elkamel, M. Fowler, and M. A. Golkar. Plug-in electric vehicle batteries degradation modeling for smart grid studies: Review, assessment and conceptual framework. *Renewable and Sustainable Energy Reviews*, 81:2609–2624, 2018.

[9] F. Alavi, E. P. Lee, N. van de Wouw, B. De Schutter, and Z. Lukszo. Fuel cell cars in a microgrid for synergies between hydrogen and electricity networks. *Applied Energy*, 192:296–304, 2017.

[10] F. Alavi, N. van de Wouw, and B. De Schutter. Min-max control of fuel-cell-car-based smart energy systems. In *European Control Conference*, pages 1223–1228. IEEE, 2016.

[11] M. Alipour, K. Zare, and M. Abapour. MINLP probabilistic scheduling model for demand response programs integrated energy hubs. *IEEE Transactions on Industrial Informatics*, 14(1):79–88, 2017.

[12] AlleCijfers.nl. Informatie gemeente amsterdam. [Online]. Available: https://allecijfers.nl/gemeente/amsterdam/. Accessed: 04-August-2020.

[13] J. Antonanzas, N. Osorio, R. Escobar, R. Urraca, F. J. Martinez-de Pison, and F. Antonanzas-Torres. Review of photovoltaic power forecasting. *Solar Energy*, 136:78–111, 2016.

[14] L. Aye, W.W.S. Charters, and C. Chaichana. Solar heat pump systems for domestic hot water. *Solar Energy*, 73(3):169–175, 2002.

[15] P. Bacher, H. Madsen, and H. A. Nielsen. Online short-term solar power forecasting. *Solar energy*, 83(10):1772–1783, 2009.

[16] A. Barbato and A. Capone. Optimization models and methods for demand-side management of residential users: A survey. *Energies*, 7(9):5787–5824, 2014.

[17] L. Bartolucci, S. Cordiner, V. Mulone, and M. Santarelli. Hybrid renewable energy systems: Influence of short term forecasting on model predictive control performance. *Energy*, 172:997–1004, 2019.

[18] S. Bashash and H. K. Fathy. Optimizing demand response of plug-in hybrid electric vehicles using quadratic programming. In *American Control Conference*, pages 716–721, 2013.

[19] A. Bemporad and M. Morari. Control of systems integrating logic, dynamics, and constraints. *Automatica*, 35(3):407–427, 1999.

[20] Berenschot and Kalavasta. Klimaatneutrale energiescenarios 2050. [Online]. Available: https://www.rijksoverheid.nl/documenten/rapporten/2020/03/31/klimaatneutrale-energiescenarios-2050. Accessed: 04-May-2020.

[21] C. Bharathi, D. Rekha, and V. Vijayakumar. Genetic algorithm based demand side management for smart grid. *Wireless Personal Communications*, 93(2):481–502, 2017.

[22] R. E. Bird and R. L. Hulstrom. Simplified clear sky model for direct and diffuse insolation on horizontal surfaces. Technical report, Solar Energy Research Institute, Golden, 1981.

[23] M. Bourdeau, X. Zhai, E. Nefzaoui, X. Guo, and P. Chatellier. Modelling and forecasting building energy consumption: A review of data-driven techniques. *Sustainable Cities and Society*, 2019.

[24] M. Bouzerdoum, A. Mellit, and A. M. Pavan. A hybrid model (SARIMA–SVM) for short-term power forecasting of a small-scale grid-connected photovoltaic plant. *Solar Energy*, 98:226–235, 2013.

[25] G. E. P. Box, G. M. Jenkins, and G. C. Reinsel. *Time Series Analysis, Forecasting and Control*. Holden Day, 1976.

[26] C. Brandoni and M. Renzi. Optimal sizing of hybrid solar micro-CHP systems for the household sector. *Applied Thermal Engineering*, 75:896–907, 2015.

[27] E. F. Camacho, D. R. Ramírez, D. Limón, D. M. De La Peña, and T. Alamo. Model predictive control techniques for hybrid systems. *Annual Reviews in Control*, 34(1):21–31, 2010.

[28] M. C. Campi and S. Garatti. A sampling-and-discarding approach to chance-constrained optimization: Feasibility and optimality. *Journal of Optimization Theory and Applications*, 148(2):257–280, 2011.

[29] R. Carli, G. Cavone, T. Pippia, B. De Schutter, and M. Dotoli. A robust MPC energy scheduling strategy for multi-carrier microgrids. In *International Conference on Automation Science and Engineering*, pages 152–158. IEEE, 2020.

[30] R. Carli, M. Dotoli, J. Jantzen, M. Kristensen, and S. B. Othman. Energy scheduling of a smart microgrid with shared photovoltaic panels and storage: The case of the Ballen marina in Samsø. *Energy*, 198:117188, 2020.

[31] G. Cau, D. Cocco, M. Petrollese, S. K. Kær, and C. Milan. Energy management strategy based on short-term generation scheduling for a renewable microgrid using a hydrogen storage system. *Energy Conversion and Management*, 87:820–831, 2014.

[32] Centraal Bureau voor Statistiek. Personenauto's; voertuigkenmerken, regio's, 1 januari. [Online]. Available: https://opendata.cbs.nl/statline/#/CBS/nl/dataset/71405ned/table?ts=1603370599291. Accessed: 5-August-2020.

[33] Centraal Bureau voor Statistiek. Verkeersprestaties personenauto's; kilometers, brandstofsoort, grondgebied. [Online]. Available: https://opendata.cbs.nl/statline/#/CBS/nl/dataset/80428ned/table?ts=1595965361977. Accessed: 04-August-2020.

[34] V. Chernozhukov, I. Fernández-Val, and A. Galichon. Quantile and probability curves without crossing. *Econometrica*, 78(3):1093–1125, 2010.

[35] K. J. Chua, S. K. Chou, and W. M. Yang. Advances in heat pump systems: A review. *Applied Energy*, 87(12):3611–3624, 2010.

[36] C. Corchero, M. Cruz-Zambrano, F. J. Heredia, et al. Optimal energy management for a residential microgrid including a vehicle-to-grid system. *IEEE Transactions on Smart Grid*, 5(4):2163–2172, 2014.

[37] F. Dababneh and L. Li. Integrated electricity and natural gas demand response for manufacturers in the smart grid. *IEEE Transactions on Smart Grid*, 2018.

[38] U. K. Das, K. S. Tey, M. Seyedmahmoudian, S. Mekhilef, M. Y. I. Idris, W. Van Deventer, B. Horan, and A. Stojcevski. Forecasting of photovoltaic power generation and model optimization: A review. *Renewable and Sustainable Energy Reviews*, 81:912–928, 2018.

[39] De Energiemanager. Tools. [Online]. Available: http://www.deenergiemanager.nl/tools.html. Accessed: 14-June-2020.

[40] M. G. De Giorgi, M. Malvoni, and P. M. Congedo. Comparison of strategies for multi-step ahead photovoltaic power forecasting models based on hybrid group method of data handling networks and least square support vector machine. *Energy*, 107:360–373, 2016.

[41] S. Dhundhara, Y. P. Verma, and A. Williams. Techno-economic analysis of the lithium-ion and lead-acid battery in microgrid systems. *Energy Conversion and Management*, 177:122–142, 2018.

[42] M. Doostizadeh and H. Ghasemi. A day-ahead electricity pricing model based on smart metering and demand-side management. *Energy*, 46(1):221–230, 2012.

[43] M. Dubarry, A. Devie, and K. McKenzie. Durability and reliability of electric vehicle batteries under electric utility grid operations: Bidirectional charging impact analysis. *Journal of Power Sources*, 358:39–49, 2017.

[44] B. Elsinga and W. G. J. H. M. van Sark. Short-term peer-to-peer solar forecasting in a network of photovoltaic systems. *Applied Energy*, 206:1464–1483, 2017.

[45] Entsoe. Day-ahead prices. [Online]. Available: https://transparency.entsoe.eu/transmission-domain/r2/dayAheadPrices/show. Accessed: 15-January-2020.

[46] S. S. Farahani, R. van der Veen, V. Oldenbroek, F. Alavi, E. H. P. Lee, N. van de Wouw, A. van Wijk, B. De Schutter, and Z. Lukszo. A hydrogen-based integrated energy and transport system: The design and analysis of the car as power plant concept. *IEEE Systems, Man, and Cybernetics Magazine*, 5(1):37–50, 2019.

[47] M. Farina, L. Giulioni, and R. Scattolini. Stochastic linear model predictive control with chance constraints – A review. *Journal of Process Control*, 44:53–67, 2016.

[48] A. H. Fathima and K. Palanisamy. Optimization in microgrids with hybrid energy systems – A review. *Renewable and Sustainable Energy Reviews*, 45:431–446, 2015.

[49] P. Firouzmakan, R. Hooshmand, M. Bornapour, and A. Khodabakhshian. A comprehensive stochastic energy management system of micro-CHP units, renewable energy sources and storage systems in microgrids considering demand response programs. *Renewable and Sustainable Energy Reviews*, 108:355–368, 2019.

[50] Fraunhofer Institute for Solar Eenrgy Systems. Photovoltaic report. [Online]. Available: https://www.ise.fraunhofer.de/content/dam/ise/de/documents/publications/studies/Photovoltaics-Report.pdf. Accessed: 26-June-2020.

[51] A. Foucquier, S. Robert, F. Suard, L. Stéphan, and A. Jay. State of the art in building modelling and energy performances prediction: A review. *Renewable and Sustainable Energy Reviews*, 23:272–288, 2013.

[52] J. Geske and D. Schumann. Willing to participate in vehicle-to-grid (V2G)? Why not! *Energy Policy*, 120:392–401, 2018.

[53] F. Golestaneh, P. Pinson, and H. B. Gooi. Very short-term nonparametric probabilistic forecasting of renewable energy generation - With application to solar energy. *IEEE Transactions on Power Systems*, 31(5):3850–3863, 2016.

[54] P. Gou and J. Yu. A nonlinear ANN equalizer with mini-batch gradient descent in 40Gbaud PAM-8 IM/DD system. *Optical Fiber Technology*, 46:113–117, 2018.

[55] Greenmatch. Heat pumps: Compare prices and suppliers of heat pumps. [Online]. Available: https://www.greenmatch.co.uk/heat-pump. Accessed: 14-October-2020.

[56] G. Grimm, M. J. Messina, S. E. Tuna, and A. R. Teel. Examples when nonlinear model predictive control is nonrobust. *Automatica*, 40(10):1729–1738, 2004.

[57] Gurobi Optimization. Inc. gurobi optimizer reference manual. [Online]. Available: https://www.gurobi.com. Accessed: 1-July-2020.

[58] R. Hanna, M. Ghonima, J. Kleissl, G. Tynan, and D. G. Victor. Evaluating business models for microgrids: Interactions of technology and policy. *Energy Policy*, 103:47–61, 2017.

[59] A. D. Hawkes, D. J. L. Brett, and N. P. Brandon. Fuel cell micro-CHP techno-economics: Part 1–model concept and formulation. *International Journal of Hydrogen Energy*, 34(23):9545–9557, 2009.

[60] T. A. N. Heirung, J. A. Paulson, J. O'Leary, and A. Mesbah. Stochastic model predictive control – how does it work? *Computers & Chemical Engineering*, 114:158–170, 2018.

[61] H. Heitsch and W. Römisch. Scenario tree modeling for multistage stochastic programs. *Mathematical Programming*, 118(2):371–406, 2009.

[62] L. Hernandez, C. Baladron, J. M. Aguiar, B. Carro, A. J. Sanchez-Esguevillas, J. Lloret, and J. Massana. A survey on electric power demand forecasting: Future trends in smart grids, microgrids and smart buildings. *IEEE Communications Surveys & Tutorials*, 16(3):1460–1495, 2014.

[63] A. Hirsch, Y. Parag, and J. Guerrero. Microgrids: A review of technologies, key drivers, and outstanding issues. *Renewable and Sustainable Energy Reviews*, 90:402–411, 2018.

[64] S. Hochreiter and J. Schmidhuber. Long short-term memory. *Neural Computation*, 9(8):1735–1780, 1997.

[65] M. Houwing, R. R. Negenborn, and B. De Schutter. Demand response with micro-CHP systems. *Proceedings of the IEEE*, 99(1):200–213, 2010.

[66] Household Energy Price Index. Price data. [Online]. Available: https://www.energypriceindex.com/latest-update/. Accessed: 22-August-2020.

[67] M. Izadbakhsh, M. Gandomkar, A. Rezvani, and A. Ahmadi. Short-term resource scheduling of a renewable energy based micro grid. *Renewable Energy*, 75:598–606, 2015.

[68] M. Jin, W. Feng, C. Marnay, and C. Spanos. Microgrid to enable optimal distributed energy retail and end-user demand response. *Applied Energy*, 210:1321–1335, 2018.

[69] A. R. Jordehi. Optimisation of demand response in electric power systems, a review. *Renewable and Sustainable Energy Reviews*, 103:308–319, 2019.

[70] J. Jung and R. P. Broadwater. Current status and future advances for wind speed and power forecasting. *Renewable and Sustainable Energy Reviews*, 31:762–777, 2014.

[71] H. Karimi and S. Jadid. Optimal energy management for multi-microgrid considering demand response programs: A stochastic multi-objective framework. *Energy*, 195:116992, 2020.

[72] J. Kim and A. Shcherbakova. Common failures of demand response. *Energy*, 36(2):873–880, 2011.

[73] M. Kim, S. Parkt, J. K. Choi, and J. Lee. Energy independence of energy trading system in microgrid. In *Innovative Smart Grid Technologies*, pages 1–4. IEEE, 2017.

[74] K. Klein, K. Huchtemann, and D. Müller. Numerical study on hybrid heat pump systems in existing buildings. *Energy and Buildings*, 69:193–201, 2014.

[75] KNMI. Klimatologie. [Online]. Available: http://projects.knmi.nl/klimatologie/uurgegevens/selectie.cgi. Accessed: 30-March-2020.

[76] W. Kong, Z. Y. Dong, Y. Jia, D. J. Hill, Y. Xu, and Y. Zhang. Short-term residential load forecasting based on LSTM recurrent neural network. *IEEE Transactions on Smart Grid*, 10(1):841–851, 2017.

[77] C. D. Korkas, S. Baldi, I. Michailidis, and E. B. Kosmatopoulos. Occupancy-based demand response and thermal comfort optimization in microgrids with renewable energy sources and energy storage. *Applied Energy*, 163:93–104, 2016.

[78] P. O. Kriett and M. Salani. Optimal control of a residential microgrid. *Energy*, 42(1):321–330, 2012.

[79] J. Lago, K. De Brabandere, F. De Ridder, and B. De Schutter. Short-term forecasting of solar irradiance without local telemetry: A generalized model using satellite data. *Solar Energy*, 173:566–577, 2018.

[80] J. S. Lai and M. W. Ellis. Fuel cell power systems and applications. *Proceedings of the IEEE*, 105(11):2166–2190, 2017.

[81] I. Lampropoulos, W. L. Kling, P. F. Ribeiro, and J. Van den Berg. History of demand side management and classification of demand response control schemes. *IEEE Power & Energy Society General Meeting*, pages 1–5, 2013.

[82] J. M. Latorre, S. Cerisola, and A. Ramos. Clustering algorithms for scenario tree generation: Application to natural hydro inflows. *European Journal of Operational Research*, 181(3):1339–1353, 2007.

[83] P. Lauret, M. David, and H. T. C. Pedro. Probabilistic solar forecasting using quantile regression models. *Energies*, 10(10):1591, 2017.

[84] Liander. Beschikbare data. [Online]. Available: https://www.liander.nl/over-liander/innovatie/open-data/data/. Accessed: 02-April-2020.

[85] S. G. Liasi and S. M. T. Bathaee. Optimizing microgrid using demand response and electric vehicles connection to microgrid. In *Smart Grid Conference*, pages 1–7, 2017.

[86] C. Liu, K. T. Chau, D. Wu, and S. Gao. Opportunities and challenges of vehicle-to-home, vehicle-to-vehicle, and vehicle-to-grid technologies. *Proceedings of the IEEE*, 101(11):2409–2427, 2013.

[87] T. Logenthiran, D. Srinivasan, and E. Phyu. Particle swarm optimization for demand side management in smart grid. *IEEE Innovative Smart Grid Technologies-Asia*, pages 1–6, 2015.

[88] E. Lorenzo. Energy collected and delivered by PV modules. *Handbook of photovoltaic science and engineering*, pages 984–1042, 2011.

[89] A. Luque and S. Hegedus. *Handbook of photovoltaic science and engineering*. John Wiley & Sons, 2011.

[90] M. M. Maghanki, B. Ghobadian, G. Najafi, and R. J. Galogah. Micro combined heat and power (MCHP) technologies and applications. *Renewable and Sustainable Energy Reviews*, 28:510–524, 2013.

[91] T. M. I. Mahlia, T. J. Saktisahdan, A. Jannifar, M. H. Hasan, and H. S. C. Matseelar. A review of available methods and development on energy storage; technology update. *Renewable and Sustainable Energy Reviews*, 33:532–545, 2014.

[92] M. S. Mahmoud. *Microgrid: Advanced Control Methods and Renewable Energy System Integration*. Elsevier, 2016.

[93] G. Majeau-Bettez, T. R. Hawkins, and A. H. Strømman. Life cycle environmental assessment of lithium-ion and nickel metal hydride batteries for plug-in hybrid and battery electric vehicles. *Environmental Science & Technology*, 45(10):4548–4554, 2011.

[94] Y. Manoharan, S. E. Hosseini, B. Butler, H. Alzhahrani, B. T. F. Senior, T. Ashuri, and J. Krohn. Hydrogen fuel cell vehicles; Current status and future prospect. *Applied Sciences*, 9(11):2296, 2019.

[95] D. Q. Mayne. Model predictive control: Recent developments and future promise. *Automatica*, 50(12):2967–2986, 2014.

[96] M. Mazidi, A. Zakariazadeh, S. Jadid, and P. Siano. Integrated scheduling of renewable generation and demand response programs in a microgrid. *Energy Conversion and Management*, 86:1118–1127, 2014.

[97] A. Mohsenian-Rad and A. Leon-Garcia. Optimal residential load control with price prediction in real-time electricity pricing environments. *IEEE Transaction on Smart Grid*, 1(2):120–133, 2010.

[98] H. Mortaji, S. H. Ow, M. Moghavvemi, and H. A. F. Almurib. Load shedding and smart-direct load control using internet of things in smart grid demand response management. *IEEE Transactions on Industry Applications*, 53(6):5155–5163, 2017.

[99] J. C. Mukherjee and A. Gupta. A review of charge scheduling of electric vehicles in smart grid. *IEEE Systems Journal*, 9(4):1541–1553, 2014.

[100] D. T. Nguyen and L. B. Le. Joint optimization of electric vehicle and home energy scheduling considering user comfort preference. *IEEE Transactions on Smart Grid*, 5(1):188–199, 2013.

[101] H. S. V. S. Kumar Nunna and S. Doolla. Demand response in smart distribution system with multiple microgrids. *IEEE Transactions on Smart Grid*, 3(4):1641–1649, 2012.

[102] N. I. Nwulu and X. Xia. Optimal dispatch for a microgrid incorporating renewables and demand response. *Renewable Energy*, 101:16–28, 2017.

[103] G. J. Offer, D. Howey, M. Contestabile, R. Clague, and N. P. Brandon. Comparative analysis of battery electric, hydrogen fuel cell and hybrid vehicles in a future sustainable road transport system. *Energy Policy*, 38(1):24–29, 2010.

[104] D. E. Olivares, A. Mehrizi-Sani, A. H. Etemadi, C. A. Cañizares, R. Iravani, M. Kazerani, A. H. Hajimiragha, O. Gomis-Bellmunt, M. Saeedifard, R. Palma-Behnke, et al. Trends in microgrid control. *IEEE Transactions on Smart Grid*, 5(4):1905–1919, 2014.

[105] P. Palensky and D. Dietrich. Demand side management: Demand response, intelligent energy systems, and smart loads. *IEEE Transactions on Industrial Informatics*, 7(3):381–388, Aug 2011.

[106] S. Parhizi, H. Lotfi, A. Khodaei, and S. Bahramirad. State of the art in research on microgrids: A review. *IEEE Access*, 3:890–925, 2015.

[107] A. Parisio, E. Rikos, and L. Glielmo. A model predictive control approach to microgrid operation optimization. *IEEE Transactions on Control Systems Technology*, 22(5):1813–1827, 2014.

[108] A. Parisio, E. Rikos, and L. Glielmo. Stochastic model predictive control for economic/environmental operation management of microgrids: An experimental case study. *Journal of Process Control*, 43:24–37, 2016.

[109] P. Pinson, H. Madsen, H. A. Nielsen, G. Papaefthymiou, and B. Klöckl. From probabilistic forecasts to statistical scenarios of short-term wind power production. *Wind Energy: An International Journal for Progress and Applications in Wind Power Conversion Technology*, 12(1):51–62, 2009.

[110] L. P. Qian, Y. J. A. Zhang, J. Huang, and Y. Wu. Demand response management via real-time electricity price control in smart grids. *IEEE Journal on Selected Areas in Communications*, 31(7):1268–1280, 2013.

[111] N. Refa and N. Hubbers. Impact of smart charging on EVs charging behaviour assessed from real charging events. *32nd Electric Vehicle Symposium*, 2019.

[112] C. Riordan and R. Hulstron. What is an air mass 1.5 spectrum? (Solar cell performance calculations). In *IEEE Conference on Photovoltaic Specialists*, pages 1085–1088. IEEE, 1990.

[113] P. Rodatz, G. Paganelli, A. Sciarretta, and L. Guzzella. Optimal power management of an experimental fuel cell/supercapacitor-powered hybrid vehicle. *Control Engineering Practice*, 13(1):41–53, 2005.

[114] H. Sak, A. W. Senior, and F. Beaufays. Long short-term memory recurrent neural network architectures for large scale acoustic modeling. *Proc. interspeech.*, 2014.

[115] T. Samad, E. Koch, and P. Stluka. Automated demand response for smart buildings and microgrids: The state of the practice and research challenges. *Proceedings of the IEEE*, 104(4):726–744, 2016.

[116] G. Santamaría-Bonfil, A. Reyes-Ballesteros, and C. Gershenson. Wind speed forecasting for wind farms: A method based on support vector regression. *Renewable Energy*, 85:790–809, 2016.

[117] G. Schildbach, L. Fagiano, C. Frei, and M. Morari. The scenario approach for stochastic model predictive control with bounds on closed-loop constraint violations. *Automatica*, 50(12):3009–3018, 2014.

[118] M. Sedighizadeh, M. Esmaili, A. Jamshidi, and M. Ghaderi. Stochastic multi-objective economic-environmental energy and reserve scheduling of microgrids considering battery energy storage system. *International Journal of Electrical Power & Energy Systems*, 106:1–16, 2019.

[119] P. Siano. Demand response and smart grids - A survey. *Renewable and Sustainable Energy Reviews*, 30:461–478, 2014.

[120] G. Sideratos and N. D. Hatziargyriou. An advanced statistical method for wind power forecasting. *IEEE Transactions on Power Systems*, 22(1):258–265, 2007.

[121] Stedin. Tarieven 2020 elektriciteit grootverbruik. [Online]. Available: `https://www.stedin.net/zakelijk/betalingen-en-facturen/tarieven`. Accessed: 6-October-2020.

[122] W. Su, Z. Yuan, and M. Y. Chow. Microgrid planning and operation: Solar energy and wind energy. In *IEEE PES General Meeting*, pages 1–7. IEEE, 2010.

[123] X. Tan, Q. Li, and H. Wang. Advances and trends of energy storage technology in microgrid. *International Journal of Electrical Power & Energy Systems*, 44(1):179–191, 2013.

[124] D. Testi, L. Urbanucci, C. Giola, E. Schito, and P. Conti. Stochastic optimal integration of decentralized heat pumps in a smart thermal and electric micro-grid. *Energy Conversion and Management*, 210:112734, 2020.

[125] C. E. Thomas. Fuel cell and battery electric vehicles compared. *International Journal of Hydrogen Energy*, 34(15):6005–6020, 2009.

[126] United Nations. Adoption of the Paris agreement. [Online]. Available: http://unfccc.int/files/essential_background/convention/application/pdf/english_paris_agreement.pdf. Accessed: 14-December-2019.

[127] U.S. Department of Energy. Benefits of demand response in electricity markets and recommendations for achieving them. Technical report, US Dept. Energy, Washington, DC, USA, 2006.

[128] S. I. Vagropoulos, G. I. Chouliaras, E. G. Kardakos, C. K. Simoglou, and A. G. Bakirtzis. Comparison of SARIMAX, SARIMA, modified SARIMA and ANN-based models for short-term PV generation forecasting. In *IEEE International Energy Conference*, pages 1–6, 2016.

[129] M. Van Der Kam and W. van Sark. Smart charging of electric vehicles with photovoltaic power and vehicle-to-grid technology in a microgrid; a case study. *Applied Energy*, 152:20–30, 2015.

[130] H. Van Ekeren, R. R. Negenborn, P. J. van Overloop, and B. De Schutter. Time-instant optimization for hybrid model predictive control of the Rhine–Meuse delta. *Journal of Hydroinformatics*, 15(2):271–292, 2013.

[131] P. Velarde, L. Valverde, J. M. Maestre, C. Ocampo-Martínez, and C. Bordons. On the comparison of stochastic model predictive control strategies applied to a hydrogen-based microgrid. *Journal of Power Sources*, 343:161–173, 2017.

[132] C. Wan, J. Zhao, Y. Song, Z. Xu, J. Lin, and Z. Hu. Photovoltaic and solar power forecasting for smart grid energy management. *CSEE Journal of Power and Energy Systems*, 1(4):38–46, 2015.

[133] R. Wang, P. Wang, G. Xiao, and S. Gong. Power demand and supply management in microgrids with uncertainties of renewable energies. *International Journal of Electrical Power & Energy Systems*, 63:260–269, 2014.

[134] D. Xu, Z. Chen, and L. Yang. Scenario tree generation approaches using K-means and LP moment matching methods. *Journal of Computational and Applied Mathematics*, 236(17):4561–4579, 2012.

[135] D. Xu, P. Li, and B. Zhao. Optimal scheduling of microgrid with consideration of demand response in smart grid. In *IEEE 12th International Conference on Networking, Sensing and Control*, pages 426–431, April 2015.

[136] D. Yang, Z. Ye, L. H. I. Lim, and Z. Dong. Very short term irradiance forecasting using the lasso. *Solar Energy*, 114:314–326, 2015.

[137] P. Yi, X. Dong, A. Iwayemi, C. Zhou, and S. Li. Real-time opportunistic scheduling for residential demand response. *IEEE Transactions on Smart Grid*, 4(1):227–234, 2013.

[138] B. Yildiz, J. I. Bilbao, and A. B. Sproul. A review and analysis of regression and machine learning models on commercial building electricity load forecasting. *Renewable and Sustainable Energy Reviews*, 73:1104–1122, 2017.

[139] A. Zakariazadeh, S. Jadid, and P. Siano. Smart microgrid energy and reserve scheduling with demand response using stochastic optimization. *International Journal of Electrical Power & Energy Systems*, 63:523–533, 2014.

[140] Zakelijke Energietarieven. Gemiddeld energie verbruik. [Online]. Available: https://zakelijkeenergietarieven.nl/grootverbruik-energie/gemiddeld-energie-verbruik/. Accessed: 14-June-2020.

[141] T. Zhang, P. Wang, H. Chen, and P. Pei. A review of automotive proton exchange membrane fuel cell degradation under start-stop operating condition. *Applied Energy*, 223:249–262, 2018.

[142] X. Zhang, R. Sharma, and Y. He. Optimal energy management of a rural microgrid system using multi-objective optimization. In *Innovative Smart Grid Technologies*, pages 1–8. IEEE, 2012.

[143] H. Zhao and F. Magoulès. A review on the prediction of building energy consumption. *Renewable and Sustainable Energy Reviews*, 16(6):3586–3592, 2012.

[144] Z. Zhao, W. C. Lee, Y. Shin, and K. B. Song. An optimal power scheduling method for demand response in home energy management system. *IEEE Transactions on Smart Grid*, 4(3):1391–1400, 2013.

[145] C. Zhou, J. Zheng, S. Liu, Y. Liu, F. Mei, Y. Pan, T. Shi, and J. Wu. Operation optimization of multi-district integrated energy system considering flexible demand response of electric and thermal loads. *Energies*, 12(20):3831, 2019.

Glossary

List of Acronyms

ANN	Artificial Neural Network
CHP	Combined Heat and Power
DR	Demand Response
EV	Electric Vehicle
MPC	Model Predictive Control
PV	Photovoltaic

List of Symbols

Symbols Related to the Model of the Microgrid

k	Time step
x_{bat}	Energy storage in the battery [kWh]
u_{bat}	Energy exchange of the battery [kWh]
δ_{bat}	Logic binary variable indicating if the battery is charging or discharging
$\eta_{\mathrm{bat}}^{\mathrm{c}}$	Charging efficiency of the battery
$\eta_{\mathrm{bat}}^{\mathrm{d}}$	Discharging efficiency of the battery
x_{hst}	Hydrogen stored in the hydrogen storage tank [kg]
u_{hst}	Hydrogen exchanged with the hydrogen storage tank [kg]
H_{elc}	Hydrogen produced by the electrolyzer [kg]
u_{elc}	Electrical energy consumed by the electrolyzer [kWh]
δ_{elc}	Logic binary variable indicating if the electrolyzer is on or off
α_{elc}	Model parameter of the electrolyzer [kg/kWh]
Q_{HP}	Thermal energy generated by the hybrid heat pump [kWh]
$u_{\mathrm{HP}}^{\mathrm{el}}$	Electrical energy consumed by the hybrid heat pump [kWh]
$u_{\mathrm{HP}}^{\mathrm{gas}}$	Gas consumed by the hybrid heat pump [kWh]
$u_{\mathrm{HP}}^{\mathrm{hyd}}$	Hydrogen consumed by the hybrid heat pump [kWh]
$\delta_{\mathrm{HP}}^{\mathrm{el}}$	Logic binary variable indicating if the hybrid heat pump is consuming electrical energy
$\delta_{\mathrm{HP}}^{\mathrm{el}}$	Logic binary variable indicating if the hybrid heat pump is consuming gas
$\delta_{\mathrm{HP}}^{\mathrm{hyd}}$	Logic binary variable indicating if the hybrid heat pump is consuming hydrogen
$\eta_{\mathrm{HP}}^{\mathrm{el}}$	Electrical energy efficiency of the hybrid heat pump
$\eta_{\mathrm{HP}}^{\mathrm{gas}}$	Gas efficiency of the hybrid heat pump
$\eta_{\mathrm{HP}}^{\mathrm{hyd}}$	Hydrogen efficiency of the hybrid heat pump
P_{CHP}	Electrical energy produced by the CHP plant [kWh]
Q_{CHP}	Thermal energy produced by the CHP plant [kWh]
x_{CHP}	Thermal energy stored in the storage component of the CHP plant [kWh]
u_{CHP}	Gas or hydrogen consumed by the CHP plant [kWh]
δ_{CHP}	Logic binary variable indicating if the CHP plant is turned on or off
$\eta_{\mathrm{CHP}}^{\mathrm{el}}$	Electrical efficiency of the CHP plant
$\eta_{\mathrm{CHP}}^{\mathrm{th}}$	Thermal efficiency of the CHP plant
x_{BEV}	Electrical energy stored in the battery EV [kWh]
u_{BEV}	Electrical energy transferred with the battery EV [kWh]
h_{BEV}	Electrical energy costs per trip for the battery EV [kWh]
$\delta_{\mathrm{BEV}}^{\mathrm{g}}$	Logic binary variable indicating if the battery EV is in generation mode
$z_{\mathrm{BEV}}^{\mathrm{g}}$	Auxiliary variable indicating the generated energy for the microgrid from the battery EV
$\eta_{\mathrm{BEV}}^{\mathrm{c}}$	Charging efficiency of the battery EV
$\eta_{\mathrm{BEV}}^{\mathrm{d}}$	Discharging efficiency of the battery EV
x_{FEV}	Hydrogen stored in the fuel cell EV [kg]
$u_{\mathrm{FEV}}^{\mathrm{hyd}}$	Hydrogen transferred with the fuel cell EV [kg]
$u_{\mathrm{FEV}}^{\mathrm{el}}$	Electrical energy transferred with the fuel cell EV [kWh]
h_{FEV}	Hydrogen costs per trip for the fuel cell EV [kg]
α_{FEV}	Model parameter of the fuel cell EV [kg/kWh]

β_{FEV}	Model parameter of the fuel cell EV [kg/h]
C_{UG}	Economic cost for the imported energy from the utility grid [€]
u_{UG}	Energy exchanged with the utility grid [kWh]
δ_{UG}	Logic binary variable indicating if energy is purchased from or sold to the utility grid
c^{p}	Purchasing price of energy [€]
c^{s}	Sale price of energy [€]
D_{c}	Thermal curtailable load [kWh]
β_{c}	Percentage of preferred power level to be curtailed
Q_{c}	Actual curtailed thermal load [kWh]
D_{r}	Rescheduable load [kWh]
$D_{\mathrm{r}}^{\mathrm{el}}$	Electrical rescheduable load [kWh]
$D_{\mathrm{r}}^{\mathrm{th}}$	Thermal rescheduable load [kWh]
β_{r}	Percentage of preferred power level to be rescheduled
$\beta_{\mathrm{r}}^{\mathrm{el}}$	Percentage of preferred electrical power level to be rescheduled
$\beta_{\mathrm{r}}^{\mathrm{th}}$	Percentage of preferred thermal power level to be rescheduled
P_{r}	Actual rescheduled electrical load [kWh]
Q_{r}	Actual rescheduled thermal load [kWh]
D_{rc}	Consumed rescheduled load [kWh]
$D_{\mathrm{rc}}^{\mathrm{el}}$	Consumed electrical rescheduled load [kWh]
$D_{\mathrm{rc}}^{\mathrm{th}}$	Consumed thermal rescheduled load [kWh]
$\delta_{\mathrm{rc}}^{\mathrm{el}}$	Logic binary variable indicating if electrical rescheduable load is consumed
$\delta_{\mathrm{rc}}^{\mathrm{th}}$	Logic binary variable indicating if thermal rescheduable load is consumed
P_{rc}	Actual consumed rescheduled electrical load [kWh]
Q_{rc}	Actual consumed rescheduled thermal load [kWh]
$l_{\mathrm{r}}^{\mathrm{el}}$	Unsatisfied rescheduled electrical load [kWh]
$l_{\mathrm{r}}^{\mathrm{th}}$	Unsatisfied rescheduled thermal load [kWh]
$T_{\mathrm{rc}}^{\mathrm{el}}$	Time needed for the unsatisfied rescheduled electrical load to be consumed [h]
$T_{\mathrm{rc}}^{\mathrm{th}}$	Time needed for the unsatisfied rescheduled thermal load to be consumed [h]
F_{el}	Defined time step when rescheduled electrical load needs to be consumed
F_{th}	Defined time step when rescheduled thermal load needs to be consumed

Symbols Related to the Constraints in the Model of the Microgrid

δ	Logic binary variable indicating different modes
T_{ON}	Minimum time the system is turned on [h]
T_{OFF}	Minimum time the system is turned off [h]
x_{EV}	Fuel stored in the EV [kWh]
$\underline{x}_{\mathrm{EV}}^{\mathrm{t}}$	Minimum fuel that needs to be stored upon departure in the EV
$\delta_{\mathrm{EV}}^{\mathrm{t}}$	Logic binary variable indicating if the EV is in transportation mode
$\underline{x}_{\mathrm{EV}}^{\mathrm{g}}$	Minimum fuel that needs to be stored in the EV before in generation mode
$\delta_{\mathrm{EV}}^{\mathrm{g}}$	Logic binary variable indicating if the EV is in generation mode
$(\cdot)^{\mathrm{el}}$	Indicating that it is about electrical energy
$(\cdot)^{\mathrm{gas}}$	Indicating that it is about gas
$(\cdot)^{\mathrm{hyd}}$	Indicating that it is about hydrogen

Symbols Related to the Stochastic Processes

P_{PV}	Photovoltaic power [kW]
P_{STC}	Photovoltaic power under standard test conditions [kW]
G_{c}	Global horizontal solar irradiance [W/m^2]
G_{STC}	Global horizontal solar irradiance under standard test conditions [W/m^2]
$G_{\mathrm{c}}^{\mathrm{cs}}$	Global horizontal solar irradiance for a clear sky day [W/m^2]
T_{c}	Cell temperature [°C]
T_{STC}	Cell temperature under standard test conditions [°C]
α	Negative power temperature coefficient
T_{amb}	Ambient temperature [°C]
NOCT	Nominal operating cell temperature [°C]
τ	Clear sky index
P_{res}	Electrical energy demand of the residential buildings [kWh]
Q_{res}	Thermal energy demand of the residential buildings [kWh]
P_{com}	Electrical energy demand of the commercial buildings [kWh]
Q_{com}	Thermal energy demand of the commercial buildings [kWh]

Symbols Related to the Forecasting Models

$\boldsymbol{\alpha}$	Vector of optimized parameters for the linear regression
p	Autoregressive order
d	Difference order
q	Moving average order
ϕ_{p}	Regular autoregressive polynomial of order p
θ_{q}	Regular moving average polynomial of order q
L	Regular lag operator
∇^{d}	Regular differentiating operator
P	Seasonal autoregressive order
D	Seasonal difference order
Q	Seasonal moving average order
Φ_{P}	Seasonal autoregressive polynomial of order P
Θ_{Q}	Seasonal moving average polynomial of order Q
L^{s}	Seasonal lag operator
$\nabla_{\mathrm{s}}^{\mathrm{D}}$	Seasonal differentiating operator
X_{t}	Forecast variable
ε_{t}	White noise
$x'_{\mathrm{k,t}}$	Exogenous input of the k^{th} exogenous input variable
β_{k}	Coefficient value of the exogenous input of the k^{th} exogenous input variable

Symbols Related to the Control of the Microgrid

$\boldsymbol{x}$	States of the system
$\boldsymbol{u}$	Inputs of the system
$\boldsymbol{y}$	Outputs of the system
$\boldsymbol{w}$	Additive disturbances to the system
f	Function of the states of the system
h	Function of the outputs of the system
N_{p}	Prediction horizon
N_{s}	Number of scenarios
B^{ij}	Branching point of scenarios i and j
Δ	Bound for the tree structure
μ	Median
J	Cost function
J_{eco}	Economic cost function
J_{dis}	Discomfort cost function
J_{dur}	Durability cost function
J_{gd}	Grid demand cost function
ρ_{c}	Penalty weight on curtailment
$\rho_{\mathrm{r}}^{\mathrm{el}}$	Penalty weight on electrical energy rescheduling
$\rho_{\mathrm{r}}^{\mathrm{th}}$	Penalty weight on thermal energy rescheduling
ρ_{EV}	Penalty weight on the state of charge of the EVs
ρ_{bat}	Penalty weight on the state of charge of the battery
ρ_{hst}	Penalty weight on the state of charge of the hydrogen storage tank
N_{EV}	Number of EVs
N_{BEV}	Number of battery EVs
N_{FEV}	Number of fuel cell EVs
ρ_{gd}	Penalty weight on the maximum transferred electrical energy between the microgrid and the utility grid
$\zeta_{\mathrm{UG}}^{\mathrm{el}}$	Auxiliary variable indicating the maximum electrical energy transfer between the microgrid and the utility grid
$z_{\mathrm{UG}}^{\mathrm{el}}$	Auxiliary variable indicating only imported electrical energy

Symbols Related to the Performance Indices

T	Simulation time steps
T_{m}	Time steps in a month
EGI	Electric grid investment performance index
EIC	Energy import costs performance index
CL	Comfort level performance index
DEV	Durability of EV performance index
ESS	Electric self-supply performance index
EI	Energy independence performance index
δ^{t}	Logic variable indicating if EV is in transportation mode